SEPARATION POTENTIAL CHARACTERIZATION AND ITS ROLE IN SELECTING NANOFILTRATION MEMBRANES FOR THE REMOVAL OF INORGANIC IONS

by

Shardul Sudhir Wadekar

Bachelor in Chemical Engineering, Institute of Chemical Technology, Mumbai, 2014

Master of Science in Civil Engineering, University of Pittsburgh, 2016

Submitted to the Graduate Faculty of

Swanson School of Engineering in partial fulfillment

of the requirements for the degree of

Doctor of Philosophy

University of Pittsburgh

2018

UNIVERSITY OF PITTSBURGH

SWANSON SCHOOL OF ENGINEERING

This dissertation was presented

by

Shardul Sudhir Wadekar

It was defended on

April 20, 2018

and approved by

Radisav D. Vidic, Ph.D., Professor, Department of Civil and Environmental Engineering

Sachin S. Velankar, Ph.D., Associate Professor, Department of Chemical and Petroleum Engineering

Robert M. Enick, Ph.D., Professor, Department of Chemical and Petroleum Engineering

Andrew Zydney, Ph.D., Professor, Department of Chemical Engineering, Pennsylvania State University

Dissertation Director: Radisav D. Vidic, Ph.D., Professor, Department of Civil and Environmental Engineering

SEPARATION POTENTIAL CHARACTERIZATION AND ITS ROLE IN SELECTING NANOFILTRATION MEMBRANES FOR THE REMOVAL OF INORGANIC IONS

Shardul Sudhir Wadekar, Ph.D.

University of Pittsburgh, 2018

Water desalination with nanofiltration (NF) and reverse osmosis (RO) membranes presents an excellent solution to meet the ever–increasing water demand. NF membranes can achieve higher permeability at lower operating pressures and hence are energetically favorable compared to RO membranes. As such the overall motivation of this study was to improve the fundamental understanding of separation potentials for NF membranes and provide sound guidance for the selection of NF membranes for particular applications.

The first objective of this study was to explain the importance of different separation potentials for the rejection of inorganic ions by two most commonly used active layers of NF membranes – polyamide (PA) and poly(piperazineamide) (PP). Effective pore size measurements, zeta potential and crossflow ion rejection were used to establish that both Donnan (charge) and steric exclusion are important for ion rejection with PP membranes and that steric exclusion was the dominant mechanism for PA membranes. Specific studies with barium and strontium ions confirmed the dominance of steric exclusion for PA membranes. Experimental studies were conducted to unravel the impact of chemical cleaning on physicochemical characteristics and

performance of PA and PP membranes. In general, chemical cleaning with HCl and NaOH increased membrane permeability and decreased ion rejection due to the increase in effective pore sizes and changes in zeta potential but PP membranes were affected significantly more than PA membranes. The second objective of this study was to evaluate the use of NF membranes for treatment of abandoned mine drainage (AMD). Laboratory–scale optimization followed by pilot–scale testing demonstrated that polymeric NF membranes could achieve >98% removal of total dissolved solids without significant decrease in permeate flux. Polymeric NF membrane achieved higher permeability and ion rejection than ceramic NF membrane. This study demonstrated that AMD can be treated with polymeric NF membranes to recover high quality permeate and highlighted the need for improving ceramic NF membranes. The results obtained in this study provide new insights into NF separation mechanisms and their use for the treatment of AMD and contribute to further improvements in current membrane technologies to provide solutions for significant environmental problems and meeting the ever–increasing demand for clean water.

TABLE OF CONTENTS

LIST OF TABLES

LIST OF FIGURES

ACKNOWLEDGEMENTS

I would firstly like to thank my Ph.D. advisor, Dr. Radisav D. Vidic for his time, efforts, knowledge, guidance and inputs, which have immensely contributed in making my Ph.D. a success. I admire your vision and your way of looking for research questions. I really appreciate you sending me to several conferences that have helped me grow both professionally and personally. Thank you very much for constantly keeping me on my toes; I am now better equipped to tackle the fickle future and meet challenges.

I would also like to thank my Ph.D. committee, Dr. Robert M. Enick, Dr. Sachin S. Velankar and Dr. Andrew Zydney (Pennsylvania State University) for working with me to improve the quality of my thesis. Thank you for your time and consideration!

Several students and professors have helped and motivated me during the course of my Ph.D. Dr. Leanne Gilbertson, Dr. Lei Li, Dr. Giannis Bourmpakis (Yanni), Dr. Vikas Khanna, Dr. Kyle Bibby, and Dr. Goetz Veser thank you for interacting, inspiring and motivating me. Dr. David Malehorn thank you for all the technical assistance with cleaning and updating the analytical instruments, thank you Dr. Susheng Tan for helping me choose the right analytical instruments for my membrane characterization. Thank you, Mr. Charles Hager, for helping me build my crossflow membrane apparatus. Thank you Mr. Jonathan Callura (Carnegie Mellon University) for help with ICP–MS analysis and Ms. Yan Wang for help with XPS analysis. Thank you Dr. Michael Rothfuss and Dr. Nicholas Franconi for building my amplifier system for

the membrane potential measurements. Thank you to the Chemical & Petroleum Engineering and Civil & Environmental Engineering staff – Ms. Erin Golen, Ms. Amy Kapp, Ms. Rita Leccia, Ms. Patricia Park and Ms. Adrian Starke.

I would also like to thank my funding sources for their support of this work. I was funded for four semesters by the Pittsburgh Plate and Glass (PPG) industries fellowship. The nanofiltration – abandoned mine drainage project was funded by the Pennsylvania Shale Alliance for Energy Research Department (SAFER PA) and the Pennsylvania Department of Community and Economic Development (PA DCED). Thank you to the Chemical Engineering Department for the Graduate Research Fellowship.

I would like to thank all my friends for their support through the four years. Alen Gusa and Omkar Lokare, my lab mates, we have spent a lot of time together. Also, thank you to all other friends for supporting me – Yan Wang, Nathalia Aquino de Carvalho, Aman Dhuwe, Swapnil Nerkar, Shrinath Ghadge, Tieyuan Zhang, Zhewei Zhang, Atoosa Mashayekhi, Amey More, Sameer Damle, Michael Taylor, Gianfranco Rodriguez, Prashant Jampani.

Very special thanks to the very special people in my world. Mamma, Pappa, Chingi and my wife Bhagyashree. Thank you for your generosity, kindness and support.

NOMENCLATURE

AFM	Atomic Force Microscopy
AGC	Adjustable Gap Cell
AMD	Abandoned or Acid Mine Drainage
APALD	Atmospheric Pressure Atomic Layer Deposition
ARD	Acid Rock Drainage
ATR–FTIR	Attenuated Total Reflection – Fourier Transform Infrared
C_f	Solute Bulk Feed Concentration (mM)
C_m	Solute Concentration at Membrane Surface (mM)
C_p	Solute Bulk Permeate Concentration (mM)
DAP	N,N'–diaminopiperazine
DAPP	1,4–bis(3–aminopropyl)–piperazine
DFT	Density Functional Theory
d_h	Hydraulic Diameter (m)
DI	Deionized
D_i	Diffusion Coefficient of ion 'i' (m^2/s)
DSPM	Donnan Steric Partitioning Pore Model
EAP	N,N'–(2–aminoethyl)–piperazine

EDS	Energy Dispersive X–ray Spectroscopy
EKA	Electro–kinetic Analyzer
EPA	Environmental Protection Agency
FA	Fully Aromatic
GPM	Gallon per minute
IC	Ion Chromatography
ICP–MS	Inductively Coupled Plasma–Mass Spectroscopy
ICP–OES	Inductively Coupled Plasma–Optical Emission Spectroscopy
IEP	Iso–Electric Point
IP	Interfacial Polymerization
J	Permeate Volume Flux (LMH)
k	Mass Transfer Coefficient (m/s)
LMH/bar	Liter per meter squared per hour per bar
LPM	Liter per minute
MF	Microfiltration
MPD	1,3–benzenediamine (m–phenylenediamine)
MWCO	Molecular Weight Cut–Off (Daltons)
NF	Nanofiltration
NF90, NF270, TS40, TS80, NFX, NFW, NFG, NF HL, XN45, NFCK	Names of polymeric nanofiltration membranes used in this study
NOM	Natural Organic Matter
P-MCL	Primary Maximum Contaminant Level (mg/L)

PA	Polyamide
PIP	Piperazine
PP	Poly(piperazineamide)
PTEs	Potentially Toxic Elements
PZC	Point of Zero Charge
Q	Feed Flow Rate (GPM)
$R = R_0$	Observed Rejection (%)
Re	Reynolds Number (–)
R_i	Intrinsic or Real Rejection (%)
RO	Reverse Osmosis
ROSA	Reverse Osmosis System Analysis
S-K	Spiegler–Kedem
S-MCL	Secondary Maximum Contaminant Level (mg/L)
SA	Semi–Aromatic
Sc	Schmidt Number (–)
SEDE	Steric Electric Dielectric Exclusion
SEM	Scanning Electron Microscope
Sh	Sherwood Number (–)
T	Temperature (°C)
TCLP	Toxicity Characteristic Leaching Procedure
TDS	Total Dissolved Solids (mg/L)
TFC	Thin Film Composite
TMC	Trimesoyl Chloride

TMS	Teorell–Meyer–Sievers
TOC	Total Organic Carbon (μg/L)
UF	Ultrafiltration
WHO	World Health Organization
ε	Spacer Porosity (%)
η	Solution Viscosity (Pa.s)
u	Feed Crossflow Velocity (m/s)
ρ	Solution Density (g/cm^3)
σ	Solute Reflection Coefficient (–)
ω	Solute Permeability (LMH)

PUBLICATIONS AND PRESENTATIONS

The following publications and presentations resulted from this work:

Accepted Publications

S.S. Wadekar, R.D. Vidic, Influence of Active Layer on Separation Potentials of Nanofiltration Membranes for Inorganic Ions, Environmental Science & Technology, 51 (2017) 5658-5665. [1]

S.S. Wadekar, T. Hayes, O.R. Lokare, D. Mittal, R.D. Vidic, Laboratory and Pilot-Scale Nanofiltration Treatment of Abandoned Mine Drainage for the Recovery of Products Suitable for Industrial Reuse, Industrial & Engineering Chemistry Research, 56 (2017) 7355-7364. [2]

S.S. Wadekar, R.D. Vidic, Comparison of ceramic and polymeric nanofiltration membranes for treatment of abandoned coal mine drainage, Desalination, 440 (2018) 135-145. [3]

Publications Under Review/In preparation

S.S. Wadekar, R.D. Vidic, Insights into the rejection of barium and strontium by nanofiltration membrane from experimental and modeling analysis, (2018), *under review with Journal of Membrane Science*. [4]

S.S. Wadekar, Y. Wang, O.R. Lokare, R.D. Vidic, Influence of chemical cleaning on the physicochemical characteristics and ion rejection by thin film composite nanofiltration membranes, (2018), *under review with Journal of Membrane Science.* [5]

Referred Conference Proceedings

S.S. Wadekar, R.D. Vidic, Optimization of abandoned mine drainage treatment by commercially available nanofiltration membranes, in: Proceedings of the 2017 American Water Works Association (AWWA)-American Membrane Technology Association (AMTA) Membrane Technology Conference and Exposition, Long Beach, California, 2017. [6]

S.S. Wadekar, R.D. Vidic, Effect of repetitive chemical cleaning on the performance of polymeric nanofiltration membranes, in: Proceedings of the 2018 American Water Works Association (AWWA)-American Membrane Technology Association (AMTA) Membrane Technology Conference and Exposition, West Palm Beach, Florida, 2018. [7]

Presentations

S.S. Wadekar, R.D. Vidic, Use of nanofiltration membranes for acid mine drainage treatment, 251st American Chemical Society (ACS) National Meeting & Exposition, Mar 13-17, 2016, San Diego, CA, USA. (oral)

S.S. Wadekar, R.D. Vidic, Role of active layer in the performance of aromatic and semi-aromatic nanofiltration membranes for water purification, Engineering Conferences International (ECI), Advanced Membrane Technology VII, Sept 13-17, 2016, Cork, Ireland. (podium poster)

S.S. Wadekar, R.D. Vidic, Optimization of abandoned mine drainage treatment by commercially available nanofiltration membranes, American Water Works Association (AWWA) – American Membrane Technology Association (AMTA), Membrane Technology Conference, Feb 13-17, 2017, Long Beach, CA, USA. (oral)

S.S. Wadekar, R.D. Vidic, Effect of repetitive chemical cleaning on the performance of polymeric nanofiltration membranes, American Water Works Association (AWWA) – American Membrane Technology Association (AMTA), Membrane Technology Conference, Mar 12-16, 2018, West Palm Beach, FL, USA. (oral)

1.0 INTRODUCTION

1.1 BACKGROUND AND MOTIVATION

Alarming increase in population growth, global warming and contamination of natural freshwater sources pose a significant threat to clean water supply in many parts of the world. A dramatic increase in water scarcity has been predicted in the coming decade in many regions including China, Southeast and Southwest Asia, India, Middle East, North Africa, South Africa and the western United States [8]. Water scarcity is the focus of the work presented in this thesis. As of 2015, it was estimated that 660 million people lack access to adequate drinking water source [9] and an unbelievable 3.5 billion people are expected to live in water stressed areas by 2050 [10]. Majority of people in rural communities rely on water sources such as rivers, lakes, groundwater and rainwater that are often contaminated with bacteria and chemicals, which may be dangerous for human consumption [11]. In addition to remote rural communities, water concerns are also wide–spread in industrial areas, where water demand is higher and where shrinking groundwater resources are becoming increasingly brackish as withdrawals continue to increase. The increasing withdrawal of water can be clearly seen from Figure 1.1. Thus, research efforts towards desalination of brackish groundwater and seawater are thriving [12]; however, increase in performance and decrease in energy demand for desalination by novel technologies, such as building more efficient membranes, are at the forefront [13]. Also, securing water in new

ways has added importance to the recovery of water from different sources including wastewater, abandoned mine drainage, etc. because water recovery from sources that are less saline is more energetically favorable (less osmotic pressure) as compared to desalination of seawater or brackish groundwater.

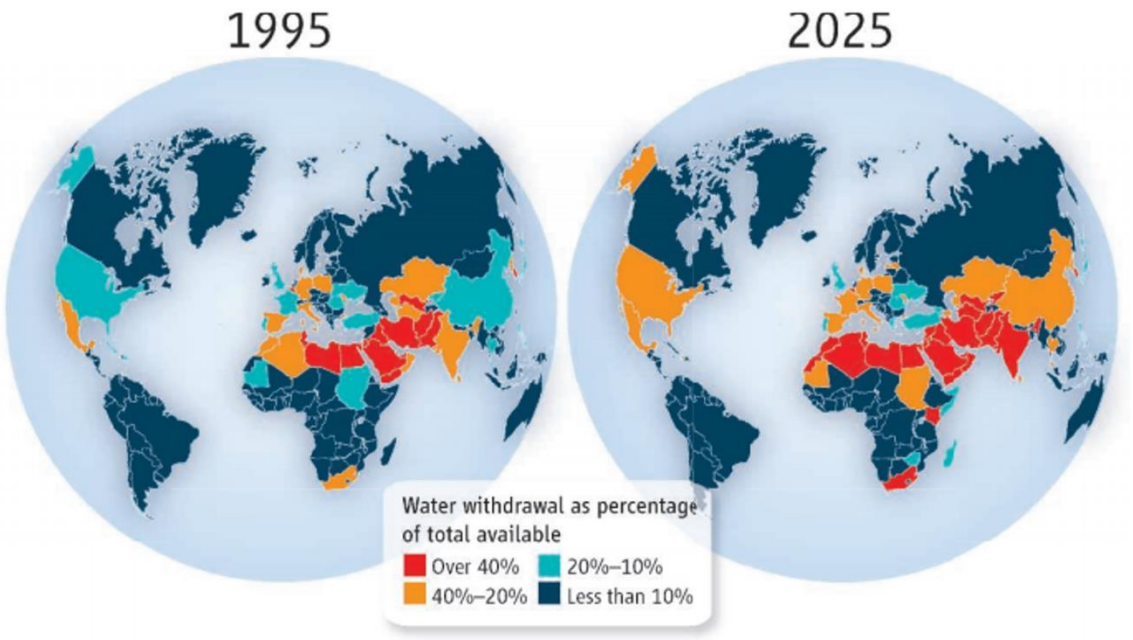

Figure 1.1. Water withdrawal in 1995 and 2025 (projected) **[10]**

1.2 ABANDONED MINE DRAINAGE

Management of water from the mining industry is becoming increasingly scrutinized and there is a growing need to treat, discharge and reuse mine water [14]. Treatment of abandoned or acid mine drainage (AMD) or acid rock drainage (ARD) has been a major research focus for over 50 years [15] because these contaminated streams represent a pervasive environmental problem for both working and abandoned mines. Natural oxidation of sulfide minerals like pyrite (FeS_2),

chalcocite (Cu_2S) and mackinawite (FeS) when exposed to water and oxygen contribute most of the contaminants in the AMD [16]. Typically, it is characterized by high acidity (pH 2–4), high sulfate concentrations (1–20 g/l), and high concentrations of potentially toxic elements (PTEs) such as Al, As, Ca, Cd, Cu, Fe, Mg, Mn, Ni, Pb and Se [17]. Generation of AMD can be explained by the following set of equations [16, 17]:

$$FeS_2 + 7/2\ O_2 + H_2O \rightarrow Fe^{+2} + 2\ SO_4^{2-} + 2H^+ \quad (1\text{-}1)$$

$$Fe^{2+} + 1/4\ O_2 + H^+ \rightarrow Fe^{3+} + 1/2\ H_2O \quad (1\text{-}2)$$

$$FeS_2 + 14\ Fe^{3+} + 8\ H_2O \rightarrow 15\ Fe^{2+} + 2\ SO_4^{2-} + 16\ H^+ \quad (1\text{-}3)$$

$$Fe^{3+} + 3\ H_2O \rightarrow Fe(OH)_3\ (s) + 3\ H^+ \quad (1\text{-}4)$$

$$FeS_2 + 15/4\ O_2 + 7/2\ H_2O \rightarrow Fe(OH)_3\ (s) + 2\ SO_4^{2-} + 4\ H^+ \quad (1\text{-}5)$$

Equation (1-1) describes the direct oxidation of pyrite in an oxic environment and equation (1-2) shows the oxidation of ferrous ions to ferric ions, which occurs depending on the availability of a sufficiently acidic and oxidizing environment that is supported by microorganisms. Ferric ions can oxidize to pyrite (Equation (1-3)) or form insoluble ferric hydroxide (Equation (1-4)). Both of these reactions produce acidity that can assist in leaching metals from other ambient rocks. Equation (1-5) summarizes equations (1-1), (1-2) and (1-4), thereby showing the acidity generation, pyrite oxidation, and precipitation of $Fe(OH)_3$ [18]. Outflow from an abandoned coal mine in southwestern Pennsylvania is shown in Figure 1.2.

Figure 1.2. Outflow from an abandoned coal mine in southwestern Pennsylvania [19]

Traditionally, lime or limestone neutralization has been used to mitigate the effects of AMD. Lime or limestone is added to increase the pH and to precipitate the sulfate as gypsum and other metals as hydroxides which is followed by gravity separation of the solid product [20-22]. This process generates large quantities of sludge contaminated with PTEs. Another important disadvantage of this process is that the sulfate concentration can only be reduced to about 1,440 mg/l (considering gypsum solubility) [17] while Environmental Protection Agency (EPA) and World Health Organization (WHO) stipulate a sulfate limit of 250 mg/l as one of the criteria for unrestricted discharge [23].

1.3 MEMBRANE TECHNOLOGY

Conventional water treatment technologies including a combination of coagulation, flocculation, clarification, filtration and disinfection are effective for some chemical contaminants but less for

others [24]. Advanced water treatment technologies include methods such as advanced oxidation, ultraviolet disinfection, membrane processes and achieve better performance along with being economically and energetically favorable. The focus of this work is on membrane processes, which collectively refers to different types of membrane technologies, namely reverse osmosis (RO), nanofiltration (NF), ultrafiltration (UF) and microfiltration (MF). These are essentially selective barriers that separate different solutes in water to varying degrees and differ depending on the size of solute or particle that passes through the membrane (i.e., pore size of the membrane) and the operating pressure. Figure 1.3 shows different membrane types and their general attributes. Since the primary interest in this work was to remove dissolved inorganic salts, the following discussion is focused on RO and NF. RO membranes almost completely remove mono– and multivalent ions while NF membranes have a slightly more open structure than RO and can reject most of the multivalent ions and some monovalent ions. NF membranes achieve higher flux but lower rejection compared to RO membranes. RO membranes were originally developed for seawater desalination in the 1960s and were made of cellulose acetate [25], however, they required high operating pressures and had high energy consumption (> 10 $kWh.m^{-3}$) [26]. Numerous improvements lead to the development of NF membranes in the late 1980s to achieve higher water permeability and reduced energy consumption [27, 28]. The focus in this work will be on nanofiltration membranes for the rejection of dissolved inorganic salts.

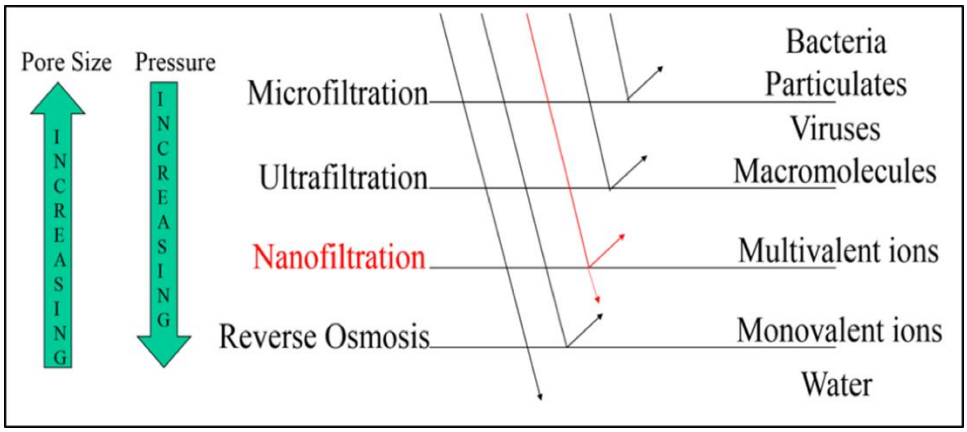

Figure 1.3. Schematic of membrane types

1.4 NANOFILTRATION MEMBRANES

NF membranes can be manufactured as thin film composites (TFC) or could also be made of various ceramics. TFC polymeric membranes include the ultrathin active layer (~20 – 200 nm) responsible for the rejection, permeability, hydrophilicity, and roughness of the composite membrane, followed typically by polysulfone support matrix (~20 – 50 μm) and a non–woven polyester fiber backing (~300 μm) for mechanical stability and strength [29]. Figure 1.4 shows a typical polymeric TFC NF membrane. The active layer can be made of different polymers including but not limited to polyamide, poly(piperazineamide), combination of polyamide and poly(piperazineamide), polyether sulfone, cellulose acetate, etc. [30]. Interfacial polymerization (IP) is the most commonly used technique for synthesizing these TFC membranes. The amine monomers in water are brought into contact with acid chloride monomers in solvent to form a thin film of polyamide on the substrate [31-34]. Two of the most commercially successful recipes to make the polyamide films are: 1) 1,3-benzenediamine (m-phenylenediamine) (MPD) with trimesoyl chloride (TMC) and piperazine (PIP) with TMC [29]. Molecular weight cut–off

(MWCO) (defined as molecular weight of a neutral organic molecule corresponding to 90% rejection by a particular membrane) is usually used to describe the tightness of a particular NF membrane. With polymeric membranes, MWCO's between 200 – 1000 can easily be established by varying the active layer chemistry, reaction times during IP, reaction temperature, etc. [35]. Ceramic membranes have recently been gaining prominence due to better resistance to fouling, easier cleaning, lower maintenance, better thermal resistance and greater mechanical strength [36, 37]. Ceramic NF membranes are commonly made using the sol–gel technique with Al_2O_3, ZrO_2 or TiO_2 as the active layer, with the latter two preferred due to greater stability [38]. They are typically available with molecular weight cut–off (MWCO) close to ~1000 Da and have been applied to remove organic molecules and natural organic matter (NOM) [39, 40]. Newer manufacturing techniques like atmospheric pressure atomic layer deposition (APALD) [41] and DNA template technology [42] are being studied to manufacture ceramic NF membranes with MWCO below 500 Da that could effectively reject multivalent ions. One ceramic membrane manufactured using DNA template technology and several polymeric TFC membranes were selected for this study because they were commercially available.

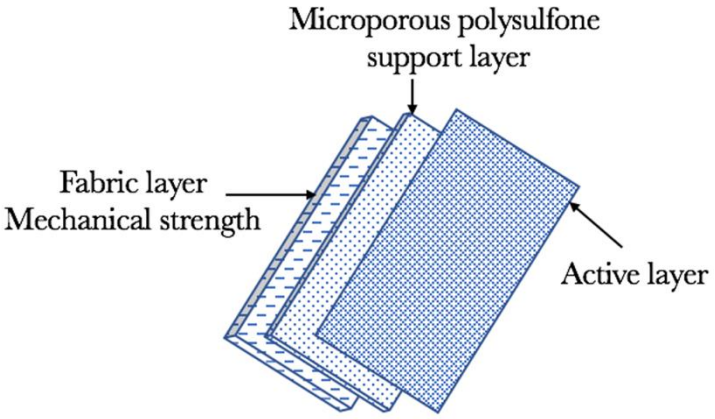

Figure 1.4. A typical thin film composite nanofiltration membrane

NF membranes utilize a number of different mechanisms to create separation between water and dissolved solutes. Specific separation mechanisms include steric (size) exclusion, charge (Donnan) exclusion, dielectric exclusion [43, 44] and are dependent on the type of membrane, feed composition, pH, temperature, etc. [45]. In addition to these separation mechanisms, precipitation, dehydration, and sorptive interactions may also be important in specific cases [46-48]. Size or steric exclusion is an important separation mechanism that is based on the physical hydrated size of a solute. However, the separation is a bit more complex compared to simple sieving because neither the size of the solutes nor the pores are uniform [49]. Charge exclusion may be a dominant rejection mechanism in cases where the solute size is smaller than the effective pore size of the membrane [50]. NF membranes are usually negatively charged because of the dissociation of the carboxylic acid groups at the active layer surface at pH above the iso–electric point (IEP) of the membrane [51]. The negatively charged membrane surface interacts with ions in the feed solution to increase repulsion of the anions in the feed. The equilibrium established as a result of these interactions is called the Donnan equilibrium and is characterized using the Donnan potential [52]. The Donnan potential is impacted by surface charge and chemsistry of the membrane surface and pH and specific ion concentration and ionic strength of the feed. Dielectric exclusion occurs due to: (1) Born effects that occur by changes to the equilibrium and dynamic properties of the solvent in the confined geometry of the nanopores, and (2) image forces due to the difference in dielectric constants between the membrane matrix and the solution [53]. The transport of ions as a result of these different separation potentials can be described by diffusion, convection and electromigration [54]. Hindered diffusion occurs in membrane processes as solute moves from a more concentrated side (i.e., feed) to the less concentrated side (i.e., permeate). Convective transport is directly related to the permeate flux

and thus to the applied operating pressure and concentration while electromigration is directly related to the charge interactions involving both Donnan and dielectric exclusion mechanisms. The importance of the exclusion mechanisms with respect to the active layer chemistries will be the focus of this study.

A membrane's capability to deliver stable performance depends not only on the characteristics of its active layer but also how easily can it be cleaned and restored to achieve its original performance. All membrane processes are affected by membrane scaling or fouling at high water recoveries. Membrane scaling or fouling is caused by the deposition of organic and colloidal matter as well as precipitation of inorganic salts on the membrane surface, which increases mass transfer resistance and affects membrane performance. It is dependent on the type and composition of the feed solution, process flow conditions, antiscalants use, etc. [55] Thus, periodic chemical cleaning to recover the permeate flux and solute rejection is an inevitable step in NF/RO membrane applications and is considered a major drawback of NF/RO filtration processes [56]. Typically, chemical cleaning is initiated when there is a 10% drop in the normalized permeate flow or a 15% increase in the normalized pressure drop (feed pressure minus concentrate pressure) or when the normalized salt passage increases by 5 – 10% [57, 58]. Several studies have addressed the impacts of different cleaning chemicals on various types of foulants [59-61] with acidic and basic cleaning strategies being most commonly applied. Interestingly, a particular cleaning chemical can have different effects on the performance of different NF membranes. Understanding the effects of cleaning chemicals on the ion rejection characteristics of different active layers of NF membranes will also be the focus of this study.

1.5 THESIS ORGANIZATION

Overall, there is a great need for improved water treatment solutions to meet the ever–increasing water demand. NF membranes present an excellent treatment option because of their ability to remove ionic impurities while achieving higher permeability at lower operating pressures (hence, energetically favorable) compared to RO membranes. However, there are still several improvements to be made with NF membranes including finding newer materials for active layers, integration of renewable energy, better mechanistic understanding of separation by different active layer types, influence of chemical cleaning agents, etc. Hence, this makes NF an exciting research area with the potential for tackling current real challenges presented by the water crisis.

The overall aim of this study was to provide better understanding of the NF process with a view of applying the technical knowledge to find solutions for the water shortage problem. Accordingly, this study was divided in two segments:

(A) Understanding the separation mechanism of different active layers in nanofiltration membranes. This section can be divided into 3 main parts:

- Unravelling the underlying separation potentials for the rejection of dissolved inorganic ions for two commonly used active layer NF membranes – polyamide and poly(piperazineamide) with a view of realizing new potential applications for the recovery of water from different sources. This was achieved by (i) Characterizing effective membrane pore radii (ii) Measuring zeta potential under different feed conditions and (iii) Conducting crossflow rejection experiments at low and high ionic strength to determine the relative importance of steric and charge (Donnan) exclusion for the two types of active layers. (CHAPTER 2.0)

- Elucidating the effects of chemical cleaning on the physicochemical characteristics and performance of two commonly used active layers of NF membranes – polyamide and poly(piperazineamide). This was studied by (i) Characterizing effective membrane pore radii (ii) Measuring zeta potential, (iii) Characterizing the chemical changes and elemental compositions of NF membranes with chemical cleaning and (iv) Conducting crossflow rejection experiments with single divalent ions and mixture of salts to illustrate the relative importance of exclusion mechanisms for the two types of active layers. (CHAPTER 3.0)

- Understanding the rejection of barium and strontium ions using a polyamide NF membrane with a view of testing the results obtained in the first two studies. This was achieved by (i) Measuring zeta potential, (ii) Studying the rejection characteristics of barium and strontium as a function of pH and (iii) Influence of crossflow velocity, feed pressure and concentration of ions on rejection was also studied and an equation was developed using the Spiegler–Kedem model to predict the rejection behavior of barium and strontium over a hundred–fold feed concentration range. (CHAPTER 4.0)

(B) Application of nanofiltration membranes for treatment of abandoned mine drainage (AMD). This section can be divided into 2 main parts:

- Testing the ability of polymeric NF membranes to treat AMD at pilot–scale for complete reuse. This was done by (i) Selection of an optimized (high rejection and high permeability) commercially available NF membrane based on laboratory–scale screening, (ii) Testing the optimized NF membrane at laboratory–scale using real AMD, (iii) Pilot–scale testing of the

optimized membrane and (iv) Fouling analysis of NF membranes used in pilot–scale testing. (CHAPTER 5.0)

- Comparing the performance of polymeric and ceramic NF membranes for treatment of AMD. This was achieved by (i) Testing the effect of permeate recovery on ion rejection with polymeric and ceramic NF membranes, (ii) Elucidating the effects of chemical cleaning with the two membranes, (iii) Studying the effect of fouling mitigation strategies (iv) Studying the fouling characteristics with and without the use of antiscalant and (v) Testing a tight polymeric NF membrane to produce permeate that meets drinking water standards. (CHAPTER 6.0)

Chapter 7.0 discusses all the key findings and provides insights into several NF related aspects that were studied in this work as future recommendations.

2.0 INFLUENCE OF ACTIVE LAYER ON SEPARATION POTENTIALS OF NANOFILTRATION MEMBRANES FOR INORGANIC IONS

This work has been published as:

S.S. Wadekar, R.D. Vidic, Influence of Active Layer on Separation Potentials of Nanofiltration Membranes for Inorganic Ions, Environmental Science & Technology, 51 (2017) 5658–5665.

Active layers of two fully aromatic and two semi–aromatic nanofiltration membranes were studied along with surface charge at different electrolyte composition and effective pore size to elucidate their influence on separation mechanisms for inorganic ions by steric, charge and dielectric exclusion. The membrane potential method used for pore size measurement is underlined as the most appropriate measurement technique for this application owing to its dependence on the diffusional potentials of inorganic ions. Crossflow rejection experiments with dilute feed composition indicate that both fully aromatic membranes achieved similar rejection despite the differences in surface charge, which suggests that rejection by these membranes is exclusively dependent on size exclusion and the contribution of charge exclusion is weak. Rejection experiments with higher ionic strength and different composition of the feed solution confirmed this hypothesis. On the other hand, increase in the ionic strength of feed solution when the charge exclusion effects are negligible due to charge screening strongly influenced ion

rejection by semi–aromatic membranes. The experimental results confirmed that charge exclusion contributes significantly to the performance of semi–aromatic membranes in addition to size exclusion. The contribution of dielectric exclusion to overall ion rejection would be more significant for fully aromatic membranes.

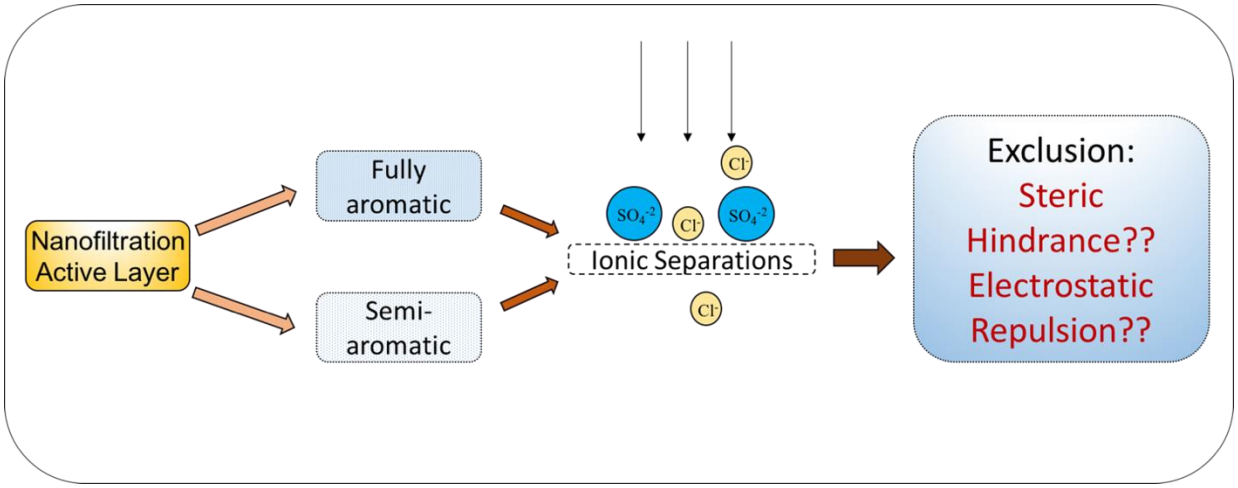

Figure 2.1. Abstract art illustrating the influence of active layer on separation potentials of nanofiltration membranes for inorganic ions

2.1 INTRODUCTION

Application of membrane technologies for water purification gained greater attention in recent years due to population boom and worldwide industrialization [62]. Major technological advancement and cost reduction lead to increased use of reverse osmosis (RO) and nanofiltration (NF) membranes in desalination, wastewater treatment and reclamation [13, 29]. Modern NF membranes are predominantly thin film composite (TFC) membranes consisting of three layers: the topmost layer is the selective active layer followed by the microporous polysulfone support

layer and a non–woven fabric layer for mechanical strength [29]. Of these, the topmost dense layer with thickness of about a few hundred nanometers is the most important layer responsible for permeability, ionic selectivity, fouling resistance, roughness and hydrophilicity of the composite membrane [63]. Ion rejection by this active layer is due to three different separation potentials: Steric hindrance (pore size effects), Donnan exclusion (by fixed surface charge) and dielectric exclusion (by Born effect and image forces) [64, 65]. Modeling efforts have attempted to explain these effects and predict the rejection behavior of NF membranes [66-68]. The separation by NF membranes was initially modeled using the Donnan steric partitioning pore model (DSPM) [66] but the steric, electric and dielectric model (SEDE) [67, 68] was developed later due to the inability of DSPM to predict the rejection of divalent cations. SEDE model is a four parameter (i.e., membrane's effective pore size, thickness to porosity ratio, volume charge density and the dielectric constant of solution inside the membrane pores) model and is able to predict the rejection performance of NF membranes reasonably well.

Interfacial polymerization (IP) is the most commonly used technique for synthesizing these TFC membranes. The amine monomers in water are brought into contact with acid chloride monomers in solvent to form a thin film of polyamide on the substrate [31-34]. Two of the most commercially successful recipes to make the polyamide films are: 1) 1,3–benzenediamine (m–phenylenediamine) (MPD) with trimesoyl chloride (TMC) and piperazine (PIP) with TMC [29]. In the first reaction scheme, both monomers (i.e., MPD and TMC) are aromatic and hence the membrane can be designated as fully aromatic (FA) while the membranes prepared using the second scheme can be designated as semi–aromatic (SA) because PIP is an aliphatic monomer. These membranes are often coated with different groups to alter membrane properties [69]. For example, it has been found that a neutral hydrophilic coating can affect surface charge, surface

roughness, permeability and salt rejection of TFC membranes [70]. Thus, understanding the role of active layers in achieving ion rejection by a particular separation mechanism is of utmost importance to understand the potential use of these membranes for specific application.

Tang et al. [63, 70] characterized seventeen commercially available RO and NF membranes and have shown how the active layer chemistries and coatings affect hydrophilicity, surface roughness and permeability of these membranes. Verissimo et al. [31] evaluated the effect of combining different aliphatic monomers (i.e., PIP, 1,4–bis(3–aminopropyl)–piperazine (DAPP), N,N'–diaminopiperazine (DAP) and N,N'–(2–aminoethyl) –piperazine (EAP)) with TMC on the performance, surface morphology and charge of composite semi–aromatic membranes. They found that water permeability was the highest for DAP–TMC membrane but that PIP–TMC membrane performed better in terms of salt rejection. In a similar study, Li et al. [32] evaluated the effect of other aliphatic monomers on salt rejection and anti–fouling properties of thin–films. Ahmad et al. [33] found that permeate flux and separation capabilities of polyamide NF membranes greatly depend on the diamine ratio and the IP reaction times while effects of polyamide chemistry on amino acid separation have also been compared [34]. Other studies have also evaluated the ionization behavior of functional groups [71-73] and surface heterogeneity [74, 75] of active layer towards understanding the rejection by these membranes. However, the underlying separation mechanisms of NF membranes with different active layers have not yet been fully unraveled because none of the previous studies attempted to fully characterize all three separation potentials as a function of active layer chemistry.

Since semi–aromatic poly(piperazineamide) and fully aromatic (polyamide) membranes are the most commonly used NF membranes, the aim of this study was to investigate the separation potentials of these active layer types in different applications. Separation potentials

(i.e., steric, Donnan (charge) and dielectric exclusion) of these active layers were characterized to elucidate their relative contribution to rejection of inorganic ions in an effort to develop new applications and to improve membrane selection process for the separation of inorganic ions. Sulfate was the key ion selected for this study since it is found in many wastewaters, surface and ground waters at widely different concentrations [76] and since it is one of the contaminants of concern in abandoned mine drainage, which is a pervasive problem in many parts of the US [77, 78]. All membranes used in this study are commercially available and hence the information about their separation potential and performance is relevant to their application in practice.

2.2 EXPERIMENTAL

2.2.1 Membranes and chemicals

Four commercially available flat sheet NF membranes were used in the study. NF90 and NF270 membranes were purchased from DOW Filmtech (Edina, MN); TS40 and TS80 were purchased from Sterlitech Corporation (Kent, WA). Key properties of these membranes reported in the literature and those provided by the manufacturers are shown in Table 2.1 and the chemical structures of the polymers forming the two types of active layers are shown in Figure A.4 in Appendix A.1. Deionized (DI) water used for water permeability experiments (resistivity = 18 kohm.cm^{-1}) was obtained using MilliQ water system (Millipore, Billerica, MA). All chemicals used were analytical grade and were purchased from Fisher Scientific (Pittsburgh, PA).

Table 2.1. Membranes used in this study

Membranes	Fully Aromatic (FA)		Semi–Aromatic (SA)	
	NF90	TS80	NF270	TS40
Polymer	Polyamide	Polyamide	Polypiperazine–amide	Polypiperazine–amide
MWCO	~200[a]	~150[c]	~200–300[b]	~200[c]

[a][76], [b][79], [c]Provided by manufacturer

2.2.2 Apparatus and filtration process

All experiments were carried out in the laboratory–scale SEPA–CFII test cell (GE Osmonics, Minnetonka, MN) shown in Figure A.3 (Appendix A.1) with usable membrane area of 140 cm^2 and has been described in detail elsewhere [6]. Pump power (Hydra–cell diaphragm pump, Wanner Engineering, MN), feed control valve and concentrate control valve were used to adjust the desired feed pressure (20 bar) and flow rate (1 GPM), which were held constant throughout the study. All experiments were performed in total recirculation mode at a constant feed pH of 5.6 ± 0.1. Temperature was maintained at 22 ± 1°C using an immersed cooling coil connected to a chiller (6500 series, Polyscience, Niles, IL). Prior to the experiment, each membrane was immersed in DI water for at least 24 hours to ensure complete wetting. Each membrane was first compacted with DI water at 50 bar and then used to filter DI water until a stable flux (LMH/bar) was reached (typical stabilization times ranged between 20–24 hours). Once, a stable flux had been established, the feed was adjusted to the required composition and the system was allowed to equilibrate for two hours. The permeate flux was measured over the next two hours during which samples were collected every 15 min for chemical analysis.

Sulfate, magnesium and calcium were introduced as $Na_2SO_4 \cdot 10H_2O$, $CaCl_2 \cdot 2H_2O$ and $MgCl_2 \cdot 6H_2O$ salts. The filtration experiments were carried out at dilute (low) and high

electrolyte concentrations to evaluate the relative importance of the Donnan (charge) exclusion effects. Experiments with dilute feed were performed at sulfate concentration of 96 mg/L with calcium and magnesium concentrations up to 40 mg/L and 24 mg/L (i.e., 1 mM each), respectively. For experiments at high ionic strength, sulfate concentration was adjusted to 650 mg/L and magnesium and calcium ions were introduced at 1,000 mg/L each. This feed composition was chosen for two reasons: it assured that the surface charge is screened at high concentrations and it also represents abandoned mine drainage [17], which is a pervasive environmental concern in many areas of the US [78]. All cations and anions were analyzed using inductively coupled plasma–optical emission spectroscopy (ICP–OES) system (5100 ICP–OES, Agilent Technologies, Santa Clara, CA) and ion chromatography (IC) system (Dionex ICS–1100 with IonPac AS22 carbonate eluent anion–exchange column, Dionex, Sunnywale, CA), respectively.

2.2.3 Attenuated total reflection – Fourier transform infrared spectroscopy (ATR–FTIR)

FTIR was used to determine the chemical composition of the active layer for all four nanofiltration membranes selected for this study. Infrared spectra were obtained using Nicolet 6700 (Thermo Scientific, Pittsburgh, PA) FTIR spectrometer with the active layer of the membrane pressed tightly against the crystal. At least two replicates were obtained for each membrane type and each spectrum was averaged from 256 scans collected from 1800 cm^{-1} to 800 cm^{-1}.

2.2.4 Membrane pore size measurements

Membrane potential technique [80] was used to measure the effective pore sizes of the NF membranes. The membrane sample (exposed area of 12.5 cm^2) was held between two acrylic half–cells (700 cm^3 each) filled with NaCl solutions at different concentrations but identical pH, temperature and hydrostatic pressure. The ratio of ion concentrations in the two half cells, $c_i^0 / c_i^{\Delta x}$, was maintained at a constant value of 2, with the active layer always facing towards the half-cell with higher concentration. NaCl concentrations ranged between 3 – 250 mM. Each experiment was repeated at least twice and the electrodes were also interchanged between the two compartments to cancel the asymmetric potential effect [80]. Prior to each experiment, the membrane was immersed in solution of lower concentration for at least 24 hours to ensure saturation of the support layer and to avoid any interference from the concentration gradient in the support layer. All the experiments were carried out at ambient temperature of 22°C with continuous stirring of each cell using magnetic stirrers. The output from Ag/AgCl electrodes (RE–5B, BASi Electronics, West Lafayette, IN) submerged in each cell was amplified (INA826EVM, Gain = 97.76, Texas Instruments, Dallas, TX) and measured by a multi–meter (Fluke 21 Series II, Fluke Corporation, Everett, WA). The membrane pore radius was calculated using the procedure described Table A.1 and the apparatus used for the measurement of the membrane potential is shown in Figure A.1 in Appendix A.1.

2.2.5 Zeta potential measurements

Zeta potential of the membranes was analyzed using Surpass 3 Electro–kinetic Analyzer (EKA) equipped with the Adjustable Gap Cell (AGC) (Anton Paar, Ashland, VA). For each measurement, two 10 mm × 20 mm membrane samples were inserted into the AGC and 1 mM KCl solution was used as electrolyte to obtain the isoelectric point of each membrane. An automatic pH sweep from ~5.6 to 2 was accomplished by the addition of 0.05 M HCl solution and from ~5.6 to 10 using 0.05 M NaOH. Following the isoelectric point determination, the membranes were also tested with the following electrolyte solutions at pH 5.6 ± 0.1: 1 mM Na_2SO_4, 1 mM Na_2SO_4 + 1 mM $CaCl_2$ and 1 mM Na_2SO_4 + 1 mM $MgCl_2$. These experiments were designed to determine the change in zeta potential of these NF membranes with the addition of divalent cations using sulfate as the base anion. Each of these experiments was repeated at least four times with a maximum standard deviation of 4 mV.

2.3 RESULTS AND DISCUSSION

2.3.1 ATR–FTIR

ATR–FTIR spectra of the four NF membranes in the range 1800 – 800 cm^{-1} are shown in Figure 2.2. This range would reflect both the active layer and the polysulfone support layer as the FTIR signal has relatively deep penetration (> 300 nm) [63]. Since the focus of this study is to differentiate between fully and semi–aromatic membranes, only the relevant peaks are discussed here and information about all other peaks is included in Appendix A.1.

As seen from Figure 2.2, the peaks at ∼1664, 1610 and 1545 cm^{-1} are present only for NF90 and TS80 membranes and are absent for NF270 and TS40 membranes. The peak at ∼1664 cm^{-1} can be assigned to C=O stretching (dominant contributor), C–N stretching and C–C–N deformation vibration in a secondary amine group [81, 82]. The peak at ∼1610 cm^{-1} is due to N–H deformation vibration for the aromatic amide [83] while the peak at ∼1545 cm^{-1} is due to amide II band for the N–H in–plane bending and N–C stretching vibration of CO–NH group [63]. These three peaks are clearly seen to be absent from the spectra obtained for the semi–aromatic membranes (NF270 and TS40). On the other hand, the peak at ∼1630 cm^{-1} is observed only in the case of NF270 and TS40 and is absent for NF90 and TS80 membranes. This peak is due to amide I band (poly(piperazineamide)) [84]. Tang el al. [63] have shown that NF90 and NF270 are uncoated NF membranes by comparing the FTIR and XPS spectra of several commercially available NF membranes. Figure 2.2 shows that the spectra for TS80 is identical to NF90 and that of TS40 is identical to NF270. Based on these results, it can be concluded that TS80 and NF90 are uncoated fully aromatic polyamide membranes and TS40 and NF270 are uncoated semi–aromatic poly(piperazineamide) membranes. Therefore, this study included two membranes that are truly representative of each category of membrane chemistry (i.e., full aromatic (MPD–TMC) and semi–aromatic (PIP–TMC)) without any coating or any modifications of the polyamide and poly(piperazineamide) active layers.

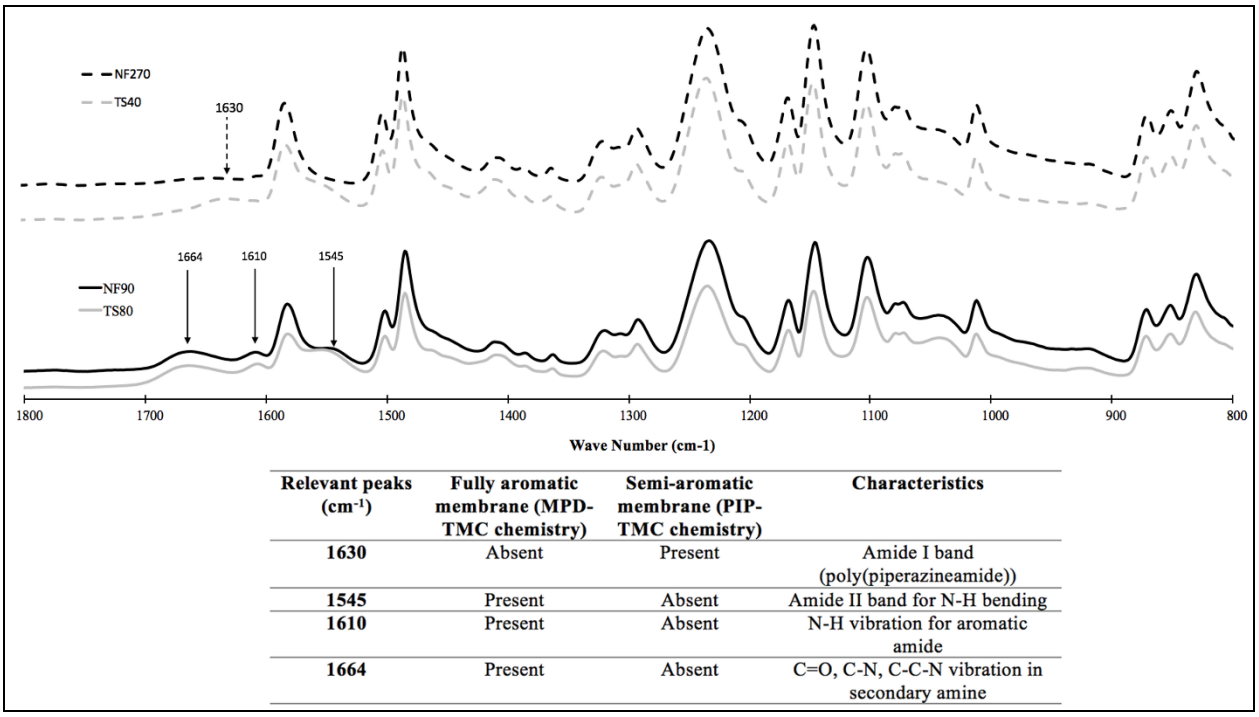

Relevant peaks (cm^{-1})	Fully aromatic membrane (MPD-TMC chemistry)	Semi-aromatic membrane (PIP-TMC chemistry)	Characteristics
1630	Absent	Present	Amide I band (poly(piperazineamide))
1545	Present	Absent	Amide II band for N-H bending
1610	Present	Absent	N-H vibration for aromatic amide
1664	Present	Absent	C=O, C-N, C-C-N vibration in secondary amine

Figure 2.2. ATR–FTIR spectra of NF270, TS40, TS80 and NF90 nanofiltration membranes

2.3.2 Effective pore size measurements

Variation of membrane potential ($\Delta\psi_m$) with chloride concentration is shown in Figure 2.3. Each point on this figure represents a mean of at least four measurements at each concentration of the single salt (NaCl). As can be seen from Figure 2.3, the membrane potential first increases with an increase in chloride concentration and then plateaus, which corresponds to the diffusion potential (i.e., limiting value at high concentration) where both the image forces and the Donnan (charge) effects are screened [80]. A maximum standard deviation of ± 0.6 mV was observed for membrane potential values when chloride concentration in solution was below 0.1 M and it was only ± 0.1 mV at the plateau of membrane potential. The asymmetry potential was below ± 0.1 mV.

The effective mean pore sizes of the four NF membranes were evaluated using plateau levels of the membrane potential (i.e., diffusion potential) where the diffusion potentials of 6.14 mV, 6.0 mV, 5.66 mV and 5.45 mV were measured for NF90, TS80, TS40 and NF270 membranes, respectively. Using the procedure described in Appendix A.1, the effective mean pore radii of 0.68 $\pm$ 0.02 nm, 0.71 $\pm$ 0.02 nm, 0.80 $\pm$ 0.03 nm and 0.87 $\pm$ 0.02 nm were calculated for NF90, TS80, TS40 and NF270 membranes, respectively. Thus, the calculated effective pore sizes of these four membranes differed only slightly (i.e., 0.19 nm difference between NF90 and NF270). Also, it was noted that the two semi–aromatic membranes (TS40 and NF270) had larger effective pore sizes as compared to the two fully aromatic membranes (NF90 and TS80). Lo et al. [85] used Density Functional Theory (DFT) analysis to suggest that the reaction between MPD and TMC (i.e., FA membranes) is much facile as compared to the reaction between PIP and TMC (i.e., SA membranes), which explains the greater crosslinking and smaller effective pore size for fully aromatic membranes.

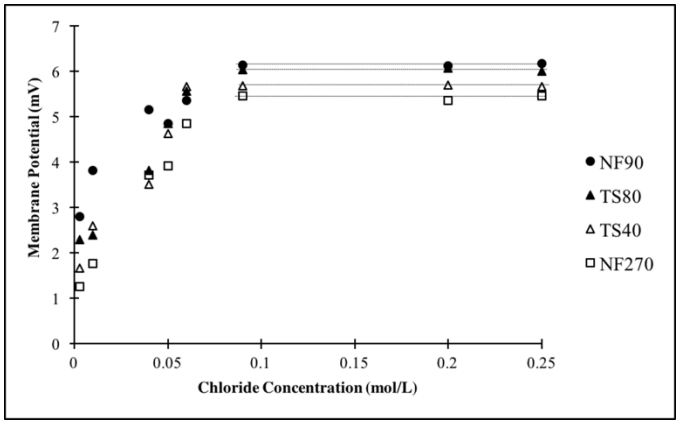

Figure 2.3. Membrane potential as a function of chloride concentration in solution

The mean pore size of NF membranes can been measured using three different techniques: 1) atomic force microscopy (AFM) [86, 87], 2) retention of neutral organic solutes of different molecular weights [66, 88] and 3) membrane potential analysis (used in this study) [68, 80]. Selection of a particular method should be based on specific application because NF membranes behave differently in different feed solutions. This study is focused on the rejection of inorganic ions and hence membrane potential technique is more suitable for pore size measurements because it is based on the diffusional potential of ionic species through the membrane pores. Hilal et al. [87] used AFM technique and reported the membrane pore radii of NF90 and NF270 membranes to be 0.257 nm and 0.341 nm, respectively. Nghiem et al. [88] reported the pore radii of NF90 and NF270 membranes as 0.34 nm and 0.42 nm, respectively, by modelling the retention data of organic solutes of different molecular weights. Mean pore sizes determined in this study differ for both membranes but they agree that pore size of NF90 is smaller than the pore size of NF270 membrane. Similarly, by modelling the retention data of neutral organic solute, mean pore radius of TS80 membrane (≈ 0.52 nm) has been reported to be smaller than that of TS40 membrane (≈0.65 nm) [89].

AFM provides a semi–visual determination of the pore size since only the membrane surface is evaluated and no transport of species takes place through the membrane. It is known that the pores in the NF membranes are non–homogeneous and hence surface evaluation of pores cannot accurately determine the mean effective membrane pore radius. In case of modeling the retention data of neutral organic solutes of different molecular weights, actual retention experiments have to be carried out in order to measure the rejections, which involves introducing a convective factor in these experiments. Hence, in addition to the dependence of the effective membrane pore radius on the steric partitioning coefficient, it is now also dependent on the

convective hindrance factor. In the case of membrane potential technique, the effective pore radius is dependent on only the diffusive hindrance factor or the steric partitioning coefficient since there are no convective forces at play. This difference in the convective and diffusive hindrance factors contributes to the observed differences in the measured effective membrane pore radii between the membrane potential technique and neutral organic molecule retention technique.

Apart from the membrane pore size measurements, the results in Figure 2.3 can also be used to determine the approximate solute concentration where the Donnan (charge) separation potential becomes negligible. As can be seen from this figure, the Donnan (charge) separation potential has already canceled out at chloride concentration of 0.09 M for all four membranes as evidenced by the leveling of the membrane potential. This observation indicated that hindered diffusion and convection are the only relevant transport mechanisms in NF systems where the ionic strength of the feed is above about 0.1 M.

2.3.3 Zeta potential measurements

Figure 2.4 (a) shows zeta potential of the four nanofiltration membranes in the pH range between 2 – 10 using 1 mM KCl as the electrolyte. It can be seen from this figure that the isoelectric points (IEPs) for NF90, TS80, NF270 and TS40 membranes are 4.60, 2.54, 2.43 and 2.40, respectively. An IEP in the neighborhood of pH 4 typically indicates that the surface is either neutral or inert [51]. Hence, the zeta potential for NF90 suggests that it has similar concentrations of dissociable acidic carboxylic groups and basic amine groups. The remaining three membranes have low IEP, which indicates dominance of dissociable acidic carboxylic groups over dissociable basic amine groups. Artug et al. [79] and Tu et al. [90] have reported the

IEP's of NF90 and NF270 at 4.2 and 2.8 and 4 and 2.8, respectively. Since the reaction between MPD and TMC (i.e., FA membranes) is much facile as compared to the reaction between PIP and TMC (i.e., SA membranes) [85], there will be more unreacted acyl chloride in the active layer in the case of PIP–TMC (i.e., SA type) and the charged carboxylic entities will impart more negative surface potential to these membranes. TS80 membrane has IEP very close to that of the SA type membranes even though it has been confirmed to be a FA type membrane (Figure 2.2). The excess carboxylic groups on TS80 membrane suggests that this membrane may have been immersed in the TMC solution for a longer time during the interfacial polymerization process as compared to NF90.

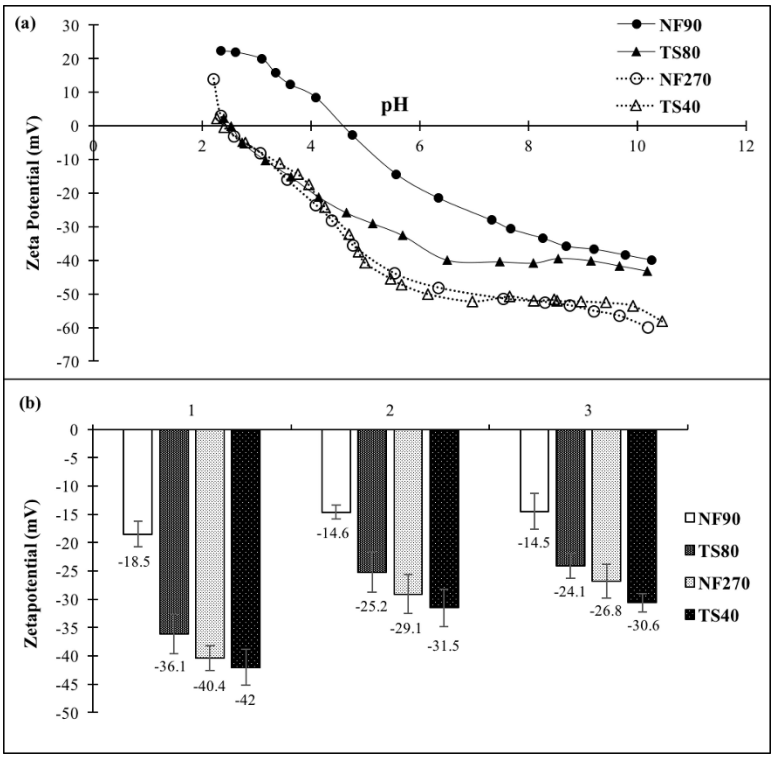

Figure 2.4. (a) Isoelectric Point (IEP) determination (with 1 mM KCl) (b) Zeta potentials with different solution composition (1) 1 mM Na_2SO_4; (2) 1 mM Na_2SO_4 + 1 mM $MgCl_2$; (3) 1 mM Na_2SO_4 + 1 mM $CaCl_2$, pH = 5.6 ± 0.1) for NF90, TS80, NF270 and TS40 membrane

Zeta potentials of the selected membranes were also measured using three different electrolytes at pH = 5.6 ± 0.1 as shown in Figure 2.4 (b). The results in this figure suggest that both SA type membranes (i.e., NF270 and TS40) have a more negative zeta potential than both FA type membranes (i.e., NF90 and TS80), which suggests that the contribution of Donnan (charge) exclusion towards the separation by SA type membranes would be greater than for FA type membranes. Figure 2.4 (b) also shows an increase in zeta potential with the addition of divalent cations to the electrolyte solution for all four membranes. Childress et al. [91, 92] proposed that the complex formation or electrostatic interactions between the divalent cations and the negatively charged membrane surface lead to adsorption of cations on membrane surface and an increase in zeta potential, which was also supported by other studies [93, 94]. It can also be observed from Figure 2.4 (b) that the relative increase in zeta potential is about the same for TS80, TS40 and NF270 membranes but is less pronounced for NF90 membrane, which is due to the fact that NF90 is less electronegative than the other three membranes (Figure 2.4 (a)). Also, the similar zeta potential values measured with the addition of Ca^{2+} and Mg^{2+} can be explained by the fact that both Ca^{2+} and Mg^{2+} have similar diffusivity and Stokes radii (Table A.2, Appendix A.1) and hence have a similar impact on the membrane surface. The main conclusion from the zeta potential study is that the semi–aromatic membranes are more electronegative and have more fixed charges on the membrane surface compared to the fully aromatic membranes.

2.3.4 Membrane performance

Membrane permeability was measured with DI water where the permeate flux was monitored for two hours and is shown in Figure 2.5. Figure 2.5 (a) shows linear dependence of measured permeate flux on operating feed pressure and hence provides evidence that the

effective pore sizes of the four membranes reflect their pure water permeability values. Also, the selected operating feed pressure of 20 bar for all crossflow rejection experiments in this study, was in between the linear 'pure water flux – operating feed pressure' range. In addition, pure water permeability values correlate well with the membrane pore radii measured using membrane potential method (Figure 2.5 (b)). An increase in the permeate flux of 143% (4.7 LMH/bar for NF90 to 11.4 LMH/bar for NF270) was measured with an increase in the effective pore radii of 28% (0.68 nm for NF90 to 0.87 nm for NF270). Similar values have previously been reported by Hilal et al. [95] and Santafe–Moros et al. [96] for NF90 and NF270 membranes. The membrane potential technique is new and not usually used in literature where the method employing MWCO's to determine the membrane pore radius has been used frequently. Hence, it is very difficult to compare the pure water permeability and membrane pore radii values of other commercial NF membranes available in literature. It would be interesting to investigate the scope of linearity of the curve shown in Figure 2.5 (b) as a function of the effective pore radii, however, such an investigation was beyond the scope of this thesis.

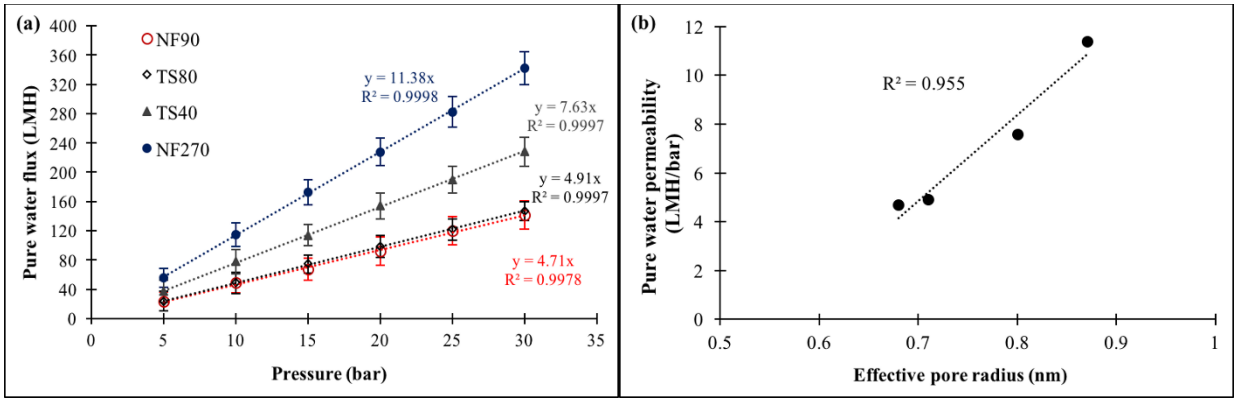

Figure 2.5. (a) Pure water flux as function of operating feed pressure and (b) Pure water permeability as a function of effective membrane pore radii

Figure 2.6 shows rejections of various ions for both dilute (Figure 2.6 (a), (b)) and concentrated (Figure 2.6 (c), (d)) feed strengths. These experiments were conducted to determine the dominant separation mechanism knowing that the surface charge is screened at high ionic strength and that the contribution of Donnan effect to separation potential would be negligible.

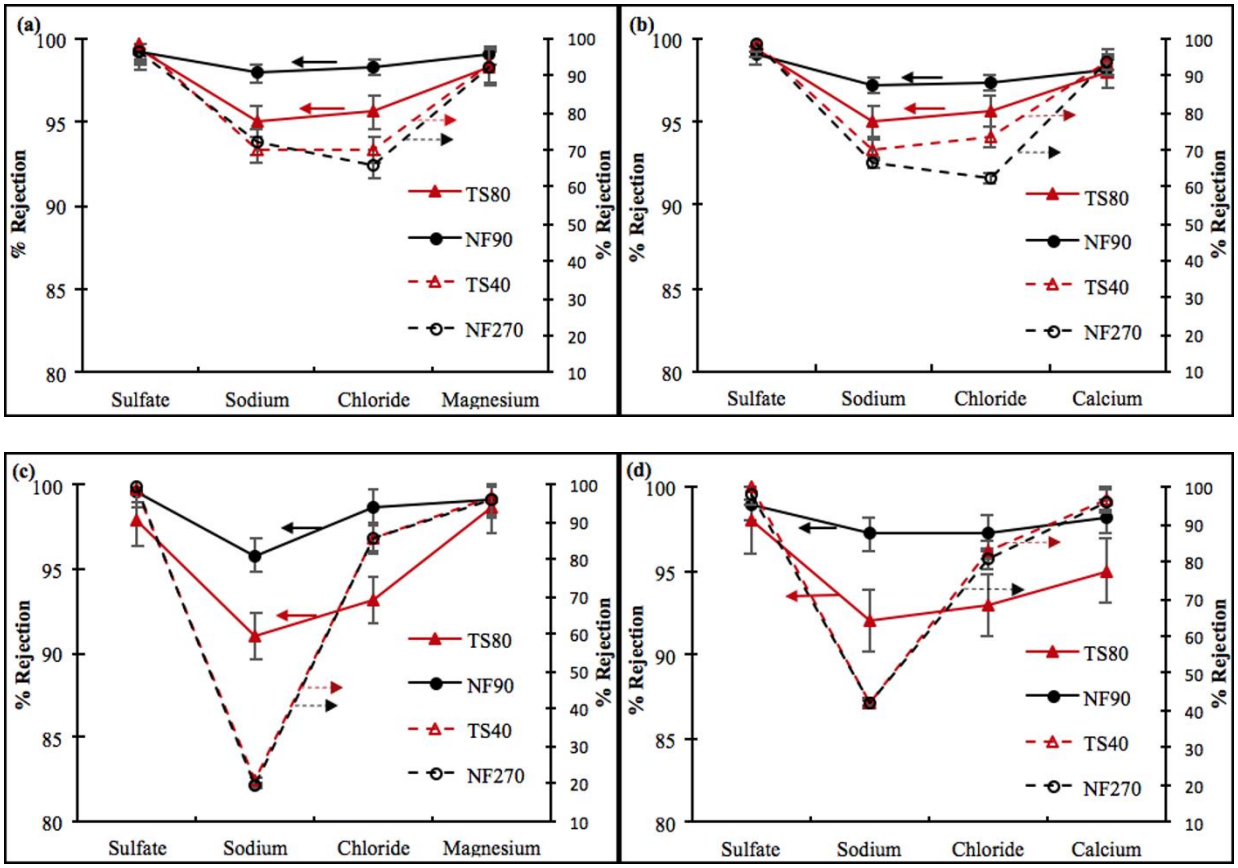

Figure 2.6. Rejection of ionic species with feed solutions: (a) 96 mg/l sulfate + 24 mg/l magnesium and (b) 96 mg/l sulfate + 40 mg/l calcium, (c) 650 mg/L sulfate + 1000 mg/L magnesium and (d) 650 mg/L sulfate + 1000 mg/L calcium

Figure 2.6 shows that sulfate rejection was always greater than 98% and that the FA type membranes performed better than SA type membranes in all cases. High sulfate rejection can be explained by negative surface charge of all four membranes for all solution

compositions investigated in this study (Figure 2.4). The rejection order of the ionic species observed in these experiments is: $R(SO_4^{2-}) > R(Cl^-)$ (for anions) and $R(Mg^{2+}) > R(Ca^{2+}) > R(Na^+)$ (for cations); rejection of magnesium being marginally more or equal to the rejection of calcium. According to the Donnan exclusion theory for single salt solutions and negatively charged membrane surfaces, the sequence of rejection of cations should be in the order $R(Na^+) > R(Mg^{2+}) \approx R(Ca^{2+})$ [97]. With single salt solutions, the effect of single valence cations on the electronegativity of the negatively charged membrane surface will be less drastic as compared to that of multi–valence cations [98] and hence, the rejection of Na^+ is expected to be greater than Mg^{2+} and Ca^{2+}. The rejection order of $R(Mg^{2+}) > R(Ca^{2+}) > R(Na^+)$ observed in Figure 2.6 with multiple ions in the feed can be explained by ionic diffusivity and Stokes radii of magnesium, calcium and sodium ions. With multiple ions in the feed, the rejected sulfate will be largely electro–neutralized by divalent cations that will also experience greater steric rejection potential than the monovalent cations owing to their larger Stokes radii (Table A.2, Appendix A.1). Hence, rejection of Mg^{2+} and Ca^{2+} will be greater than Na^+. When comparing the rejection of Mg^{2+} and Ca^{2+}, the ionic diffusivity and Stokes radii play a major role. Because Mg^{2+} has lower ionic diffusivity and larger stokes radius than Ca^{2+} (Table A.2, Appendix A.1), it will be rejected more than Ca^{2+}. In the case of anions, SO_4^{2-} with a valence of –2 will experience greater electronegative repulsion from the negatively charged membrane surface as opposed to Cl^-. In addition, SO_4^{2-} has larger Stokes radius and lower ionic diffusivity than Cl^- (Table A.2, Appendix A.1), which will also contribute towards greater rejection of SO_4^{2-} than Cl^-.

In the case of dilute feed composition (Figure 2.6 (a) and (b)), both Donnan (charge) and steric effects would contribute to ion rejection [98]. FA type membranes achieved > 98% rejection of calcium and magnesium ions while the SA type membranes achieved 92 – 94%

rejection of these cations. Also, FA membranes achieved > 95% rejection of sodium and chloride ions in each case while the rejection of these ions by SA membranes ranged between 62 – 73%. The fact that SA membranes achieved lower ion rejection despite having more electronegative surfaces than FA membranes (Figure 2.4) clearly suggests that the steric rejection potential can be more dominant in determining the overall rejection by a particular membrane. Lower rejection by SA type membranes is explained by their larger effective pore size compared to FA type membranes. Comparison between two membranes of the same category (i.e. FA membrane type) shows that both FA membranes achieved similar rejection of all ions although TS80 membrane is more electronegative than NF90 membrane (Figure 2.4). Such behavior suggests that the contribution of charge effects (Donnan potential) towards rejection by FA type membranes is weak. Slightly better rejection of sodium and chloride ions by NF90 membrane is due to smaller pores compared to TS80 membrane.

For high feed ionic strength (i.e., addition of 1,000 mg/L of calcium or magnesium to the feed), the rejection of divalent ions (i.e., sulfate, magnesium and calcium) changed only slightly (3% or less) for both FA and SA type membranes (Figure 2.6 (c) and (d)). However, the rejection of sodium and chloride ions was affected by the elevated ion concentrations in the feed (Figure 2.6 (c), (d)) as compared to those achieved with dilute feed (Figure 2.6 (a), (b)). The decrease in the rejection of sodium with an increase in feed concentration was significant for SA membranes where it decreased by at least 30% compared to the dilute feed conditions while it changed by 5% or less for FA membranes. This decrease in rejection for semi–aromatic membranes occurs when the Donnan separation potential has been screened out and is no longer assisting the separation, which suggests that Donnan potential contributed significantly to separation at dilute feed conditions for SA membranes. Additional ion rejection experiments were also carried out at

low and high ionic feed strengths with different feed composition. The results from these experiments also support the conclusion of dominant dependence of fully aromatic membranes on steric exclusion potential and that of semi–aromatic membranes on both steric and Donnan exclusion potential and are discussed in the Appendix A.1 (Figure A.2). It is also important to note that the addition of cations to the feed is accompanied by the increase in chloride concentration because all cations were added as their chloride salts. The quantum of chloride ions diffusing to the permeate side is dependent on the sodium ions diffusing through the membrane to maintain electroneutrality because the divalent cations are effectively rejected by all membranes. Hence, there is a relative increase in chloride rejection with an increase in the ionic strength of the feed.

Crossflow rejection experiments with dilute feed indicated that fully aromatic membranes achieved similar rejection despite the differences in surface charge and suggest that the rejection by FA membranes is predominantly dependent on the pore size effects (i.e., size exclusion) and that the contribution of Donnan (charge) effects is rather weak. Also, rejection experiments with high ionic strength feed confirmed the weak contribution of Donnan (charge) exclusion effects on the rejection of inorganic ions by these membranes. On the other hand, increase in the ionic strength of the feed solution when the Donnan exclusion effects are negligible due to charge screening strongly influenced ion rejection by semi–aromatic membranes, which confirmed that the Donnan (charge) exclusion contributes significantly to the performance of SA membranes in addition to steric hindrance. These results suggest that the fully aromatic nanofiltration membranes would be preferred over semi–aromatic nanofiltration membranes in applications that require complete removal of inorganic ions (e.g., desalination) while the later would be better suited for applications requiring fractional rejections of ionic species (e.g., dairy industry).

2.3.5 Other mechanisms

Another important mechanism for the separation by nanofiltration membranes is by dielectric exclusion, which is explained in terms of: (1) Born effects that occur by changes to the equilibrium and dynamic properties of the solvent in the confined geometry of the nanopores, and (2) image forces due to the difference in dielectric constants between the membrane matrix and the solution [53]. Comparison of dielectric exclusion potential for the two membrane types (i.e., fully aromatic and semi–aromatic) is difficult because dielectric exclusion occurs by several concomitant factors and only a qualitative discussion is possible. When considering only the effect of image forces, the contribution of dielectric exclusion to rejection is expected to decrease with an increase in the ionic strength of the feed because each ion will interact not only with its own polarization charge (i.e., image force) but also with the polarization charges induced by neighboring ions, which screens the image forces. Both membrane materials have similar dielectric constants of ~ 3 [47, 99] and the contribution of image force to the overall dielectric exclusion can be expected to be similar for both membrane types. In addition to screening of interactions by polarization charges induced by neighboring ions, polarization charges are also induced by fixed membrane charges. This screening will be stronger in the case of semi–aromatic nanofiltration membranes than that for fully aromatic nanofiltration membranes because they have greater fixed surface charge (Figure 2.4). Considering the Born effects, the structural changes of water in a confined medium affect the free energy of ion transfer from external solution into nanopores of the NF membranes [100]. Yaroshchuk [53] showed that the rejection by dielectric effects is more prominent for smaller pores. Because fully aromatic membranes have narrower pores than semi–aromatic membranes, the contribution of Born

effects to rejection by dielectric exclusion would be higher for FA membranes than SA membranes. The screening by fixed membrane charges is expected to be greater in the case of semi–aromatic membranes and it is reasonable to expect that the contribution to the overall rejection by dielectric exclusion would be more prominent in the case of fully aromatic nanofiltration membranes.

2.4 CONCLUSIONS

This study contributes significantly to understanding the separation mechanisms of two types of commonly used nanofiltration membranes with a view of realizing new potential applications. We first analyze the active layer chemistries of four commercially available nanofiltration membranes with two different active layer chemistries: fully aromatic or polyamide (1,3–benzenediamine (m–phenylenediamine) (MPD) with trimesoyl chloride (TMC) and semi–aromatic or poly(piperazineamide) (piperazine (PIP) with TMC) to prove that these membranes are representative of the respective categories with no coatings or modification of the active layer. Effective membrane pore size and zeta potential characterization of the four membranes suggests that semi–aromatic membranes have relatively larger pore sizes and that they are more electronegative for all feed compositions tested. Crossflow rejection experiments at low and high feed ionic strength suggest that Donnan (charge) exclusion is significant for semi–aromatic membranes and that these membranes should be preferred in applications requiring partial ion removal (e.g., dairy industry) or charged based separations (e.g., charged organic separations), while fully aromatic membranes should be considered in desalination applications. Qualitative analysis suggests that the contribution of dielectric exclusion to overall rejection by fully

aromatic membranes would be more significant than semi–aromatic membranes. This study offers additional insights into how the separation potentials of polyamide and poly(piperazineamide) active layer chemistries vary even with a very small difference in the effective membrane pore size.

3.0 INFLUENCE OF CHEMICAL CLEANING ON PHYSICOCHEMICAL CHARACTERISTICS AND ION REJECTION BY NANOFILTRATION MEMBRANES

This work is under review as:

S.S. Wadekar, Y. Wang, O. R. Lokare, R.D. Vidic, Influence of chemical cleaning on physicochemical characteristics and ion rejection by thin film composite nanofiltration membranes, (2018), *under review with Journal of Membrane Science*.

The impact of chemical cleaning on the rejection of inorganic ions by different nanofiltration membranes was determined to be dependent on the physicochemical characteristics and separation potentials of their active layers. The active layers underwent no chemical changes after cleaning with HCl or NaOH. Cleaning with NaOH decreased the negative zeta potential values for membranes with greater concentration of carboxylic acid groups on the membrane surface rendering the zeta potential to be always negative. Effective membrane pore radii increased post cleaning, especially for poly(piperazineamide) membranes. Exposure to NaOH was found to cause an increasing swelling of the membrane active layer after each cleaning, which was clearly evident for poly(piperazineamide) membranes. Rejection of sulfate decreased only slightly even for poly(piperazineamide) membranes despite their appreciable increase in pore radii. Such behavior can be explained by the impact of charge exclusion on ion rejection that was enhanced by the reduction in zeta potential after NaOH cleaning. A 23%

increase in the effective pore radii for the poly(piperazineamide) membranes after NaOH cleaning for 18 h lead to 25, 36, 53 and 62% decrease in the rejection of magnesium, calcium, sodium and chloride ions, respectively. However, only a 7% decrease in the rejection of sulfate ions was observed. This behavior can be explained by the 16% decrease in zeta potential. The increase in permeability after chemical cleaning is in agreement with a decrease in the rejection of inorganic ions. The effective pore radii measured using the membrane potential technique correlated well with DI water permeability for all membranes before and after cleaning. The importance of charge exclusion in rejection of inorganic ions was highlighted by the observed differences in rejection and permeability values when testing membranes after chemical cleaning with NaOH for 9 and 18 h.

3.1 INTRODUCTION

The use of nanofiltration (NF) and reverse osmosis (RO) membranes for desalination purposes, wastewater treatment and recovery has been continuously escalating owing to the cost reduction and technological advancements [13, 62]. Typical modern NF membranes are thin film composite (TFC) membranes made of three layers: topmost is the ultrathin active layer (~20 – 200 nm) responsible for the rejection, permeability, hydrophilicity, and roughness of the composite membrane, followed by a polysulfone support matrix (~20 – 50 μm) and a non–woven polyester fiber backing (~300 μm) for mechanical stability and strength [29]. A membrane's capability to deliver stable performance not only depends on the characteristics of its active layer but also how easily can it be cleaned to restore its original performance. All membrane processes are affected by membrane scaling or fouling at high water recoveries.

Membrane scaling or fouling that is usually caused by the deposition of organic and colloidal matter as well as precipitation of inorganic salts on the membrane surface increases mass transfer resistance and greatly affects membrane performance. It is dependent on the type and composition of the feed solution, process flow conditions, antiscalants use, etc. [55] Thus, periodic chemical cleaning to recover the permeate flux and solute rejection is an inevitable step in NF/RO membrane applications and is considered a major drawback of NF/RO filtration processes [56]. Typically, chemical cleaning is initiated when there is a 10% drop in the normalized permeate flow or a 15% increase in the normalized pressure drop (feed pressure minus concentrate pressure) or when the normalized salt passage increases by 5 – 10% [57, 58].

Several studies have addressed the impacts of different cleaning chemicals on various types of foulants [59-61] with acidic and basic cleaning solutions being most common. However, effects of cleaning chemicals on the membrane performance have only been more recently addressed. A need for extensive research on cleaning of NF membranes [55, 56, 101] addressed studies on the effects of chemical cleaning on NF membrane performance [102-111]. Interestingly, a particular cleaning chemical can have different effects on the performance of different NF membranes. For instance, Fujioka et al. [109] reported a permeability increase of 54% for NF270 membrane with caustic cleaning at pH 12 while Tu et al. [110] reported a permeability increase of 5% with caustic cleaning with ESPA2 membrane. In several cases, even contradictory results have been reported. Liikanen at el. [59] reported a 15 – 20% decrease in conductivity rejection as a result of caustic cleaning with NF255 membrane and on the contrary, Al–Amoudi et al. [107] reported an increase in NaCl rejection with the DK and DL membranes with after cleaning. In general, the impact of chemical cleaning on the rejection of inorganic salts remains rather inconclusive in the literature.

NF membranes have been shown to achieve rejection of ionic species by three important mechanisms: size (steric), charge (Donnan) and dielectric exclusion [65, 112]. These mechanisms vary with different NF active layers and feed composition. We have shown that semi–aromatic poly(piperazineamide) (PP) (i.e., piperazine – trimesoyl chloride type chemistry) NF membranes rely on both charge and size exclusion to achieve rejection of ionic species as opposed to fully aromatic polyamide (PA) (i.e., 1,3–benzenediamine – trimesoyl chloride type chemistry) NF membranes where size exclusion is the dominant separation mechanism [1]. In addition, Freger et al. [86] have also found that PA membranes were more rigid and presumably more regularly packed than PP membranes. Most of the studies to understand the impacts of chemical cleaning on the performance of NF/RO membrane have used organic molecules [102-105] and only few studies have used magnesium sulfate [107, 111] as solute. No study has used a mixture of salts to explain the effects of chemical cleaning, which may explain the dearth of knowledge related to the effect of chemical cleaning on the rejection of inorganic salts. In order to understand the role of charge (Donnan) exclusion in addition to the normally studied size exclusion phenomenon it is important to study the rejection characteristics with divalent salts or a mixture of salts.

The aim of this study was to investigate the impact of acidic and caustic chemical cleaning on separation characteristics of two types of commonly used nanofiltration active layer membrane types – polyamide (PA) and poly(piperazineamide) (PP). Chemical cleaning was simulated by exposing pristine membrane samples to analytical grade HCl (pH 2) and NaOH (pH 12) solutions for different cleaning times. Chemical changes to the active layer chemistry post cleaning were monitored using ATR–FTIR and XPS, surface charge characteristics were studied by measuring zeta potentials and any conformal changes were monitored by measuring the

effective membrane pore radii using the membrane potential method. Performance changes were quantified by ion rejection and permeability measurements carried out using a variety of feed solutions to understand size and charge exclusion mechanisms for the two types of active layers post chemical cleaning.

3.2 EXPERIMENTAL

3.2.1 Membranes and chemicals

Four commercially available flat sheet NF membranes, two each of fully aromatic polyamide (PA) and semi–aromatic poly(piperazineamide) (PP) active layer chemistry were selected for the study. All membranes were thin film composites with a polysulfone support layer followed by a fabric for mechanical support. These membranes have been tested elsewhere and it has been confirmed that they are truly representative of each category of membrane chemistry (i.e., fully aromatic PA and semi–aromatic PP) without any coating or any modifications of the PA and PP active layers [1, 113]. NF90 and NF270 membranes were purchased from DOW Filmtech (Edina, MN); TS40 and TS80 were purchased from Sterlitech Corporation (Kent, WA) and key properties of these membranes are shown in Table 3.1. MilliQ deionized (DI) water (resistivity = 18 kohm.cm^{-1}, Millipore, Billerica, MA) was used to prepare all test solutions. Analytical grade $Na_2SO_4.10H_2O$, $CaCl_2.2H_2O$, $MgCl_2.6H_2O$, HCl and NaOH were purchased from Fisher Scientific (Pittsburgh, PA).

Table 3.1. Characteristics of membranes used in this study

Membranes	Fully Aromatic (PA)		Semi – Aromatic (PP)	
	NF90	TS80	NF270	TS40
Active layer	Polyamide	Polyamide	Poly(piperazine–amide)	Poly(piperazine–amide)
MWCO	~200[a]	~150[b]	~200 – 300[c]	~200[b]
Effective mean pore radii (nm)[d]	0.68 ± 0.02	0.71 ± 0.02	0.87 ± 0.02	0.8 ± 0.03

[a][79], [b][76], [c]Provided by manufacturer, [d][1]

3.2.2 Filtration and chemical cleaning process

All rejection experiments were carried out in the laboratory–scale SEPA–CFII test cell (GE Osmonics, Minnetonka, MN) with a usable membrane area of 140 cm^2 [6, 114]. New membrane was immersed in DI water for 24 hours to allow for complete wetting. Considering a typical membrane life of 4 – 5 years with chemical cleaning applied once every 3 – 4 months [115, 116], a membrane encounters a total of 15 – 18 h of contact with the chemical cleaning solution. Hence, 9 and 18 h were selected to simulate repetitive membrane cleaning cycles over average half and full life of the membrane. Chemical cleaning was performed by soaking the membranes in HCl (at pH 2) or NaOH (at pH 12) in aluminum foil covered Pyrex glass bottles with PTFE (polytetrafluoroethylene) caps and the contents were mixed on a shaker for 9 or 18 h at 23°C. Post cleaning, each membrane was gently rinsed with flowing DI water and tested in the SEPA–CFII crossflow unit after compaction at 50 bar for 1 h to avoid any compression effects during testing. The feed pressure was adjusted to 20 bar and the system was operated until stable permeate flux was established. The feed solution was adjusted to a desired composition and the system was monitored for 2 – 3 h until stable permeability and feed/permeate conductivities were verified. Samples were then collected to determine ion rejections. Rejection experiments were

conducted with both pristine and chemically cleaned NF membranes with 1 mM sulfate in the feed. Sulfate was selected as target ion instead of commonly used sodium chloride because NF membranes are primarily used to reject divalent ions. Crossflow rejection tests were also performed with 1 mM sodium sulfate + 1 mM calcium chloride + 1 mM magnesium chloride as feed in order to elucidate the relative importance between steric and charge exclusion mechanisms. All experiments were conducted in total recirculation mode (i.e., circulating the permeate, concentrate and reject back to the feed tank to maintain constant feed concentration) at a constant feed pH = 5.6 ± 0.1, temperature = 23 ± 1°C, feed flow rate = 1 GPM (corresponding crossflow velocity = 0.77 m/s) and feed pressure = 20 bar. All rejection experiments were performed in duplicate within 2 hours after chemical cleaning.

3.2.3 Membrane characterization

3.2.3.1 Attenuated total reflection – Fourier transform infrared spectroscopy (ATR–FTIR)

Infrared spectra were obtained using VERTEX–70LS FTIR spectrometer (Bruker, Billerica, MA) with the active layer of the membrane pressed tightly against the ZnSe crystal to determine the chemical composition of the active layer before and after chemical cleaning. At least two replicates were obtained for each membrane type and each spectrum was averaged from 256 scans collected from 1800 cm^{-1} to 800 cm^{-1}.

3.2.3.2 X–ray photoelectron spectroscopy (XPS)

X–ray photoelectron spectroscopy (XPS) analysis was performed to quantify elemental composition before and after chemical cleaning using ESCALAB 250Xi instrument (Thermo

Scientific, Pittsburgh, PA) with a monochromatic Al Kα X–ray source (1486.7 eV, 650 μm spot size). High resolution scans with a step size of 0.1 eV were collected for carbon (C 1s), oxygen (O 1s), nitrogen (N 1s), chloride (Cl 2p) and sodium (Na 1s). A minimum of three replicate analysis was performed for each membrane sample that was vacuum dried for ≈ 12 h.

3.2.3.3 Membrane pore size measurements

Effective membrane pore sizes were measured using the membrane potential technique [80] to quantify the effect of chemical cleaning using the experimental protocol developed previously [1, 80]. Briefly, a membrane sample with an exposed area of 12.5 cm^2 was inserted between two acrylic half cells (700 cm^3 each) filled with NaCl solutions at different concentrations but identical hydrostatic pressure, pH and temperature. NaCl concentrations in the two half cells were adjusted to 3 – 250 mM with the active layer always facing towards the half cell with higher concentration and the potential difference was measured using Ag/AgCl electrodes (RE–5B, BASi Electronics, West Lafayette, IN). Each experiment was repeated at least twice and the electrodes were interchanged between the two compartments to cancel the asymmetric potential effect [80]. Prior to each experiment, the membrane was immersed in solution of lower concentration for at least 24 hours to ensure saturation of the support layer and to avoid any interference from the concentration gradient in the support layer. All experiments were performed at ambient temperature of 23°C with continuous stirring. The membrane pore radius was calculated using the measured membrane potential and diffusion coefficients and Stokes radii for sodium and chloride ions.

3.2.3.4 Zeta potential measurements

Surpass 3 Electro–kinetic analyzer equipped with the Adjustable Gap Cell (AGC) (Anton Paar, Ashland, VA) was used for zeta potential measurements with 1 mM KCl solution as electrolyte. An automatic pH sweep from ~5.6 to 2 was accomplished by the addition of 0.05 M HCl solution and from ~5.6 to 10 using 0.05 M NaOH. These experiments were designed to determine the change in surface charge characteristics post chemical cleaning. Each of these experiments was repeated at least three times with a maximum standard deviation of 3.6 mV.

3.3 RESULTS AND DISCUSSION

3.3.1 Membrane characterization

Several membrane characterization techniques were used to evaluate the effects of chemical cleaning. ATIR–FTIR and XPS were used to determine any changes in the chemical composition of active layers. Changes in the surface charge were analyzed using zeta potential measurements and any conformal changes were evaluated based on the effective membrane pore radii. Also, membrane surface and cross section were imaged using scanning electron microscope (SEM) and are discussed in Appendix A.2.

3.3.1.1 ATR–FTIR analysis

ATR–FTIR spectra of the four NF membranes before and after chemical cleaning are shown in Figure 3.1. To investigate interactions between the cleaning chemicals and active layer, the scan was performed in the range of 800 – 1800 cm^{-1} to capture all peaks corresponding to the

polyamide and poly(piperazineamide) active layers [63]. However, FTIR signal has relatively deep penetration (> 300 nm) and peaks corresponding to the polysulfone support layer were also detected. Since the main focus of this study is to characterize the membranes before and after chemical cleaning tests, only relevant results will be discussed. Full peak characterization [63] and evidence showing that NF90 and TS80 membranes correspond to uncoated PA and that NF270 and TS40 membranes correspond to uncoated PP can be found elsewhere [1, 113]. Important characteristic peaks to differentiate between the two types of active layer chemistries are highlighted in Figure 3.1.

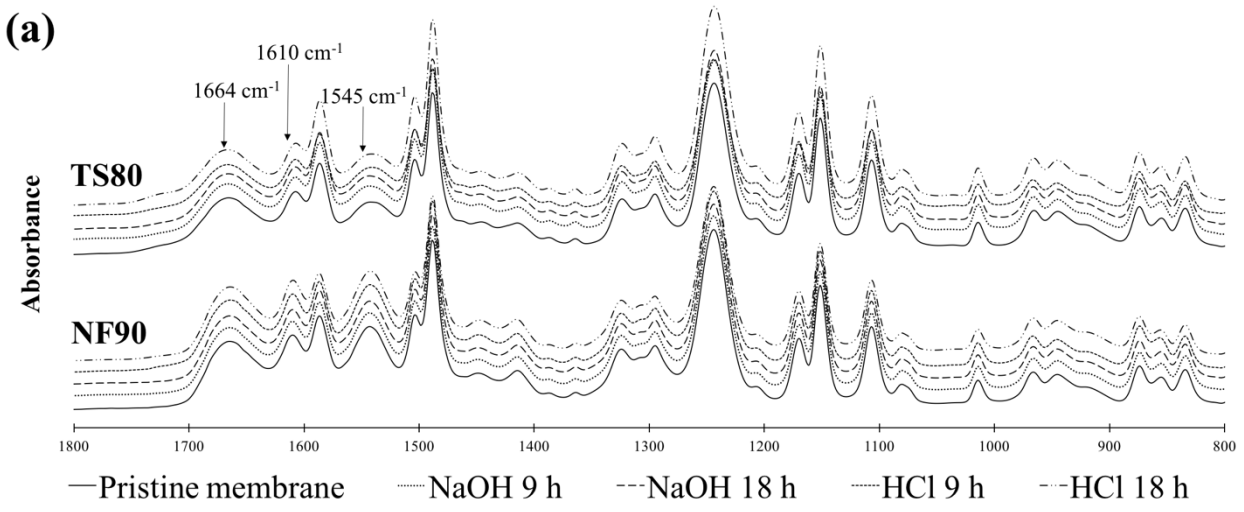

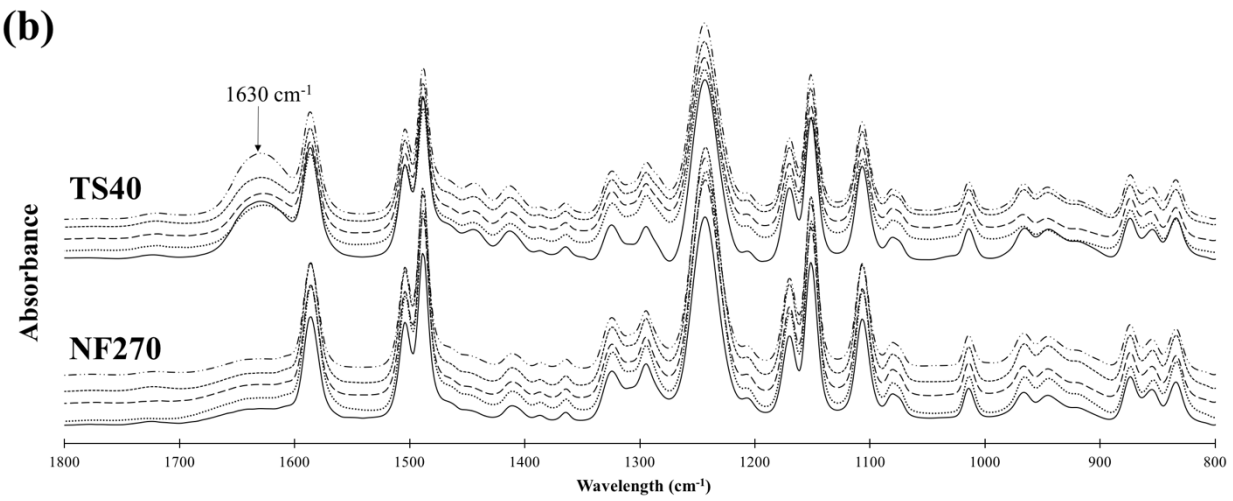

Figure 3.1. ATR–FTIR spectra of (a) fully aromatic polyamide, i.e., TS80 and NF90 and (b) semi–aromatic poly(piperazineamide), i.e., TS40 and NF270 membranes before and after chemical cleaning

As can be seen in Figure 3.1, ATR–FTIR scans had identical characteristic peaks for virgin and chemically cleaned membranes indicating that these membranes are chemically resistant to HCl (pH 2) and NaOH (pH 12) solutions even after 18 h of exposure at 23°C. Recently, Kallioinen et al. [111] reported minor changes in the chemical structure of nanofiltration membranes as observed by IR spectra with commercial membrane cleaning solution. However, these changes were observed at 70°C while these results are in agreement with those observed in other cleaning studies at lower temperatures [105].

ATR–FTIR analysis can also be used to determine the relative active layer thickness of these four NF membranes based on the intensity ratio between the characteristic peaks corresponding to the active layer and that corresponding to the polysulfone support layer [117]. Peaks at 1545 and 1630 cm^{-1} that correspond to the Amide II band for N–H bending in PA membranes and Amide I band in PP membranes respectively [63] were chosen to quantify PA and PP in the active layers, respectively. Peaks at 1488, 1504 and 1587 cm^{-1} correspond to the

aromatic in–plane ring bend stretching vibration assignable to the polysulfone support matrix [118] and the peak at 1587 cm^{-1} was chosen to quantify the active layer thicknesses. Table 3.2 shows relevant intensity ratios (i.e., $I_{1545/1587}$ for PA and $I_{1630/1587}$ for PP) for the four membranes tested in this study. The intensity ratios are ranked in the following order: NF90 > TS80 > TS40 > NF270, which means that the active layer thicknesses of these membranes will also be in the same order. Generally, the active layer thickness of PA membranes were greater than PP membranes, which can be explained by the much facile reaction between MPD and TMC in PA membranes compared to that between PIP and TMC in PP membranes) [85]. For reference, the active layer thickness of NF270 membrane was reported to be around 15 – 40 nm [105].

Table 3.2. Intensity ratios between the bands at 1545 and 1587 cm^{-1} ($I_{1545/1587}$) for pristine fully aromatic polyamide (NF90, TS80) membranes and between the bands at 1630 and 1587 cm^{-1} ($I_{1630/1587}$) for pristine semi–aromatic poly(piperazineamide) membranes (TS40, NF270)

Membranes	Intensity Ratio
NF90	0.884
TS80	0.580
TS40	0.332
NF270	0.170

3.3.1.2 XPS analysis

Because the penetration depth in XPS analysis is < 10 nm [119], this technique provides quantitative analysis of just the active layers of NF membranes and can be used to approximate the degree of crosslinking in their active layer. Figure 3.2 shows elemental composition of active

layers of the four NF membranes before and after chemical cleaning. No discernible changes in the elemental composition were detected for any cleaning procedure, which is consistent with ATR–FTIR findings. Fully crosslinked and fully linear PA membranes can be represented as C_6H_4ON and $C_{15}H_{10}O_4N_2$, respectively while PP membranes can be represented as C_5H_5ON and $C_{13}H_{12}O_4N_2$, respectively [63]. The corresponding carbon content in fully crosslinked and fully linear PA membranes is 75 and 71.4% and 71.4 and 68.4% for PP membranes, respectively (H was excluded from calculation since XPS is not suitable for analyzing hydrogen atoms). The carbon content of the active layers in NF90 and TS80 membranes was 74.3% ± 0.4% and 73.0% ± 0.2%, respectively indicating that NF90 membrane had relatively higher crosslinking than the TS80 membrane. The carbon content in the active layer of TS40 and NF270 membranes was 70.7% ± 0.1% and 69.6% ± 0.3%, respectively indicating that the degree of crosslinking was relatively higher for TS40 membrane than NF270 membrane. Representative XPS survey spectra and high resolution scans for carbon (C 1s), oxygen (O 1s), nitrogen (N 1s), chloride (Cl 2p) and sodium (Na 1s) are included in Appendix A.2 (Figures A.7 and A.8).

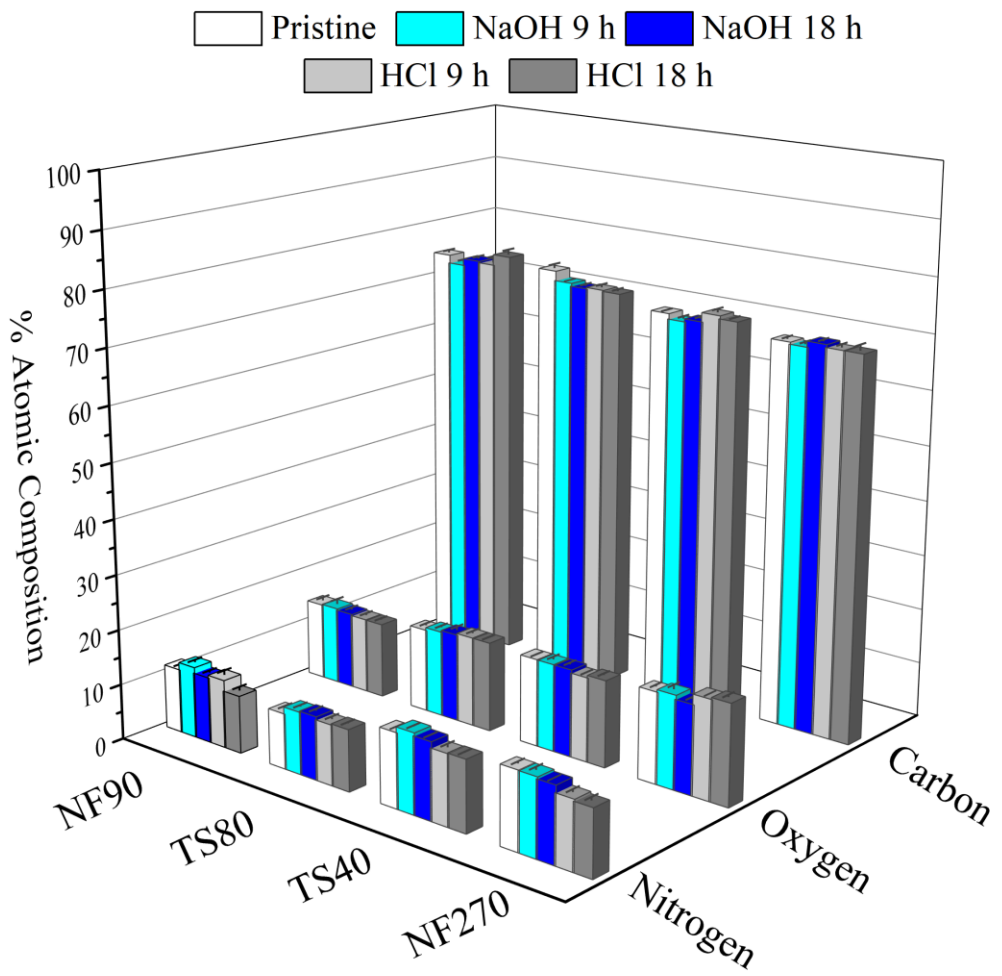

Figure 3.2. Percent atomic compositions of active layers determined using XPS for fully aromatic polyamide i.e., NF90, TS80 and semi–aromatic poly(piperazineamide) i.e., TS40, NF270 membranes before and after chemical cleaning

3.3.1.3 Zeta potential measurements

Figure 3.3 shows zeta potential of the four membranes in the pH range between 2 and 10 using 1 mM KCl as electrolyte. The iso–electric point (IEP) (i.e., pH at which there is an equal surface concentration of dissociated carboxylic acid and amine groups) for the pristine NF90, TS80, TS40 and NF270 membranes was measured as 4.60, 2.54, 2.43, and 2.40, respectively. These values are close to those reported in the literature [79, 90, 113]. An IEP in the

neighborhood of 4 typically indicates that the surface is either inert or neutral and an IEP close to 3 indicates dominance of dissociable acidic carboxylic groups over dissociable basic amine groups [51]. The results of this study suggest that NF90 membrane had similar concentrations of dissociable acidic and basic groups at the membrane surface while the dissociable carboxylic acid groups dominated in the remaining three membranes, i.e., TS80, TS40 and NF270.

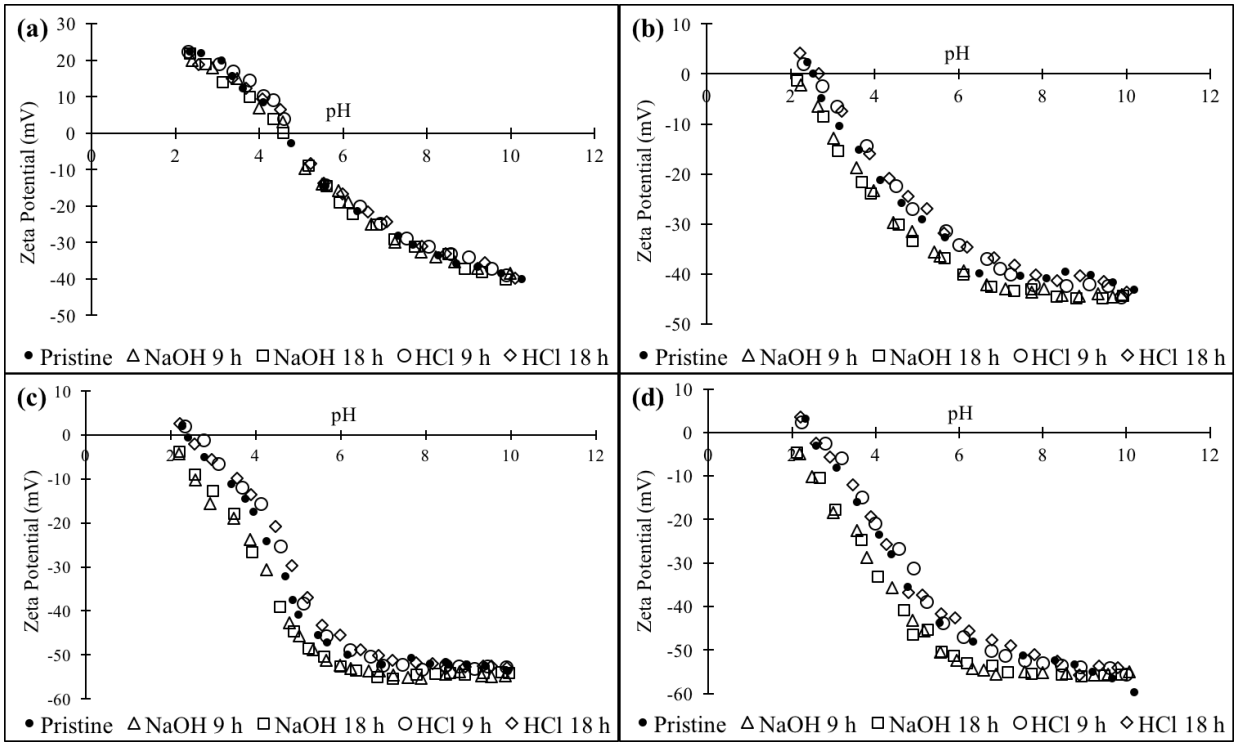

Figure 3.3. Zeta potential with 1 mM KCl as electrolyte for fully aromatic polyamide i.e., (a) NF90, (b) TS80 and semi–aromatic poly(piperazineamide) i.e., (c) TS40, (d) NF270 membranes before and after chemical cleaning

Cleaning with HCl had no significant impact on zeta potential of all four membranes because the observed changes were between 0.5 – 5%. Furthermore, NaOH cleaning of NF90 membrane (Figure 3.3 (a)), which was shown to have equal concentration of dissociable carboxylic and amine groups on the membrane surface, also had negligible impacts (< 3%

change). Discernible changes in the zeta potential of NF90 membrane were reported after cleaning with commercial cleaning solutions [105]. These commercial cleaning solutions included MC11 (a caustic cleaning formulation at pH 11.2 with blended detergent builders, pH buffer and chelating agents including ethylenediaminetetraacetic acid (EDTA), sodium tripolyphosphate (SDP) and trisodium phosphate (TSP)), MC3 (an acidic cleaning formulation at pH 3 consisting of organic acids, detergent builders and chelating agent SDP) and PC98 (a caustic cleaning formulation at pH 11 containing amphoteric surfactants and the chelating agent EDTA), which may explain the difference in the observed effects. On the other hand, zeta potential of TS80, TS40 and NF270 membranes (Figure 3.3 (b), (c) and (d)) became slightly more negative after cleaning with NaOH solution. Figure 3.4 shows zeta potential for the four membranes at pH = 5.6 ± 0.1 with 1 mM KCl as electrolyte before and after chemical cleaning. With NaOH cleaning, the decrease in zeta potentials ranged between 10 – 16% with the maximum decrease corresponding to NF270 membrane where the zeta potential decreased (i.e., became more negative) from –43.8 ± 1.6 mV for the pristine membrane to –50.6 mV ± 2.7. Moreover, the IEP's of TS80, TS40 and NF270 membranes could not be detected after cleaning with NaOH as the zeta potential remained negative over the entire pH range from 2 – 10. These results indicate that there is a correlation between the relative concentration of carboxylic and amine groups on the membrane surface and cleaning with NaOH. Simon et al. [103] reported no significant changes in zeta potential of NF270 membrane after cleaning with NaOH while Tian et al. [120] suggested that NaOH could react with hydrophilic surface functional groups, thereby leading to a surface charge modification as observed in our study. Al–Amoudi et al. [108] also reported changes in the measured zeta potential for three different poly(piperazineamide) NF membranes post chemical cleaning with HCl, NaOH, SDS and EDTA.

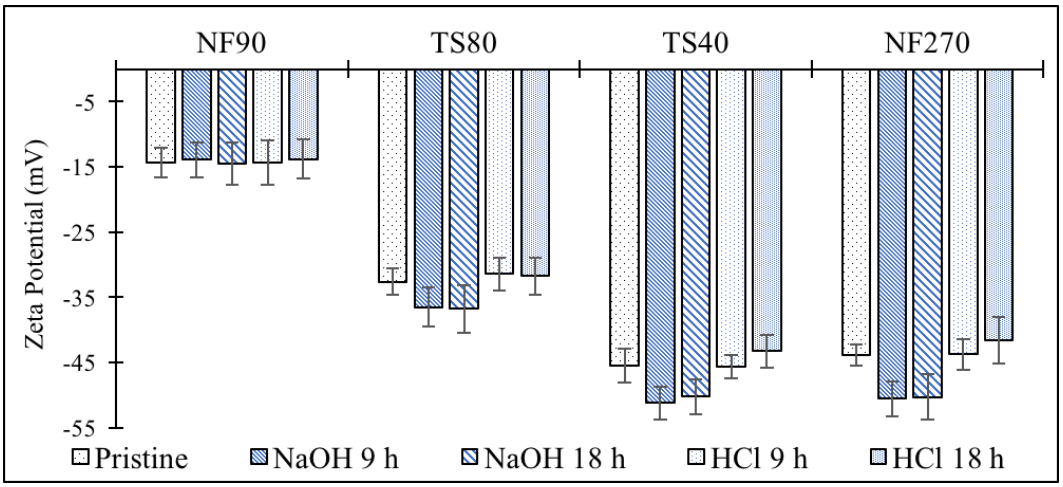

Figure 3.4. Zeta potentials at pH = 5.6 ± 0.1 with 1 mM KCl as electrolyte for fully aromatic polyamide i.e., NF90, TS80 and semi–aromatic poly(piperazineamide) i.e., TS40, NF270 membranes before and after chemical cleaning

3.3.1.4 Membrane pore size measurements

Membrane potential technique was chosen to determine the effective pore radii of NF membranes because it is based on the diffusion potentials of ionic species [1] and can be used to explain changes in the ion rejection characteristics post chemical cleaning. Figure 3.5 (a) shows the measured membrane potential and Figure 3.5 (b) shows the calculated effective pore radii of the four tested NF membranes before and after chemical cleaning. As can be seen in these figures, the effective membrane pore radii of all membranes increased due to chemical cleaning with the PP membranes being affected more than the PA membranes.

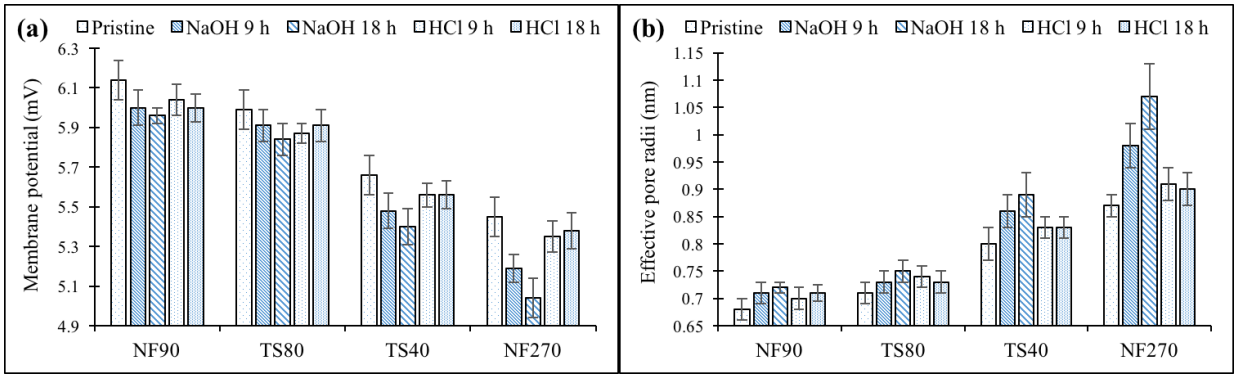

Figure 3.5. (a) Measured membrane potential and (b) Calculated effective pore radii of fully aromatic polyamide i.e., NF90, TS80 and semi–aromatic poly(piperazineamide) i.e., TS40, NF270 membranes before and after chemical cleaning

Cleaning the PA membranes with NaOH increased the effective membrane pore radii by 3 – 6% and minimal changes were measured with increasing NaOH cleaning time. The increase in the effective pore radii in the case of PP membranes was more severe and a further increase with longer exposure time is evident from the results shown in Figure 3.5 (b). Pore radii of NF270 membrane increased after NaOH cleaning for 9 h from 0.87 ± 0.02 nm to 0.98 ± 0.04 nm (an increase of 12.6%) and that for TS40 membrane increased by 7.5% from 0.8 ± 0.02 nm to 0.86 ± 0.03 nm. When cleaning with NaOH for 18 h, a total pore radii increase of 23% and 11% for NF270 and TS40 membranes, respectively was measured. The repulsive electrostatic interactions between deprotonated (negatively charged) carboxylic acid groups that dominate on the active layer surface at high pH that lead to swelling of the membrane polymer matrix [105] might explain the observed greater increase in the effective pore radii with NaOH cleaning when compared to HCl cleaning. As shown in Sections 3.3.1.1 and 3.3.1.3, the PP membranes had lower active layer thickness and higher concentration of carboxylic acid groups compared to PA membranes, which can explain the higher impact on the effective pore radii by chemical cleaning

with NaOH solution. Although TS80 membrane has higher concentration of carboxylic acid groups (like the case with PP membranes) on the active layer (Section 3.3.1.3), it was not significantly affected by NaOH cleaning. Such behavior might be explained by the greater active layer thickness of this membrane and possibly a higher degree of crosslinking that helps to counteract the conformational changes induced by the repulsive negatively charged carboxylic acid groups as compared to the PP membranes. The observed impact of NaOH cleaning time on the effective pore radii is novel and very interesting. It provides evidence that NaOH has capability to cause significant swelling of the membrane active layer, which is more pronounced at longer cleaning times. This effect was clearly seen with PP membranes and suggests that membranes with lower active layer thicknesses might be severely affected.

Also, cleaning with HCl at pH 2 affected all four membranes similarly and the effective membrane pore radii increased by 3 – 5%. For instance, the effective pore radii of NF90 membrane after exposure to HCl for 9 hours increased by 3% while the corresponding increase for NF270 membrane was 4.6%. It is important to note that extending the cleaning time with HCl did not further increase the measured effective pore radii for all membranes as opposed to the case with NaOH cleaning.

3.3.2 Membrane performance

Most of the studies explaining the effects of different cleaning chemicals have been quantified based on the rejection of organic molecules [102-105, 109] and very few have used $MgSO_4$ rejection characteristics [107, 111]. Considering that both size and charge (Donnan) exclusion effects are important for the performance of NF membranes [64, 65], it is important to establish the impact of chemical cleaning on the rejection of different ionic species to explain the

importance of size and charge (Donnan) exclusion effects. Therefore, permeability and rejection characteristics before and after chemical cleaning were evaluated with 1 mM Na_2SO_4 and also with a mixture of 1 mM Na_2SO_4 + 1 mM $MgCl_2$ + 1 mM $CaCl_2$.

3.3.2.1 Ion rejection

Sulfate rejection for all four membranes before and after chemical cleaning is shown in Figure 3.6. As can be seen in this figure, all pristine membranes achieved more than 98% sulfate rejection and both PP and PA membranes achieved similar sulfate rejections despite their differences in pore radii, which can be explained by the higher negative zeta potential of PP membranes (Figure 3.4).

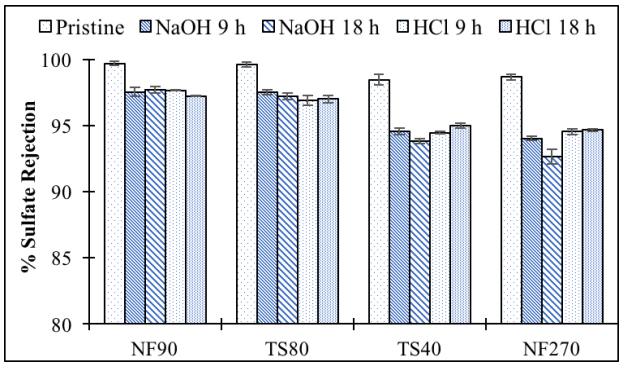

Figure 3.6. Rejection of sulfate by fully aromatic polyamide (i.e., NF90 and TS80) and semi–aromatic poly(piperazineamide) (i.e., TS40 and NF270) membranes before and after chemical cleaning (feed Na_2SO_4 = 1 mM, operating pressure = 20 bar, temperature = 23°C, pH = 5.6, crossflow velocity = 0.77 m/s)

Sulfate rejection decreased after HCl and NaOH cleaning and the cleaning time had almost no impact on the measured sulfate rejection. Marginal decrease in sulfate rejection (< 2.5%) was observed for PA membranes after HCl and NaOH cleaning. These minimal changes can be explained by very small increase in membrane pore radii as shown in Section 3.3.1.4.

While the exposure of PP membranes to NaOH lead to an increase in pore radii that was more pronounced with longer cleaning time, these changes were not reflected in sulfate rejection. The decrease in sulfate rejection after NaOH cleaning for 9 h (4 – 5%) was similar to that observed for HCl cleaning (≈ 4%) even though the increase in their effective pore sizes were higher after cleaning with NaOH (Figure 5 (b)). In addition, cleaning of TS40 and NF270 membranes with NaOH for 18 h increased their effective pore radii by 11 and 23%, respectively but sulfate rejections decreased by only 4.7 and 6%, respectively (Figure 3.6). These changes can be explained by the increased negative zeta potential with PP membranes as observed in Figures 3.3 (c), (d) and 3.4. PP membranes rely on both charge (Donnan) and size exclusion for separation of inorganic ions at ionic strengths < 0.09 M [1] and the importance of charge exclusion for ion rejection is highlighted by the observed sulfate rejection after chemical cleaning with NaOH. Interestingly, no decrease in rejection of a negatively charged organic molecule sulfamethoxazole by NF270 membrane was reported after chemical cleaning with NaOH [103]. This further emphasizes the importance of charge exclusion for PP membranes and suggests that permeate flux measurements and/or rejection experiments with monovalent ions may not always be a correct approach to evaluate the impact of chemical cleaning on NF membranes.

Experimental results with a salt mixture (i.e., 1 mM Na_2SO_4 + 1 mM $MgCl_2$ + 1 mM $CaCl_2$) are illustrated in Figure 3.7. Rejection achieved by the four pristine membranes for all ions were in the order NF90 > TS80 > TS40 > NF270 and correlated well with their measured effective pore radii (Section 3.3.1.4) [1]. The observed rejection order of cations, i.e., $R(Mg^{2+}) > R(Ca^{2+}) > R(Na^{+})$ and that of anions, i.e., $R(SO^{2-}) > R(Cl^{-})$ can be explained by ion diffusivities [47] and Stokes radii with lower ionic diffusivity and higher Stokes radii corresponding to higher rejection. Rejection of all ionic species decreased after chemical cleaning. However, the type of

cleaning chemical or the time of cleaning did not impact ion rejection by PA membranes. Rejection of divalent and monovalent ions by both PA membranes decreased by < 2% and < 4%, respectively. On the other hand, performance deterioration for PP membranes was more pronounced after cleaning with NaOH than after cleaning with HCl. For example, rejection of divalent ions decreased by 3 – 4% for TS80 membrane and 6 – 9% for NF270 membrane after cleaning with HCl. Rejection of divalent ions is dependent on charge (Donnan) exclusion [97, 98] and the impact of changes in the effective pore sizes due to chemical cleaning is illustrated by the rejection of monovalent ions. Similar zeta potential was measured for TS40 and NF270 membranes after cleaning with HCl (Figure 3.4) and the decrease in the rejection of divalent ions was similar even with a slightly higher effective pore radii of the NF270 membrane (Figure 3.5). The effect of higher pore radii can be readily seen in the rejection of monovalent ionic species where the rejection of sodium decreased by 16% for TS40 and by 23% for NF270 membrane.

The impact of NaOH cleaning on PP membranes was similar to that of HCl cleaning when considering sulfate rejection (i.e., decrease by 5 – 7%). However, the decrease in the rejection of all other ions was dependent on the duration of cleaning. For instance, when cleaning TS40 membrane with NaOH for 9 h, the rejections of magnesium, calcium, sodium and chloride ions decreased by 5, 10, 29 and 25%, respectively while the corresponding decrease after cleaning for 18 h was 9, 14, 43 and 38%, respectively. On the other hand, the 23% increase in the effective pore radii for the NF270 membrane after NaOH cleaning (Section 3.3.1.4) lead to a decrease in the rejection of magnesium, calcium, sodium and chloride ions by 25, 36, 53 and 62%, respectively. Relatively small decrease in the rejection of sulfate ions (7%) can be explained by the 16% increase in zeta potential after NaOH cleaning (Figure 3.4). The observed further performance deterioration with longer NaOH cleaning time suggests that NaOH has a

capability to slowly interact with the membrane surface leading to extensive conformal changes in the active layer of PP membranes as detected by the increase in the effective membrane pore sizes. NF membranes are often cleaned with an acid after cleaning with a base to achieve pore tightening [55, 106]. However, extensive conformal changes leading to swelling of the membrane polymer matrix with longer NaOH cleaning times may be difficult to reverse with HCl cleaning.

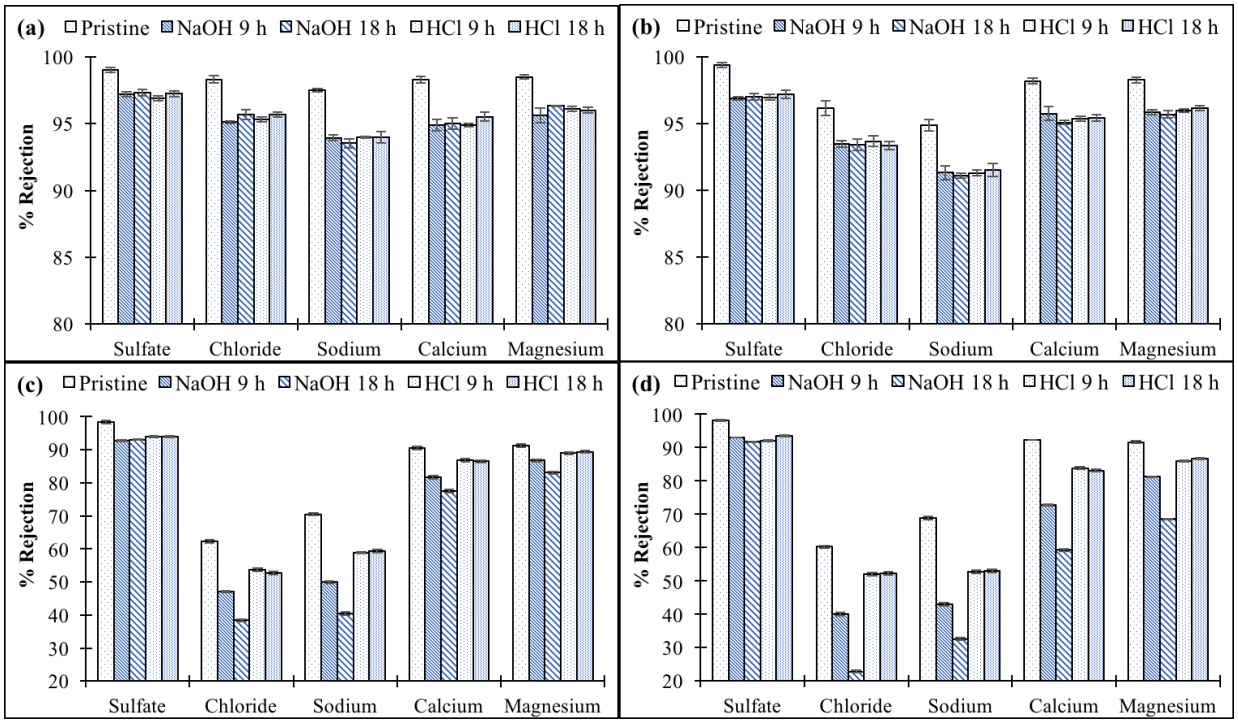

Figure 3.7. Ion rejection by fully aromatic polyamide i.e., (a) NF90, (b) TS80 and semi–aromatic poly(piperazineamide) i.e., (c) TS40, (d) NF270 membranes before and after chemical cleaning with feed composition: 1 mM Na_2SO_4 + 1 mM $MgCl_2$ + 1 mM $CaCl_2$ at operating pressure = 20 bar, temperature = 23°C, pH = 5.6, crossflow velocity = 0.77 m/s

3.3.2.2 Permeability

Experimentally measured permeability values for the four membranes before and after chemical cleaning are shown in Figure 3.8. As would be expected from the analysis of the effective pore radii, pristine NF90 had the lowest permeability (4.7 ± 0.02 LMH/bar) and NF270 membrane had the highest (11.4 ± 0.05 LMH/bar). As can be seen in Figures 3.8 (a) and (b), all membranes experienced an increase in permeability after chemical cleaning but the type of cleaning chemical or the cleaning time had very little impact on measured permeability values of PA membranes (i.e., NF90 and TS80). Cleaning time with HCl had no impact on permeability increase for PP membranes (i.e., TS40 and NF270) (Figures 3.8 (c) and (d)), but longer cleaning with NaOH lead to a further increase in membrane permeability. These changes corresponded to the measured effective membrane pore radii and the observed ion rejections.

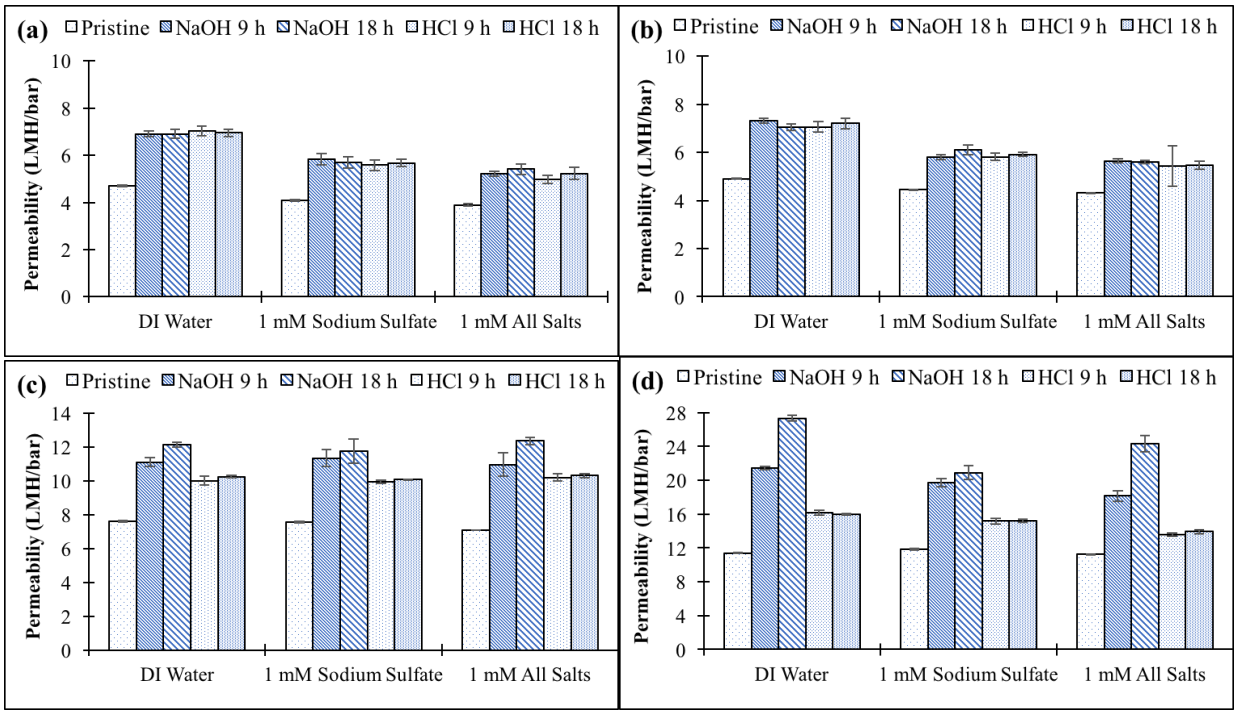

Figure 3.8. Permeability of fully aromatic polyamide i.e., (a) NF90, (b) TS80 and semi–aromatic poly(piperazineamide) (c) TS40, (d) NF270 membranes before and after chemical cleaning with DI water, 1 mM Na_2SO_4 and 1 mM Na_2SO_4 + 1 mM $MgCl_2$ + 1 mM $CaCl_2$ at operating pressure = 20 bar, temperature = 23°C, pH = 5.6, crossflow velocity = 0.77 m/s

Figure 3.9 shows that DI water permeability correlates well with the measured pore radii for all cleaning cases irrespective of the membrane type, degree of crosslinking and thickness of active layer. The measurement of the effective membrane pore radii using the membrane potential method relies on hindered diffusion across the membrane and inherently incorporates all relevant membrane parameters to obtain the effective pore radii. A maximum increase in permeability of 482% (4.70 ± 0.02 LMH/bar for pristine NF90 to 27.4 ± 0.3 LMH/bar for NF270 cleaned with NaOH for 18 h) was measured with an increase in the effective pore radii of 57.4% (0.68 ± 0.02 nm for pristine NF90 to 1.07 ± 0.06 nm for NF270 cleaned with NaOH for 18 h).

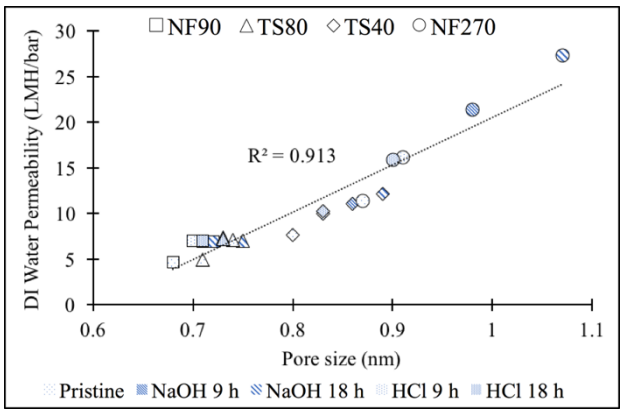

Figure 3.9. DI water permeability as a function of effective pore radii for all membranes at all test conditions

Another important phenomenon with PP membranes is that < 5% difference in their permeability values was measured with 1 mM Na_2SO_4 for 9 and 18 h of cleaning with NaOH, which was not the case when the feed contained a mixture of salts (i.e., 1 mM Na_2SO_4 + 1 mM $MgCl_2$ + 1 mM $CaCl_2$). In that case, the permeability exhibited an increase from 10.9 to 12.4 LMH/bar for TS40 membrane (13% increase) and from 18.2 to 24.3 LMH/bar for NF270 membrane (33.5% increase) when NaOH cleaning time was extended from 9 to 18 h. At the same time, the effective pore radii increased from 0.86 to 0.89 nm for TS40 membrane (3.5% increase) and from 0.98 to 1.07 nm for the NF270 membrane (9.2% increase) (Section 3.3.1.4). When only Na_2SO_4 is present in the feed solution, electrostatic repulsion is the dominant rejection mechanism and it is increased by the lowering of zeta potential with NaOH cleaning (Figures 3.3 (c), (d) and 3.4). The increase in the pore radii had negligible effect on the rejection of sulfate and similar permeability values were measured. However, the increased effective pore radius was unable to effectively reject the monovalent ions when feed contained a mixture of salts as feed, which translated to increased permeability difference with PP membranes after NaOH cleaning for 9 and 18 h. This effectively highlights the role of charge exclusion in

addition to size exclusion as an important separation mechanisms for PP membranes both before and after cleaning.

3.4 CONCLUSIONS

The impact of chemical cleaning on physicochemical characteristics and separation performance of nanofiltration membranes was determined to be dependent on the type of active layer chemistry. ATR–FTIR and XPS analysis indicated no chemical changes to the membrane active layers after chemical cleaning with HCl or NaOH. The active layer thicknesses of the membranes selected for this study decreased in the order NF90 > TS80 > TS40 > NF270. The degree of crosslinking in the active layer was higher for NF90 membrane than TS80 membrane (PA membranes) and that for TS40 membrane was higher than NF270 membrane (PP membranes). Membrane cleaning with HCl did not have significant impact on zeta potential while cleaning with NaOH further reduced zeta potentials for membranes with high concentration of carboxylic acid groups on the surface (i.e., TS80, TS40 and NF270). The effective pore radii of all membranes increased as a result of chemical cleaning and poly(piperazineamide) membranes were more affected than polyamide membranes. HCl cleaning resulted in larger effective membrane pore radii for all membranes by 3 – 5%. Cleaning with NaOH had a much more pronounced impact on the effective pore radii and an increase of as high as 23% was observed for a PP membrane (NF270) after exposure for 18 h. This study offers evidence that NaOH can cause increased swelling of the active layer with an increase in cleaning time and this was particularly evident for poly(piperazineamide) membranes. The PP membranes

are particularly vulnerable when it comes to regaining the permeability and rejection characteristics of pristine membrane if NaOH is used as a cleaning solution.

Ion rejection test with single salt (1 mM Na_2SO_4) and a mixture of salts (1 mM Na_2SO_4 + 1 mM $MgCl_2$ + 1 mM $CaCl_2$) revealed that rejection of all ions decreased after chemical cleaning. Rejection of sulfate for poly(piperazineamide) membranes decreased only slightly despite a fairly significant increase in the effective pore radii, which can be explained by their dependence on charge exclusion mechanism for ion rejection that was actually enhanced by a decrease in zeta potential by NaOH cleaning. The impact of the increased effective pore radii was readily seen in the rejection of monovalent ions when the feed was adjusted to a mixture of salts. The 23% increase in the effective pore radii for the NF270 membrane after NaOH cleaning for 18 h lead to a decrease of 25, 36, 53 and 62% rejection of magnesium, calcium, sodium and chloride ions, respectively. At the same time, only a 7% decrease in the rejection of sulfate ions was observed, which can be explained by the 16% decrease in zeta potential.

The changes in permeability due to chemical cleaning were in agreement with the changes in rejection (i.e., a decrease in ion rejection corresponds to an increase in membrane permeability). The effective pore radii measured using the membrane potential technique correlated well with DI water permeability for all membranes before and after cleaning. The importance of charge exclusion in rejection of inorganic ions was highlighted by the observed differences in rejection and permeability values when testing these membranes post cleaning with NaOH for 9 and 18 h. This study significantly contributes to help understand the lesser known effects of chemical cleaning of the rejection behavior of inorganic ions and its dependence on the physicochemical characteristics and separation potentials of two commonly used active layers of nanofiltration membranes.

4.0 INSIGHTS INTO THE REJECTION OF BARIUM AND STRONTIUM BY NANOFILTRATION MEMBRANE FROM EXPERIMENTAL AND MODELING ANALYSIS

This work is under review as:

S.S. Wadekar, R.D. Vidic, Insights into the rejection of barium and strontium by nanofiltration membrane from experimental and modeling analysis, (2018), *under review with Journal of Membrane Science*.

Better understanding of treatment approaches to remove barium and strontium from aqueous solutions is required to address potential drinking water risk from unconventional gas industry. A polyamide nanofiltration membrane was investigated to explain rejection of barium and strontium ions from single salt solutions at environmentally relevant conditions. Both ions did not specifically adsorb onto the membrane surface even with a hundred–fold feed concentration increase. Electrostatic effects and H^+ rejection did not impact rejection. Size exclusion was determined to be most dominant in achieving very high ion rejections. Concentration polarization modulus decreased with increase in crossflow velocity, decrease in operating pressure and increase in feed concentration because of increase in shear mass transfer rate, decrease in permeate convection and increase in feed osmotic pressure, respectively. Increase in feed pressure resulted in higher permeate flux but ion rejection did not change at

pressures above 15 – 20 bar. Spiegler–Kedem model explained experimental data very well and permeability and reflection coefficients for these solutes indicate that both are equally rejected. Maximum rejection of 99.5% and minimum of 92% indicates exceptional rejection capability by this nanofiltration membrane while achieving appreciable permeability of 3.9 – 5.9 LMH/bar.

4.1 INTRODUCTION

Heavy metals including zinc, cadmium, arsenic, manganese, lead, nickel, chromium and copper are under much scrutiny owing to their toxicity to living organisms and problems associated due to their long persistence in the environment [121]. Major sources of heavy metals in the environment include industrial activities, such as, fuel industry, battery manufacturing, mining, electroplating, etc. [122] Their influence on human health has been well studied [123] and the main industrial sources of these heavy metals have been regulated.

Unconventional (shale) gas extraction is a fast growing industry that is producing 48.28 billion cubic feet per day of dry shale gas in the USA as of November 2017 [124]. However, apart from economic benefits from this industry, it is also important to consider potential adverse environmental impacts from shale gas extraction. Management of wastewater (i.e., flowback and produced water) generated by this process is one of the most important environmental concerns with this industry [125, 126]. Flowback and produced water contain total dissolved solids (TDS) as high as 200,000 – 300,000 mg/L [127] dominated by sodium, chloride, calcium, magnesium, barium and strontium ions in addition to organics [128]. Currently, this industry predominantly relies on deep underground injection to dispose this highly saline water [129] and the reuse of this water for hydraulic fracturing is limited to Marcellus Shale play. Direct treatment of this

wastewater with pressure–driven NF or reverse osmosis (RO) membranes is not feasible due to very high osmotic pressures [130]. Barium (Toxicity Characteristic Leaching Procedure (TCLP) listed heavy metal) and strontium are currently not found in fresh water resources at elevated levels but may become a major environmental concern because of extreme levels in this wastewater (Ba is present at 3,000 – 6,000 mg/L and Sr at 1,600 – 12,000 mg/L) [130]. In addition to unconventional gas wastewater, strontium can also be found in the nuclear waste streams [131-133]. The Primary Maximum Contaminant Level (P–MCL) for barium in drinking water is set at 2 mg/L and strontium has a health reference level set at 1.5 mg/L by US Environmental Protection Agency [134, 135]. Thus, barium and strontium may become an important concern in the future and their removal by nanofiltration was the major focus for this study.

Traditional approach for treating heavy metal contaminated streams includes hydroxide precipitation, which leads to formation of a highly–contaminated solid waste [136]. Also, the metals are lost in waste streams and cannot be recovered. In recent years, nanofiltration (NF) membranes have been increasingly applied for the removal and/or recovery of metals from aqueous streams [137-144]. Several recent studies focused on understanding the separation mechanisms for metal ions in NF systems [66, 145, 146] and the role of the three different separation potentials: size, charge (Donnan) and dielectric exclusion [68, 99, 147]. None of these studies focused on the rejection of barium and very few evaluated the removal of strontium using NF membranes [131-133, 148].

We performed a systematic study to understand the rejection mechanism for barium and strontium from single salt solutions by a polyamide NF membrane in a crossflow system operated at varying feed pressures (5 – 30 bar) and feed concentrations (0.36 – 36.4 mM Ba/Sr).

Rejection of these ions was explained using Spiegler–Kedem model and the role of concentration polarization was also elucidated.

4.2 MATERIALS AND METHODS

NF90 membrane, a fully aromatic polyamide membrane with a polysulfone support, purchased from Dow Filmtech (Edina, MN) was used in this study. All reagents used were of analytical grade and were purchased from Fisher Scientific (Pittsburgh, PA). Barium chloride dihydrate ($BaCl_2.2H_2O$) and strontium chloride hexahydrate ($SrCl_2.6H_2O$) were used for all experiments and dilute HCl and NaOH were used for pH adjustment. All aqueous solutions were prepared with deionized (DI) water (conductivity < 1 μS/cm, resistivity = 18.2 kohm.cm^{-1}, pH = 5.6 $\pm$ 0.2) obtained in–house using MilliQ water system (Millipore, Billerica, MA). All cations and anions were analyzed using inductively coupled plasma–optical emission spectroscopy (5100 ICP–OES, Agilent Technologies, Santa Clara, CA) and ion chromatography (IC) (Dionex ICS–1100 with IonPac AS22 carbonate eluent anion–exchange column, Dionex, Sunnywale, CA), respectively. pH was monitored using Orion Versastar Pro (Thermo Scientific, Pittsburgh, PA). Zeta potential of the membranes was analyzed using Surpass 3 Electro–kinetic Analyzer (EKA), using the Adjustable Gap Cell (AGC) (Anton Paar, Ashland, VA). For each measurement, two 10 mm $\times$ 20 mm membrane samples were inserted into the AGC and the automatic pH sweep was conducted with different concentrations of barium and strontium in the

aqueous solution. Each zeta potential analysis was repeated at least four times with a maximum standard deviation of 1.7 mV.

All experiments were carried out in the crossflow laboratory–scale SEPA–CFII test cell (GE Osmonics, Minnetonka, MN) with usable membrane area of 140 cm^2 [6, 114]. Prior to every experiment, membrane was immersed in DI water for at least 24 hours to ensure complete wetting. The membrane was first compacted with DI water in the crossflow module at feed pressure of 30 bar and flow rate of 1.5 GPM (highest pressure and flow rate used in this study) and then used to filter DI water until a stable flux (LMH/bar) was reached. The feed was then adjusted to the required composition and the system was allowed to equilibrate for two hours when the permeate flux was recorded and samples were collected for chemical analysis. For all experiments, the temperature was fixed at 23 $\pm$ 1°C while the operating feed pressure varied between 5 – 30 bar, feed flow rate between 0.5 – 1 GPM (corresponding to a crossflow velocities between 0.39 – 1.16 m/s), feed pH between 2 – 10 and feed concentration between 0.36 – 36.4 mM barium or strontium. All crossflow experiments were conducted in duplicates.

4.3 MODELING

Observed rejection (R_0) was measured by analyzing the bulk feed (C_f) and permeate (C_p) solute concentrations. Actual or intrinsic rejection (R_i) was modeled using the film theory [44, 149] by considering the effect of concentration polarization as shown below:

$$R_0 = 1 - \frac{C_p}{C_f} \tag{4-1}$$

$$R_i = 1 - \frac{C_p}{C_m} = \frac{R_0 \,.\, \exp\left(\frac{J}{k}\right)}{1 - R_0 \left[1 - \exp\left(\frac{J}{k}\right)\right]} \tag{4-2}$$

where, C_m is the solute concentration at the membrane surface determined using film theory (Equation (4-2)), J is the permeate flux and k is the mass transfer coefficient in the polarization layer. k is approximated using Sherwood (Sh) relationship with Deissler correlation for flow in channels and tubes [44] as follows:

$$Sh = 0.023 \,.\, Re^{0.875} \,.\, Sc^{0.25} \tag{4-3}$$

$$Sh = \frac{k \,.\, d_h}{D}\,;\; Re = \frac{u \,.\, \rho \,.\, d_h}{\eta}\,;\; Sc = \frac{\eta}{\rho \,.\, D} \tag{4-4}$$

where, Re is the Reynolds number, Sc is the Schmidt number, D is the diffusion coefficient for the salt, d_h is the hydraulic diameter, u is the crossflow velocity, ρ and η are density and dynamic viscosity of the aqueous solution. ρ and η are taken to be equal to that of pure water and salt diffusion coefficient is calculated using the individual diffusion coefficients (D_+, D_-) and valences (z_+, z_-) of the ions as shown below:

$$D = \frac{(z_+ - z_-) \cdot D_+ \cdot D_-}{z_+ \cdot D_+ - z_- \cdot D_-} \quad (4\text{-}5)$$

Hydraulic diameter for a parallelogram type feed spacer (Figure 4.1) used in the study was calculated using the correlations developed for spacer filled membrane systems [149, 150]:

$$d_h = \frac{d_f \cdot \epsilon}{(d_f/2h_{sp}) + (1 - \epsilon)} \quad (4\text{-}6)$$

$$\text{where, porosity} = \epsilon = 1 - \frac{\pi \cdot d_f^2}{2 \cdot l_m \cdot h_{sp} \cdot \sin\theta} \quad (4\text{-}7)$$

d_f, h_{sp}, l_m and θ are the fiber thickness, spacer thickness, mesh size and angle in the direction of feed flow, respectively.

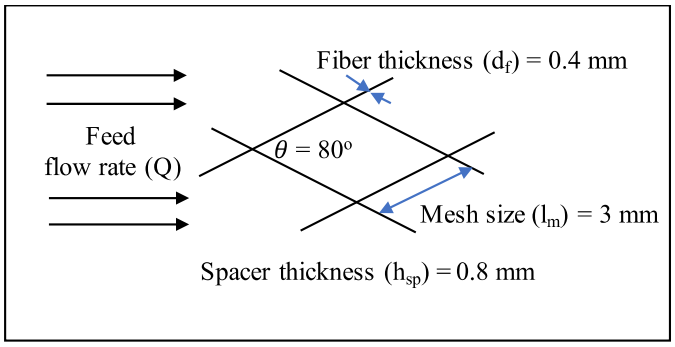

Figure 4.1. Feed spacer dimensions

The porosity of the spacer was calculated as 89.37% and the hydraulic diameter as 1.0032 mm. The crossflow velocity can now be approximated knowing the feed flow rate (Q), flow area of the channel (A = 95 mm × 1 mm) and spacer porosity (ϵ = 0.8937). Three feed flowrates i.e. 0.5, 1 and 1.5 GPM were investigated in this study and correspond to 0.39, 0.77 and 1.16 m/s crossflow velocities, respectively.

Spiegler–Kedem (S–K) equation [151] was used to predict rejection of barium and strontium over a hundred–fold variation in the feed salt concentration (i.e., 0.36 – 36.4 mM). This model considers the membrane as a black box (i.e., no consideration of membrane characteristics or separation mechanisms) and includes convective (because of the pressure gradient) and diffusive (because of the concentration gradient) fluxes. The S–K equation is given as follows [138, 151]:

$$R_i = \frac{\sigma\,.(1-F)}{1-\sigma\,.\,F} \text{ where } F = \exp(-\frac{1-\sigma}{\omega}\,.\,J) \quad (4\text{-}8)$$

where, R_i is the actual or intrinsic rejection, σ is the reflection coefficient for solute, ω is the solute permeability (LMH) and J is the permeate volume flux (LMH). A non–linear parameter (χ^2) (i.e., error) was calculated to assess model validity based of the difference between actual rejection determined experimentally (R_{exp}) and that determined by the S–K model (R_{cal}) [152]:

$$\chi^2 = \sum \frac{(R_{exp} - R_{cal})^2}{R_{cal}} \quad (4\text{-}9)$$

Concentration polarization (CP) was quantified using the CP modulus, which is the ratio of solute concentration at the membrane surface (C_m, i.e. modeled using the film theory) and solute concentration in the bulk feed (C_f) [137, 153]:

$$CP\ modulus = {C_m}/{C_f} \quad (4\text{-}10)$$

4.4 RESULTS AND DISCUSSION

Rejection of heavy metal ions (i.e., barium and strontium) in crossflow experiments at different feed pH, concentration and pressure was used to develop a Spiegler–Kedem model for a fully aromatic polyamide (1,3–benzenediamine (m–phenylenediamine) with trimesoyl chloride i.e. MPD – TMC chemistry) [63, 113] NF membrane with a MWCO of about 200 [76]. A mean effective pore radius of 0.68 ± 0.02 nm using the membrane potential method [1] and 0.34 nm by modeling the retention data of organic solutes of different molecular weights [88] for the NF90 membrane has been reported previously and is higher than the Stokes radii of the main ions of interest in this study as shown in Table 4.1.

Table 4.1. Diffusion coefficient (D_i) [47] and Stokes radii ($r_{i,s}$) of ions used in this study

Ions	$D_i \times 10^{-9}$ (m^2/s)	$r_{i,s}$ (nm)
Ba^{2+}	0.847	0.288
Sr^{2+}	0.791	0.308
Cl^-	2.032	0.12
H^+	9.311	0.026

4.4.1 Zeta potential measurements

Membrane surface charge is due to dissociation of unreacted carboxylic and amine groups in the polyamide active layer or specific adsorption of different solutes and is a function of the composition and ionic strength of the electrolyte solution in contact with the membrane surface [51]. The membrane surface charge imparts electrostatic repulsion/attraction for ions in the feed and has been shown to affect their rejection [79, 92].

Figure 4.2 shows the change in zeta potential of NF90 membrane as a function of solution pH at different feed concentrations of barium or strontium. Amphoteric behavior of NF90 is governed by the presence of both amine ($–NH_2$) and carboxylic acid groups (–COOH). Similar values of the zeta potential measured for NF90 with barium and strontium can be explained by their similar diffusion coefficients and Stokes radii as shown in Table 4.1. The iso–electric point (IEP) for NF90 was always in the vicinity of 4 for the fairly large range of barium and strontium concentrations (i.e., 0.36 to 36.4 mM). The IEP for this membrane measured using a non–adsorbing salt like KCl was also close to 4 [79, 90], which suggests that barium and strontium do not adsorb strongly on the membrane surface. Specific adsorption of divalent cations has been

attributed to electrostatic interactions between cations in solution and negatively charged carboxylic acid groups [91] and has been observed to change membrane characteristics [138, 154]. Specific adsorption of cobalt ions, for example, has been shown to change the amphoteric nature of an NF membrane so that it is always positively charged [138]. The tests with NF90 membrane also showed that cobalt adsorbs strongly on membrane surface so that the zeta potential is always positive (Figure A.9, Appendix A.3). Figure 4.2 indicates that increasing concentrations of barium or strontium lead to a slight upward shift in zeta potential at pH above IEP and an overlap of zeta potential curves at higher concentrations.

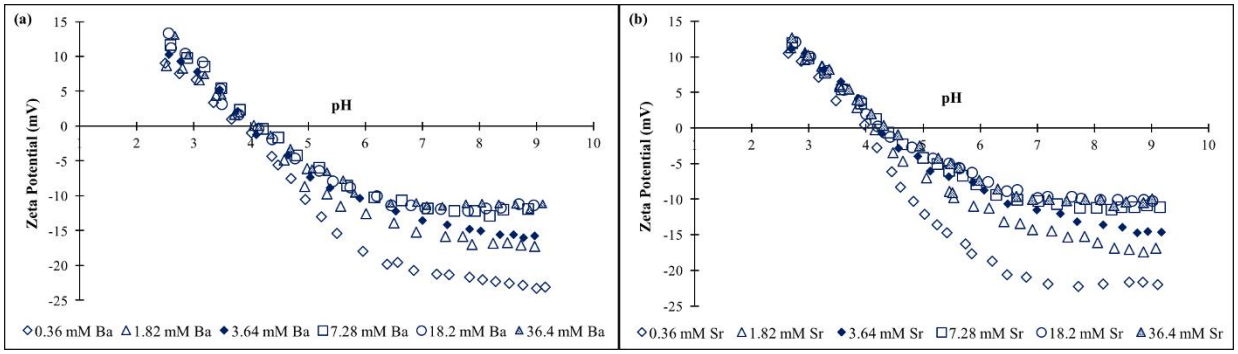

Figure 4.2. Zeta potential curves for varying concentrations of (a) barium chloride (b) strontium chloride as a function of pH

These results indicate that the membrane surface was virtually saturated with these divalent ions once their concentration exceeded 18.2 mM, which can be explained by the compression of the electrical double layer at high ionic strength and can be quantified by the change in the characteristic Debye length [51]. As seen from Figure 4.3, the Debye length calculated at the respective feed concentrations, decreases exponentially and hence no relative change to the Debye length at high ionic strength would explain the absence of any change in the measured zeta potentials with increasing concentrations of barium and strontium [155]. These

results further support the conclusion that neither barium or strontium ions adsorbed on the NF90 membrane surface.

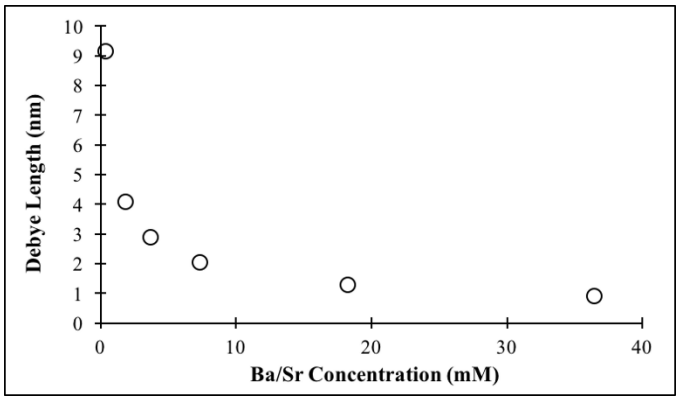

Figure 4.3. Characteristic Debye length with increasing feed concentration of barium or strontium

4.4.2 Influence of pH on ion rejection

pH plays a very important role in the rejection of ionic species [132, 141, 142, 144, 156]. The rejection characteristics of NF90 for barium and strontium ions were studied as a function of pH to help understand the underlying rejection mechanisms. The influence of pH on the rejection of barium and strontium was studied in the range of 2 – 10 at constant feed temperature of 23 ± 1 °C, feed pressure of 20 bar, crossflow velocity of 1.16 m/s and feed concentration of 3.64 mM Ba/Sr (Figure 4.4).

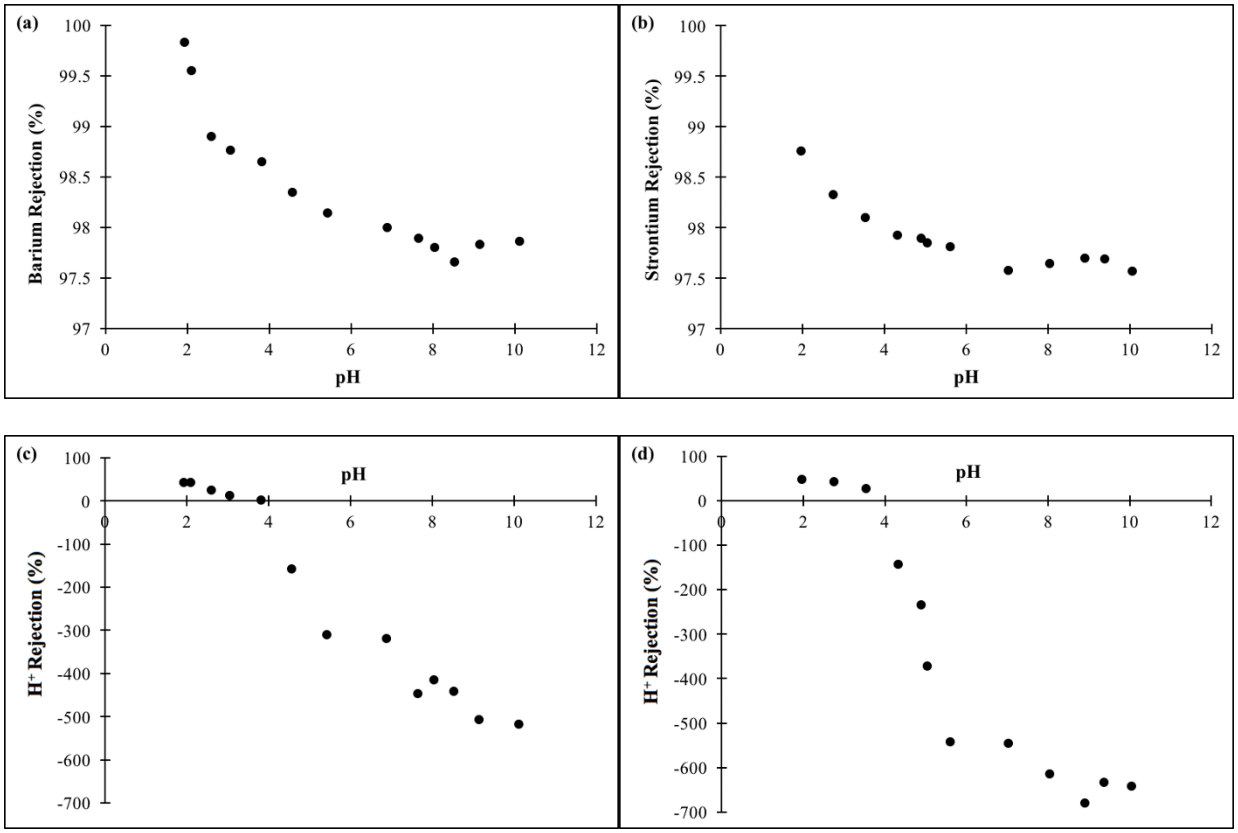

Figure 4.4. Influence of pH on rejection characteristics of (a) barium, (b) strontium, (c) and (d) H^+ rejection in case of barium and strontium, respectively. (Experimental conditions: Feed crossflow velocity = 1.16 m/s, feed concentration = 3.64 mM, T = 23 $\pm$ 1°C)

Electrostatic effects, steric exclusion and H^+ permeation are the most important mechanisms for the rejection heavy metal ions [138, 141, 157, 158]. H^+ rejection was calculated using the measured feed and permeate pH at steady state conditions. Each pH measurement was performed at least twice (maximum error in measurement = $\pm$ 0.2 pH unit) and an average was used for H^+ rejection calculations. Figures 4.4 (a) and (b) show variation in barium and strontium rejection, respectively while (c) and (d) show rejection of H^+ in each case as a function of feed pH. Rejection of both barium and strontium is the highest at low pH and decreases with pH increase until a plateau is reached at around pH 8. Ba^{2+} and Sr^{2+} rejection by NF90 was very

similar (99.5 – 97.5%), which can be explained by similar membrane surface charge in the presence of these ions (Figure 4.2) and similar diffusion coefficients and Stokes radii of these ions (Table 4.1).

Based on the zeta potential studies and rejection analysis as a function of pH, the rejection mechanism for Ba^{2+} and Sr^{2+} can be explained by dividing the pH range into 3 regions: (1) pH < IEP, where the membrane is positively charged (Figure 4.2) and H^+ rejection is positive (Figures 4.4 (c) and (d)), (2) pH ≈ IEP, where the membrane does not have any charge and (3) pH > IEP, where the membrane is negatively charged (Figure 4.2) and H^+ rejection is negative (Figures 4.4 (c) and (d)). The observed high rejection of divalent ions at pH < 4 may be attributed to the electrostatic repulsion by the positively charged membrane surface. The fact that H^+ ions are being concentrated in the feed at pH < 4 (i.e., strong positive rejection of H^+ ions) did not affect rejection of barium or strontium. In some cases, increased rejection of heavy metal ions has been explained by a decrease in H^+ rejection [138]. Because the membrane surface is neutral at IEP, ion rejection should decrease around the IEP if the electrostatic effects significantly contributed to rejection. However, that was not the case because observed barium and strontium rejections decreased only slightly (~ 0.5 – 0.8%) and were still very high (98.4% for barium and 98% for strontium). Because H^+ rejection was close to 0% at pH ≈ 4, neither the electrostatic effects nor the H^+ permeation are relevant for the rejection of barium and strontium.

At pH > 4, the zeta potential was increasingly negative (Figure 4.2) and the H^+ rejection decreased strongly (Figure 4.4). Because the decreased rejection of H^+ ions did not increase the rejection of barium and strontium, we ascertain that H^+ permeation is not relevant for the rejection of barium and strontium by NF90 in any pH range investigated in this study. In addition, increase in negative surface charge when pH increased from 4 to 10 resulted in a

marginal decrease (~0.3 – 0.5%) in the rejection of barium and strontium. Increase in strontium rejection with an increase in pH was previously explained by the formation of $Sr(OH)_2$ solids [131]. However, thermodynamic calculations (PHREEQC, Version 3.1.7, USGS) revealed that $Sr(OH)_2$ formation is not possible at pH below 10.

Besides electrostatic interactions and H^+ permeation, it is important to consider size exclusion, which is the dominant separation mechanism for fully aromatic polyamide nanofiltration membranes [1]. It is important to note that the positive surface charge arises from the dissociation of amine groups while the negative charge arises from the dissociation of carboxylic groups [51]. These changes affect the pore size characteristics by conformal changes to the polyamide active layer whereby the pore size increases at higher pH because of the strong electrostatic repulsive interactions between the hydrolyzed carboxylic acid groups on the membrane surface [102, 105]. Hence, an increase in the effective pore size is expected at higher pH (pH > IEP), which decreases barium and strontium rejection. Similar behavior was reported for cadmium, lead, copper, nickel, cobalt and manganese [137, 140, 141, 144, 159, 160].

4.4.3 Influence of crossflow velocity on ion rejection

Figure 4.5 shows the permeate flux as a function of crossflow velocity (0.39, 0.77 and 1.16 m/s) at two different feed concentrations (0.36 and 36.4 mM) of barium chloride. The permeate flux increased with an increase in crossflow velocity at all feed pressures evaluated in this study because of the increase in the shear rate at the membrane surface leading to decreased solute accumulation. This increase is more pronounced at lower feed concentration (i.e., 0.36 mM, Figure 4.5 (a)), where the permeate flux at 30 bar feed pressure increased from 139.3 to 177.9 LMH (i.e., a 28% increase) as compared to an increase from 109 to 122.6 LMH (i.e., a

12% increase) at 36.4 mM (Figure 4.5 (b)). Similar behavior was observed in the case of strontium chloride (Figure A.10 in Appendix A.3). Higher feed pressure increases the convective solute transport towards the membrane surface thereby increasing the concentration polarization (CP) modulus [138, 142]. This can be clearly observed in Figure 4.6, where CP modulus increased from 1.24 to 3.16 for a feed pressure increase from 5 to 30 bar at barium chloride feed concentration of 0.36 mM and crossflow velocity of 0.39 m/s. Also, the CP modulus is higher at lower ionic feed strength (Figure 4.6), which explains greater impact of crossflow velocity on permeate flux at lower feed concentration.

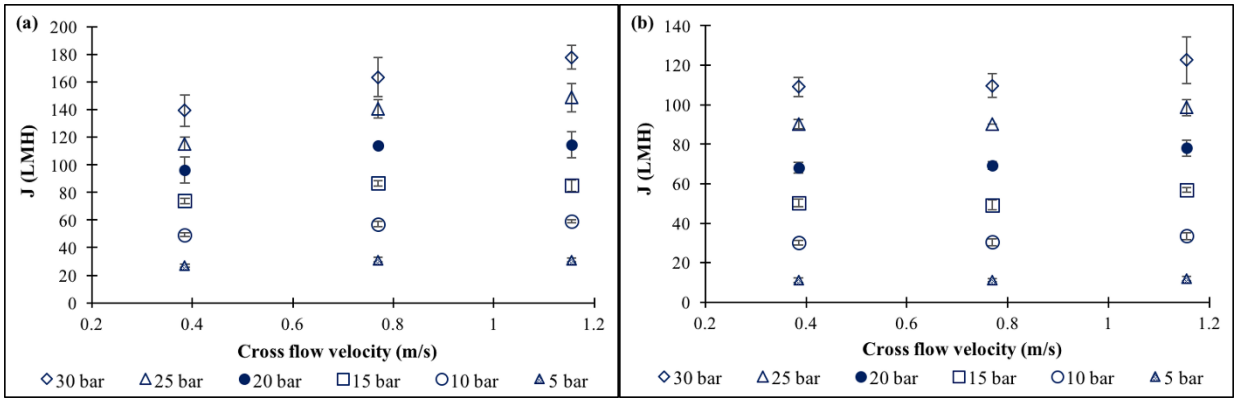

Figure 4.5. Permeate flux as a function of feed crossflow velocity for (a) 0.36 mM and (b) 36.4 mM barium chloride feed concentration (Experimental conditions: Feed pH = 5.6 ± 0.2, T = 23 ± 1°C

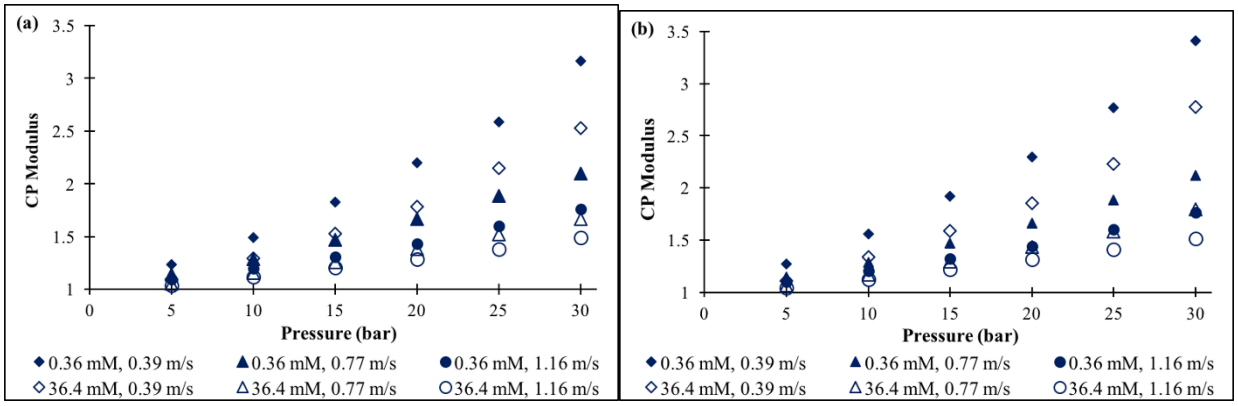

Figure 4.6. CP modulus as a function of operating feed pressure for (a) barium chloride and (b) strontium chloride (Experimental conditions: Feed pH = 5.6 ± 0.2, T = 23 ± 1°C)

The difference between the observed and actual (intrinsic) rejection for these divalent cations (Figure 4.7 for $BaCl_2$ and Figure A.11 in Appendix A.3 for $SrCl_2$) clearly illustrates the impact of crossflow velocity on membrane performance. The observed ion rejection increases with an increase in crossflow velocity for both barium and strontium but the increase is less pronounced at higher crossflow velocities because of much lower CP modulus (Figure 4.6). Also, the difference between the observed and actual rejection is less pronounced at higher ionic strength (i.e., 36.4 mM, Figure 4.7 (b)) because of the lower CP modulus (Figure 4.6 (a)). The overlap of actual rejection values for all pressures at both feed concentrations suggest that the effects of crossflow velocity on concentration polarization phenomenon can be correctly accounted by the film theory.

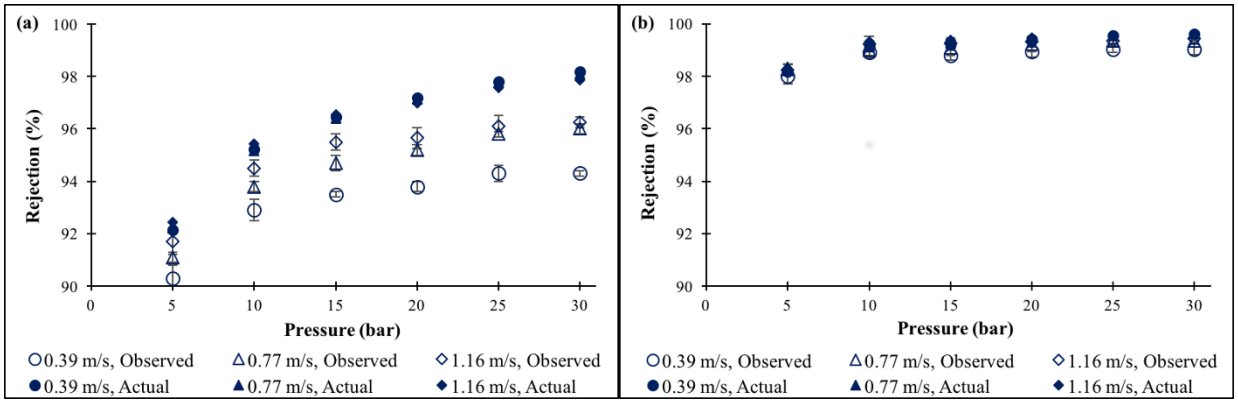

Figure 4.7. Impact of operating feed pressure on the observed and actual (intrinsic) ion rejection for (a) 0.36 mM and (b) 36.4 mM barium chloride concentration (Experimental conditions: Feed pH = 5.6 ± 0.2, T = 23 ± 1°C)

4.4.4 Influence of feed pressure and concentration on ion rejection

The effect of feed pressure and concentration on the rejection of barium and strontium was evaluated to establish the range of NF90 applicability for the removal of barium and strontium. Figure 4.8 shows the variation in permeate flux (J) (Figure 4.8 (a)), CP modulus (Figure 4.8 (b)) and barium rejection (observed and actual rejections are plotted in Figures 4.8 (c) and (d), respectively) with increasing operating feed pressure at constant crossflow velocity (i.e., 1.16 m/s), pH (i.e., 5.6 ± 0.2) and temperature (i.e., 23 ± 1 °C). The permeability measured at the lowest feed concentration used in this study (i.e., 0.36 mM) was very similar to pure water permeability of 6.14 LMH/bar. However, it decreased significantly with an increase in feed concentration (Figure 4.8 (a)) because of the increase in osmotic pressure [151]. A permeability decrease of 1.95 LMH/bar (i.e., from 5.88 to 3.93 LMH/bar) was observed for a 100–fold feed concentration increase from 0.36 to 36.4 mM salt. Ion rejection increased only slightly for more concentrated solutions compared to less concentrated solutions with an increase in feed pressure (Figure 4.8 (c)), which can be explained by the higher CP modulus values observed in the case of

less concentrated solutions (Figure 4.8 (b)). For instance, the observed rejection of 0.36 mM barium increased from 91.7 to 96.5% (i.e., a 5.2% increase) for an increase in feed pressure from 5 to 30 bar while an increase of only 1.2% (i.e., from 98.2 to 99.5%) was observed with 36.4 mM barium in the feed (Figure 4.8 (c)). Also, observed barium rejection increased with an increase in feed pressure and leveled off beyond 15 – 20 bar for all salt concentrations evaluated in this study. Identical behavior was observed for strontium chloride (Figure A.12, Appendix A.3).

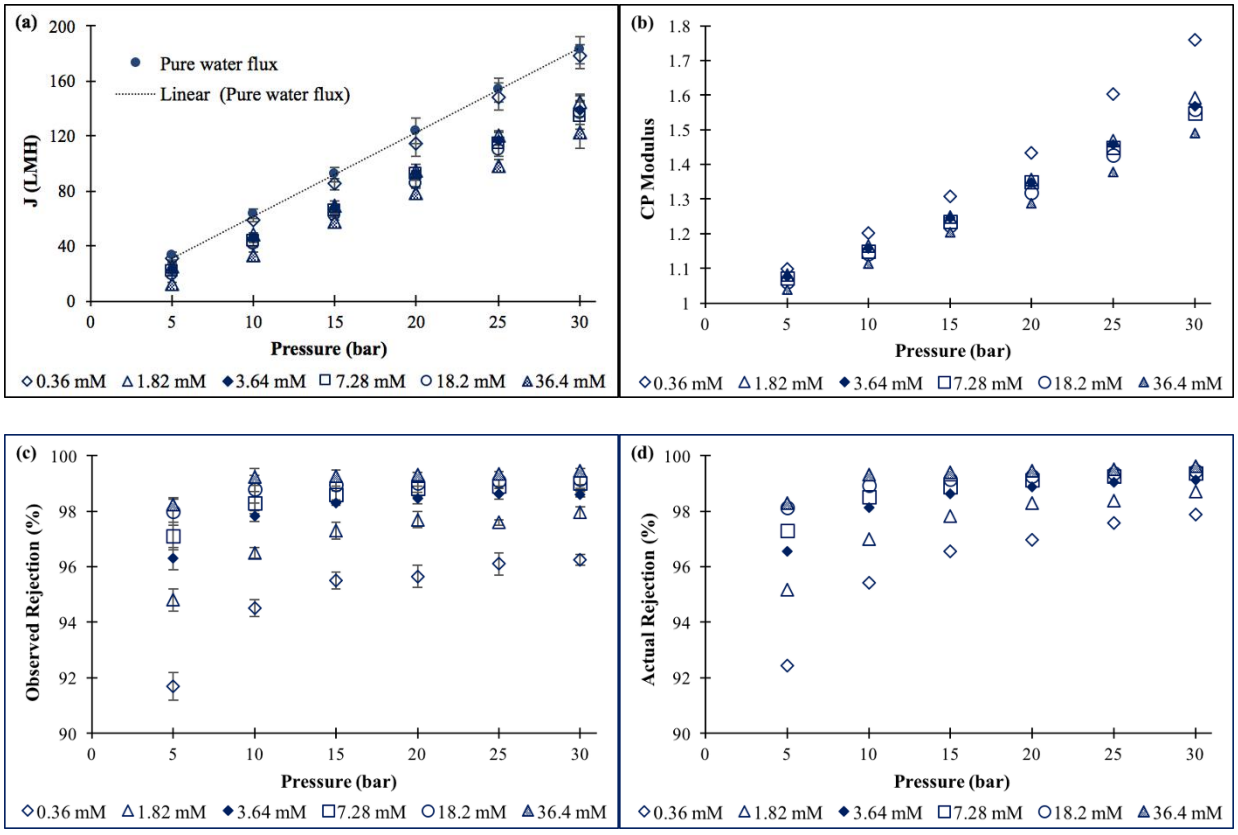

Figure 4.8. Impact of operating feed pressure on (a) permeate flux, (b) CP modulus, (c) observed rejection, and (d) actual (intrinsic) rejection for barium chloride (Experimental conditions: Feed crossflow velocity = 1.16 m/s, pH = 5.6 ± 0.2, T = 23 ± 1°C)

The effect of feed concentration on the observed rejection and permeate flux is shown in Figure 4.9. The permeate flux decreased with an increase in the initial feed

concentration of solute at all feed pressures evaluated in this study (Figure 4.9 (a)). The osmotic pressure at the membrane surface increases with an increase in feed concentration, which reduces the driving force and the resulting permeate flux [140-142]. Osmotic pressure of 0.013 bar was calculated at the membrane surface (i.e., considering concentration polarization) for 0.36 mM barium concentration in the feed. It increased to 1.18 bar (~ 2 orders of magnitude increase) at 36.4 mM Ba concentration, which explains the decrease in driving force. Even more interesting is the observed ion rejection that increased with an increase in the initial feed concentration of solute (Figure 4.9 (b)), which is not commonly observed. Shielding of the membrane charge at high ionic strength is usually offered as the main reason for decrease in ion rejection with an increase in feed concentration [142, 144, 154]. However, increase in rejection with an increase in feed concentration has also been reported in some cases [132, 138, 159]. As described above, NF90 membrane is negatively charged at pH = 5.6 ± 0.2 and this charge becomes less negative with increasing barium or strontium feed concentration (Figure 4.2). It appears that the relative increase in zeta potential aids in the rejection of barium cations. Similar characteristics were observed with strontium ions (Figure A.13 in the Appendix A.3). Ding et al. have also reported an increase in strontium rejection with an increase in feed concentration [132].

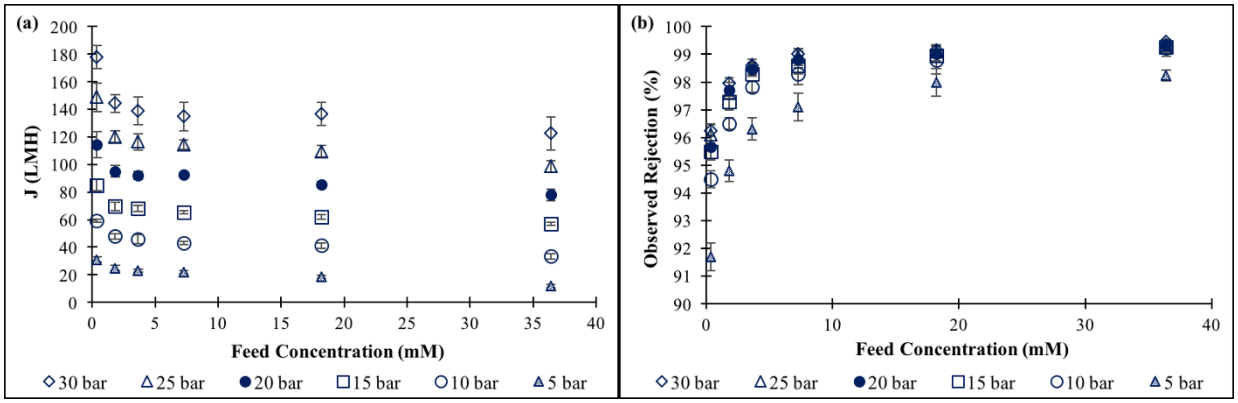

Figure 4.9. Impact of feed barium chloride concentration on (a) permeate flux and (b) observed ion rejection

(Experimental conditions: Feed crossflow velocity = 1.16 m/s, pH = 5.6 ± 0.2, T = 23 ± 1°C)

Very high rejection (92 – 99.5%) of both barium and strontium along with an appreciable permeability (5.9 – 3.9 LMH/bar) measured with NF90 membrane suggests that this membrane is very effective in separating these divalent cations under very challenging conditions. Because the ion rejection did not change significantly once the feed pressure exceeded 15 – 20 bar (Figure 4.8 (c) and (d)), it could be assumed that 20 bar is the optimal feed pressure when considering NF90 membrane for the rejection of barium and strontium ions. Recommended crossflow velocity is 1.16 m/s because of reduced concentration polarization modulus compared to other velocities evaluated in this study (Figure 4.6).

4.4.5 Modeling ion rejection

The Spiegler–Kedem (S–K) model provided an excellent fit to experimentally observed ion rejections for both barium and strontium (Figure 4.10). The evaluated concentration dependent transport parameters over a hundred–fold variation in feed concentration are given in

Table 4.2. The quality of fit or error (χ^2) (Equation (4-9)) was less than 10^{-3} for all feed concentrations investigated indicating that the S–K model describes the rejection behavior of NF90 for both barium and strontium very well. The model correctly describes the increase in rejection with an increase in feed pressure (Equation (4-8) indicates that the ion rejection increases with increasing permeate flux and reaches a limiting value R = σ at infinitely high flux) and with an increase in feed concentration.

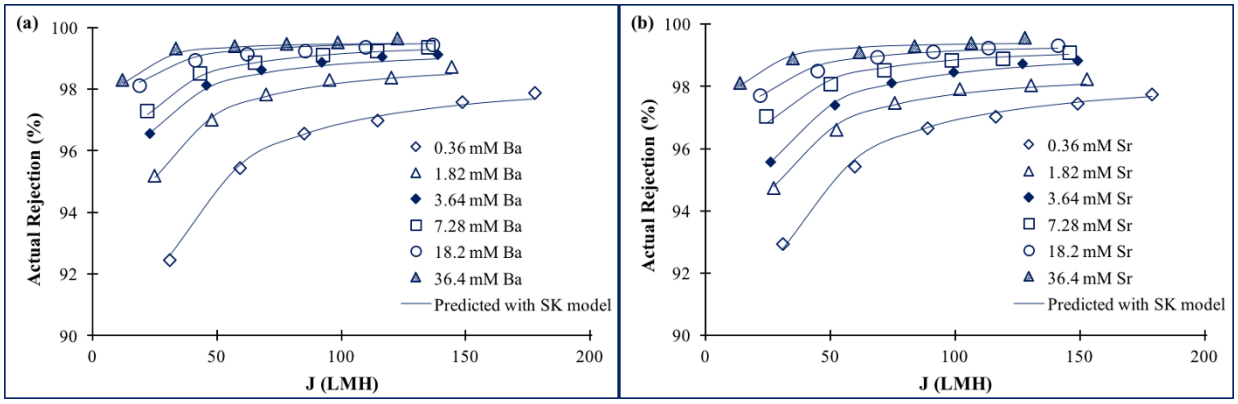

Figure 4.10. Spiegler–Kedem model prediction (lines) and actual (intrinsic) rejection of (a) barium and (b) strontium as a function of permeate flux (Experimental conditions: Feed crossflow velocity = 1.16 m/s, pH = 5.6 $\pm$ 0.2, T = 23 $\pm$ 1°C)

Table 4.2. Spiegler–Kedem reflection coefficient (σ) and solute permeability (ω) for barium chloride and strontium chloride

Feed Concentration (mM)	S–K model parameters					
	σ		ω (LMH)		Quality of fit (χ^2)	
	$BaCl_2$	$SrCl_2$	$BaCl_2$	$SrCl_2$	$BaCl_2$	$SrCl_2$
0.36	0.982	0.981	2.14	2.05	9.5×10^{-4}	9.9×10^{-4}
1.82	0.988	0.983	1.1	1.23	9.3×10^{-4}	8.1×10^{-4}
3.64	0.992	0.991	0.71	1.07	6.8×10^{-4}	2.3×10^{-4}
7.28	0.995	0.992	0.579	0.691	4.5×10^{-4}	7.8×10^{-4}
18.2	0.995	0.993	0.291	0.433	5.4×10^{-4}	3.8×10^{-4}
36.4	0.995	0.994	0.189	0.231	6.9×10^{-4}	8.7×10^{-4}

As can be seen in Table 4.2, the reflection coefficient (σ) increases while the solute permeability (ω) decreases with an increase in feed concentration. Comparison of concentration dependent S–K model parameters with those obtained for cobalt chloride at similar operating conditions [138] indicate that the reflection coefficient (σ) is lower and solute permeability (ω) is higher for cobalt, which explains lower rejection of cobalt compared to barium and strontium with a similar polyamide NF membrane. Very high reflection coefficient and low solute permeability coefficient of the S–K model provide further evidence that NF90 membrane is very efficient in rejecting both barium and strontium. Figure 4.11 shows that both rejection and feed concentration are strongly correlated to solute permeability for barium chloride as evidenced by very high values of the correlation coefficient (R^2). Very similar model

parameters and quality of fit were obtained for experimental results with strontium chloride (Table 4.2). This may be expected owing to the similar rejection characteristics, ionic diffusivities and Stokes radii for barium and strontium. However, identical values using the S–K model with very good quality of fit further support that electrostatic (Donnan/charge) exclusion had negligible impact on the rejection of these cations.

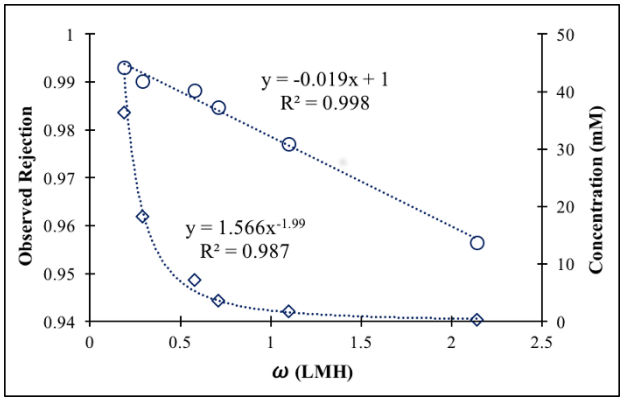

Figure 4.11. Characteristics of observed rejection and feed concentration as a function of modeled solute permeability using Spiegler–Kedem model (Experimental conditions: Feed pressure = 20 bar, crossflow velocity = 1.16 m/s, pH = 5.6 ± 0.2, T = 23 ± 1°C)

Combining correlations shown in Figure 4.11 offers a very simple model (Eq (11)) to predict the rejection of barium and strontium by NF90 membrane over a hundred–fold variation in feed concentration:

$$R_0 = 1 - 0.0238/{C_f}^{0.5} \quad \text{..... (11)}$$

Experimental and modeling results discussed above offer convincing evidence that Spiegler–Kedem model can accurately predict rejection of barium and strontium over a hundred–

fold feed concentration range (i.e., 0.36 – 36.4 mM) by a tight polyamide nanofiltration membrane.

4.5 CONCLUSIONS

A polyamide nanofiltration membrane (NF90) was investigated for the rejection of barium and strontium ions from single salt solutions at relevant process conditions. Analysis of the zeta potential of NF90 membrane at varying concentrations of barium and strontium revealed that neither of these ions specifically adsorb onto the membrane surface as the iso–electric point of the membrane did not change even with a hundred–fold increase in solute concentration. Combining these results with the observed rejection performance at different feed pH lead to a conclusion that electrostatic effects and H^+ rejection do not contribute to rejection of these cations and that size exclusion is the dominant separation mechanism. Increase in the effective pore size by conformal changes to the polyamide active skin layer were responsible for the marginal decrease in the observed rejection (≈ 1 – 2%) with increasing pH for both barium and strontium ions.

Concentration polarization modulus decreased with increase in crossflow velocity, decrease in feed pressure and increase in bulk feed concentration because of increase in shear mass transfer rate, decrease in permeate convection and increase in feed osmotic pressure, respectively. The permeate flux increased with increase in feed pressure but ion rejection stabilized at around 15 – 20 bar for both barium and strontium. Hence, feed pressure of 20 bar and crossflow velocity of 1.16 m/s are recommended as optimal operating conditions based on the observed ion rejection and concentration polarization modulus. Spiegler–Kedem model fitted

very well with the experimental data. The concentration dependent model transport parameters (i.e., permeability and reflection coefficient for solute) indicate that both barium and strontium are equally rejected by the NF90 membrane at all conditions. Maximum rejection of 99.5% and minimum of 92% indicate exceptional performance of NF90 membrane while achieving appreciable permeability between 3.9 – 5.9 LMH/bar.

5.0 LABORATORY AND PILOT–SCALE NANOFILTRATION TREATMENT OF ABANDONED MINE DRAINAGE FOR THE RECOVERY OF PRODUCTS SUITABLE FOR INDUSTRIAL REUSE

This work has been published as:

S.S. Wadekar, T. Hayes, O.R. Lokare, D. Mittal, R.D. Vidic, Laboratory and Pilot–Scale Nanofiltration Treatment of Abandoned Mine Drainage for the Recovery of Products Suitable for Industrial Reuse, Industrial & Engineering Chemistry Research, 56 (2017) 7355–7364.

Because of the problems with sludge formation and inability to meet water reuse standards with traditional limestone neutralization, nanofiltration (NF) has been evaluated for treatment of abandoned mine drainage (AMD). This study contributes to the process of selecting NF membranes based on laboratory–scale studies that is validated in pilot–scale system with real AMD under relevant process conditions to recover: (1) treated water stream (NF permeate) that can serve as a substitute for fresh water in industrial applications, and (2) concentrated sulfate stream (NF reject) that is well–suited to control divalent cations in the produced water from unconventional gas extraction by sulfate precipitation and enable its reuse for hydraulic fracturing of subsequent wells. Eight commercially available NF membranes were tested with synthetic and real AMD in laboratory–scale dead–end and crossflow membrane filtration modules. NF90 membrane was selected for pilot–scale study that consisted of aeration and

sedimentation for iron control, bag filtration and ultrafiltration for particulate control and NF. The system was operated for 208 hours using real AMD at 10 bar and 3.5 GPM feed flow rate and consistently achieved more than 98% removal of TDS at 57% water recovery with a nominal pressure drop of 1.7 bar. Pressure drop monitoring and water permeability tests post pilot–scale study along with chemical equilibrium calculations indicated that no fouling/scaling of the membranes occurred.

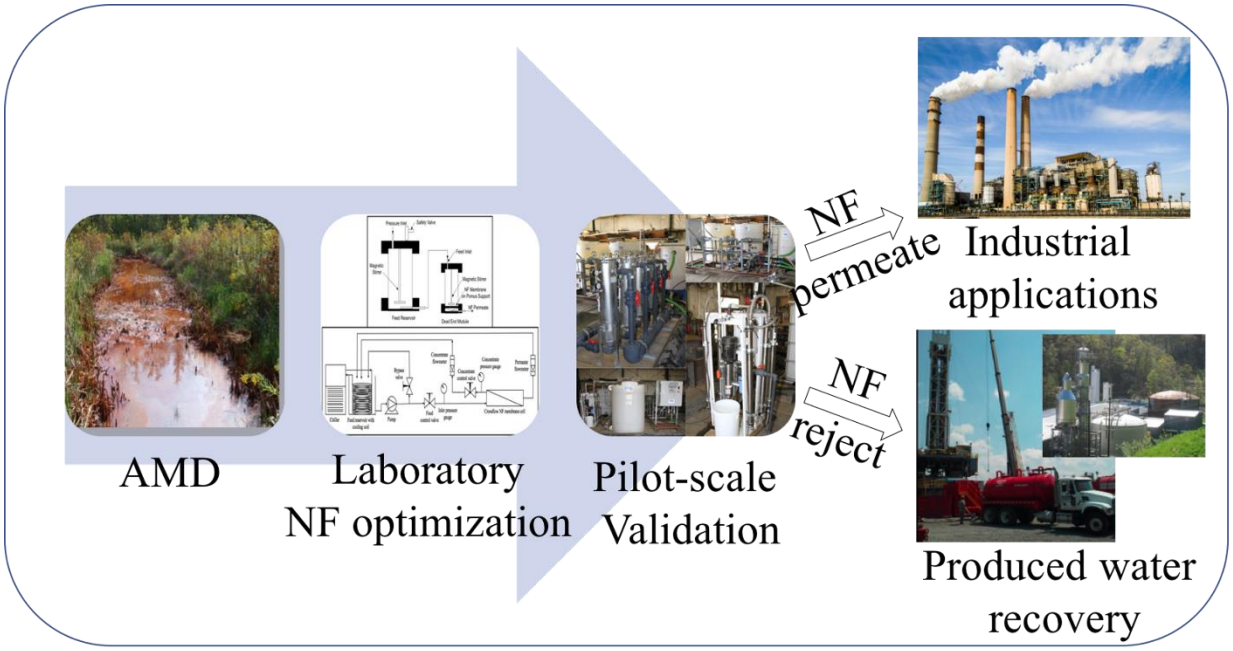

Figure 5.1. Abstract art illustrating the optimized treatment of abandoned coal mine drainage to recover products suitable for industrial reuse using nanofiltration membranes

5.1 INTRODUCTION

Treatment of abandoned or acid mine drainage (AMD) or acid rock drainage (ARD) has been a major research focus for over 50 years [15] because these contaminated streams represent a pervasive environmental problem for both working and abandoned mines. Natural oxidation of sulfide minerals like pyrite (FeS_2), chalcocite (Cu_2S) and mackinawite (FeS) when exposed to water and oxygen contributes most of the contaminants in the AMD [16]. Both underground and open pit mines, as well as tunnels, mill tailings, waste rock dumps and concentrate stockpiles contribute to the AMD problem. The presence of microorganisms, temperature, geology of the mining region and the availability of water and oxygen affect the final composition of the AMD [22]. Typically, AMD is characterized by high acidity (pH 2 – 4), high sulfate concentrations (1 – 20 g/l), and high concentrations of potentially toxic elements (PTEs) such as Al, As, Ca, Cd, Cu, Fe, Mg, Mn, Ni, Pb and Se [17].

Traditionally, lime or limestone neutralization has been used to mitigate the effects of AMD. Lime or limestone is added to increase the pH and to precipitate the sulfate as gypsum and other metals as hydroxides which is followed by gravity separation of the solid product [20-22]. This process generates large quantities of sludge contaminated with PTEs. Another important disadvantage of this process is that the sulfate concentration can only be reduced to about 1,440 mg/l (considering gypsum equilibrium) [17] while Environmental Protection Agency (EPA) and World Health Organization (WHO) stipulate a sulfate limit of 250 mg/l as one of the criteria for unrestricted discharge [23]. Use of sulfate reducing bacteria or cation exchange resin for sulfate removal have been ruled out because of the dependence on external carbon source and costs, respectively [161, 162].

Nanofiltration (NF) has been investigated as a promising technology for AMD treatment [14, 23, 76, 156, 163-167]. Visser et al. [156] studied several commercially available NF membranes with AMD from a South African coal mine and found that NF membranes were capable of rejecting 95 – 99% of sulfate in the feed. The effects of pH, feed pressure, temperature and solution chemistries on sulfate removal have also been documented [14, 17, 76, 165, 167]. Rieger et al. [23] concluded that the rejection of polyvalent ions by NF membranes was comparable to RO membranes and that precipitation of solutes had a significant scaling impact on the process efficiency of both membrane types. Krieg et al. [76] have shown that the rejection of sulfate was highly dependent on the counter ions in the feed. However, there still exists a knowledge gap for the application of this technology for AMD treatment at full–scale as there are very few long–term pilot–scale studies to validate the process parameters and long–term system performance. Bertrand et al. [116] have discussed the product water quality and permeability during the first two years of operation of a NF plant treating water from an iron mine to drinking water standards. NF was preceded by lime softening, sand filtration and addition of an antiscalant. They reported water recovery of 65% with the permeate quality meeting drinking water standards for the entire period. Pilot–scale studies with NF membranes have been conducted for seawater softening [168], improving final drinking water quality [169], and treatment of recycled water [170] and industrial effluents [171].

Along with the recovery of treated water from AMD discharge, the membrane concentrate (reject) produced by nanofiltration membranes can also be utilized for the recovery of flowback and produced water generated by the extraction of natural gas from unconventional (shale) reservoirs using hydraulic fracturing [172, 173]. Recent pilot–scale study showed that mixing AMD with flowback water results in effective removal of barium and strontium while the sulfate

concentration in the effluent can be controlled below 100 mg/l by adjusting the mixing ratio of these waste streams. Also, it was shown that > 99% of radium in the flowback water can be efficiently removed in the form of barite sludge by mixing the sulfate containing AMD with flowback water [174].

In this study, commercial NF membranes were first tested in the laboratory–scale dead–end and crossflow systems using synthetic and real AMD samples to compare these membranes based on sulfate rejection and permeate flux. The selected NF membrane was then studied at a pilot–scale with real AMD to investigate its applicability for full–scale AMD treatment by monitoring the rejection of sulfate and other ions in the feed stream together with permeate flux and pressure drop. Permeability tests with used NF modules were conducted to determine if fouling/scaling had occurred. This comprehensive study offers a protocol for screening NF membranes and provides further support for the use of NF in the recovery of AMD where the permeate stream can serve as a substitute for fresh water in industrial applications while the reject stream is well suited for the control of divalent cations in produced water from unconventional gas extraction to enable its reuse for hydraulic fracturing of subsequent wells.

5.2 EXPERIMENTAL

5.2.1 AMD collection and characterization

AMD samples were obtained from two different locations in Pennsylvania that were considered as possible sources for pilot–scale testing and their characteristics are shown in Table 5.1. AMD A was selected for pilot–scale testing because of easier accessibility while AMD B

was selected for laboratory–scale studies because its composition was similar to AMD A and because the use of different samples for the screening study expands the general applicability of the screening protocol and provides additional information about the ability of NF treatment to respond to natural variability of the source water.

Table 5.1. Characteristics of AMDs selected for this study

Ions	Concentration (mg/L)	
	AMD A	AMD B
Sulfate	786	650 ± 3.5
Chloride	44	76 ± 2.6
Sodium	236	200 ± 3.4
Calcium	107	120 ± 1.3
Magnesium	26	40 ± 2.2
Iron	200	60 ± 3
TDS	1320	1150 ± 10.6
pH	6.6	5.7 ± 0.2

5.2.2 Membranes and chemicals

Eight commercially available flat sheet NF membranes from four different manufacturers that represented three different active layer chemistries (i.e., polyamide, poly(piperazineamide) and cellulose acetate) with a molecular weight cut–off (MWCO) in the range of ~200 – 800 Daltons were used for the laboratory–scale study (Table 5.2). NF90 and NF270 membranes were purchased from DOW Filmtech (Edina, MN) while NF CK and NF HL (GE Osmonics, Minnetonka, MN), NFX, NFW and NFG (Synder Filtration, Vacaville, CA) and XN 45 (Trisep,

Goleta, CA) were all purchased from Sterlitech Corporation (Kent, WA). Water permeability tests were conducted with deionized (DI) water (resistivity = 18 kohm.cm^{-1}) obtained in-house from MilliQ water system (Millipore, Billerica, MA). All chemicals used in this study were analytical grade and were purchased from Fisher Scientific (Pittsburgh, PA).

Table 5.2. Characteristics of NF membranes used in this study

Membranes	MWCO	Active Layer
NF90	~200[a]	Polyamide
NFX	~150-300	Polyamide
NFW	~300-500	Polyamide
NFG	~600-800	Polyamide
NF270	~200-300[b]	Polypiperazine amide
NF HL	~150-300	Polypiperazine amide
XN 45	~500	Polypiperazine amide
NF CK	~400-600	Cellulose acetate

a[76], b[79]

For the pilot–scale study, four NF90–400/34i spiral would membrane modules (nominal active area of 37 m^2 per module) were purchased from DOW Filmtech (Edina, MN). Antiscalant RL9004 used in the pilot–scale study was purchased from ChemTreat (Glen Allen, VA).

5.2.3 Apparatus and filtration process

5.2.3.1 Laboratory–scale studies

Laboratory–scale experiments were carried out in dead–end and crossflow filtration systems. The schematic of the dead–end system is shown in Figure 5.2. The dead–end module

capacity of 340 ml was extended with external 800–ml reservoir to facilitate longer filtration tests. The membrane with exposed area of 44 cm^2 was supported by a porous metal plate and magnetic stirring was used to ensure feed concentration uniformity. Crossflow experiments were carried out in the laboratory–scale test cell SEPA–CFII (GE Osmonics, Minnetonka, MN) with a usable membrane area of 140 cm^2 shown in Figure 5.3 and is explained in detail elsewhere [6]. Feed solution was pumped (Hydra–cell diaphragm pump, Wanner Engineering, MN) from the feed reservoir to the crossflow unit and the concentrate and feed control valves were used to adjust the pressure and flow rate for each experiment. Feed reservoir temperature was maintained using an immersed cooling coil attached to a chiller (6500 series, Polyscience, Niles, IL).

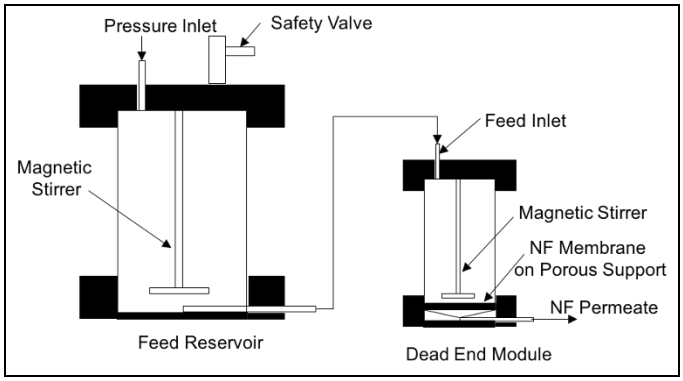

Figure 5.2. Schematic of the dead–end NF system

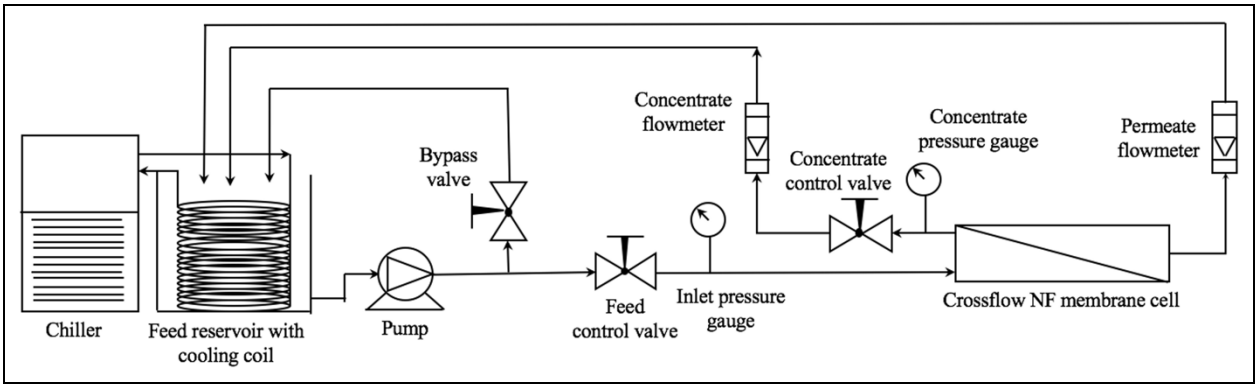

Figure 5.3. Schematic of the crossflow NF system

Pristine membrane used for each experiment was first immersed in DI water for at least 24 hours to ensure that the membrane pores are completely wetted and then compacted with DI water at 50 bar for one hour to ensure that there would be no compaction effects during testing. The membrane was then used to filter DI water at experimental conditions until a stable flux (LMH/bar) was reached. Once stable flux had been established, the feed was changed to a desired composition and the permeate flux was measured over the next two hours during which samples were collected every 15 minutes for chemical characterization. All experiments were conducted at a constant pressure of 10 bar and temperature of 22 $\pm$ 1°C. pH was not altered during any of the experiments and remained at 5.6 ± 0.1 at all times. The rejection of various ions was calculated as:

$$\text{R (\%)} = \frac{c_i^{feed} - c_i^{permeate}}{c_i^{feed}} \times 100$$

where, R is the observed rejection and c_i^{feed} and $c_i^{permeate}$ are the concentrations of ion 'i' in the feed and the permeate, respectively. Cations were analyzed using Inductively Coupled Plasma – Optical Emission Spectroscopy (ICP–OES) (Model 5100, Agilent Technologies, Santa Clara, CA) and anions were analyzed using ion chromatography (IC) (Dionex ICS–1100, Sunnywale, CA) with the IonPac AS22 carbonate eluent anion–exchange column after suitable dilutions with DI water.

Initial experiments in the dead–end filtration system were carried to screen the eight commercial NF membranes obtained for this study with respect to sulfate rejection using the synthetic solution (AMD I) containing 650 mg/L of sulfate. The membranes shortlisted based on

these experiments were tested with real AMD B in the dead–end filtration system. Crossflow experiments with membranes selected from these tests were conducted with two solutions: synthetic solution containing 650 mg/L sulfate, 200 mg/L magnesium and 200 mg/L calcium (AMD II) and real AMD B. Prior to these tests, AMD B was subjected to aeration to precipitate iron and filtration through 0.22 μm pore size membrane to remove the particulates that formed in the solution. All ions were added as $Na_2SO_4.10H_2O$, $CaCl_2.2H_2O$ and $MgCl_2.6H_2O$ salts.

5.2.3.2 Pilot–scale study

The pilot–scale system consisted of aeration and sedimentation for iron control, followed by a bag filter and ultrafiltration membrane (QUA Pure Technology, Canonsburg, PA) with a total membrane area of 2 m^2 for particulate control before treatment with a set of four spiral wound NF membranes connected in series. The process flow diagram of the pilot–scale system is shown in Figure 5.4.

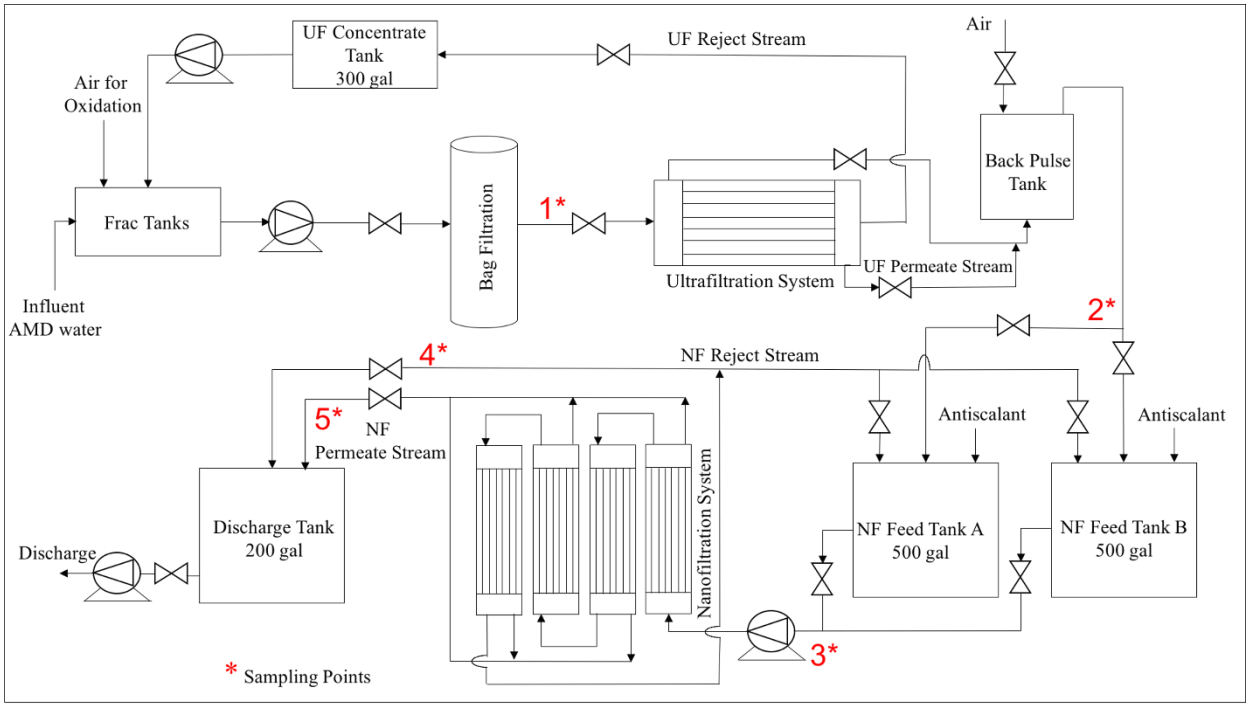

Figure 5.4. Process flow diagram of the pilot–scale system

AMD was shipped to the pilot plant location by water trucks and stored in 20,000 gallon frac tanks. Aeration was carried out in the frac tanks followed by sedimentation to separate the iron precipitates that formed in the tank. Treated AMD was first passed through four bag filters operated in parallel to remove large particles followed by UF as a final pre–treatment step prior to the NF system. Periodic backpulsing was required to clean the particles and sediments that accumulated in the UF membrane and maintain steady permeate flux. UF reject stream was recycled back to the frac tanks while the UF permeate stream was directed to 500–gal NF feed tanks A and B. These tanks served as blending tanks for pH adjustment and the addition of antiscalant prior to NF treatment. The NF system was operated continuously using the blended AMD from one feed tank while the other was being filled with UF permeate and NF reject. Four NF elements were connected in series with permeate streams from all four filters blended together into a single stream to represent the performance of commercial NF membrane elements

at full–scale. Selection of four NF elements in series was based on the calculations done with the Reverse Osmosis System Analysis software provided by Dow Filmtech. Figure 5.5 shows the pilot plant in operation.

Figure 5.5. Pilot plant in operation. Top left: Four bag filters operating in parallel; Top right: Ultrafiltration module (UF membrane is the horizontal white filter); Bottom left: NF reject and UF permeate blending tanks; Bottom right: Four spiral wound NF module

Operational parameters that were monitored throughout the study included pressure drop across the bag filters, UF and NF units, temperatures and flowrates. Nanofiltration system was operated at a pressure of 10 bar and inlet feed flow rate of 3.5 GPM due to feed pump constraints

thereby achieving 57% water recovery. With these input conditions, a permeate flow rate of 2 GPM could be achieved at a nominal pressure drop of 1.7 bar across the NF system during the entire 208 hours of pilot–scale operation. The performance of the pilot plant was characterized by water quality at several locations as indicated on Figure 5.4. Onsite analysis of these samples was performed for pH, conductivity, sulfate, iron and hardness using methods listed in Table 5.3. Following the startup period, hourly monitoring of sulfate concentration was performed until a steady state had been achieved. The sulfate concentration in the feed was increased from about 700 ppm to about 1,700 ppm by adding NF reject to the feed tanks to test the capability of the membrane system to treat more challenging AMD streams. Each batch of feed for the NF unit was prepared by blending 140 gallons of the NF reject stream with 325 gallons of the UF permeate. Six samples collected throughout the pilot–scale testing were sent to a commercial analytical laboratory (Test America, Pittsburgh, PA) for detailed chemical characterization that included sulfate and chloride, along with major and trace metals (Ag, Al, As, Ba, Be, Ca, Cd, Co, Cr, Cu, Fe, K, Mg, Mn, Ni, Pb, Sb, Se, Tl, V, Zn), total dissolved solids (TDS) and total organic carbon (TOC).

Table 5.3. Instruments and methods used for onsite analytical determinations

Instrument	Parameter	Method
Hach DR2700	Sulfate	Hach Method 8051 using SulfaVer® Powder Pillows
	Iron	Hach Method 8008 using FerroVer® Powder Pillows
Hach Digital Titrator Kit	Hardness	Hach Method 8213

5.3 RESULTS AND DISCUSSION

5.3.1 Laboratory–scale optimization

5.3.1.1 Dead–end experiments

Figure 5.6 shows rejection and permeate flux from screening experiments using AMD I by eight NF membranes obtained in a dead–end test system. Sulfate rejection was selected as the primary screening factor because it is the most important AMD constituent that governs the usability of NF permeate and reject for industrial applications [18, 22, 77] and because ion rejection by NF membranes is most influenced by divalent ions [98]. As can be seen from Figure 5.6 (a), all membranes were able to achieve between 80 – 92% sulfate rejection with NFG membrane being the only exception. Low sulfate rejection by NFG (20%) can be explained by its MWCO of ~600 – 800 Daltons (Table 5.2). Hence, the NFG membrane was eliminated from further consideration. NF CK membrane achieved the highest sulfate rejection of 92% despite having relatively high MWCO but it also exhibited the lowest permeate flux of only 1.2 LMH/bar. Interactions of cellulose acetate with ionic solutions are different than those of polyamide or polypiperazine amide [175, 176], which may explain higher sulfate rejection by cellulose acetate membrane despite having slightly higher MWCO. However, because of very low permeate flux, NF CK membrane was also eliminated from further consideration. The remaining thin film composite (TFC) membranes can be broadly classified into two groups based on the active layer chemistry: polyamide (NF90, NFX and NFW) and polypiperazine amide (NF270, NF HL and XN 45). It has been shown that the rejection mechanisms of TFC membranes are influenced by the type of active layer chemistry [1, 33, 34]. Hence, NF90 membrane was selected from the polyamide group for further study as it achieved better rejection

than NFW membrane and higher permeate flux than both NFX and NFW membranes. Also, NF270 membrane was selected from the polypiperazine amide group because it exhibited higher sulfate rejection and higher permeate flux than the other two membranes.

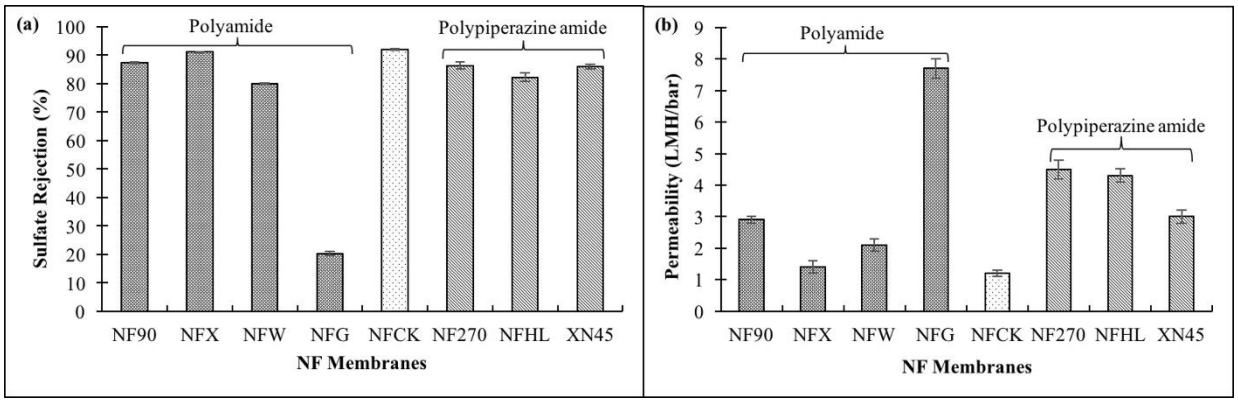

Figure 5.6. (a) Sulfate rejection and (b) permeate flux for 8 commercial NF membranes with synthetic AMD I in dead–end module

Dead–end filtration tests with these membranes using real AMD (i.e., AMD B) revealed that NF90 achieved 75% sulfate rejection while NF270 could only achieve about 45% sulfate rejection. It is important to note that the sulfate rejection decreased with real AMD when compared with the results obtained with synthetic solution shown on Figure 5.6 (a) because of the complex composition of real AMD that contains many other ions like Ca, Mg and Cl along with Ni, Se as well as some organic compounds. The membrane surface becomes more positively charged in the presence of cations because of preferential adsorption of these ions, which contributes to the reduced rejection of the negatively charged sulfate ions [91, 93, 177]. Krieg et al. [76] reported a decrease in sulfate rejection in the presence of sodium and chloride ions. Also, NF270 is a looser membrane [14] compared to NF90 (Table 5.2) and would therefore

be less effective in rejecting sulfate ions. These screening experiments suggested that NF90 membrane would be preferred over NF270 for treatment of real AMD.

5.3.1.2 Crossflow experiments

Tests with NF90 and NF270 membranes in the crossflow module with synthetic and real AMD were performed for more than 4 hours at constant feed concentration (i.e., both permeate and reject were returned back to the feed tank) using AMD II (i.e., synthetic solution). Figure 5.7 shows that NF90 achieved > 97% rejection of all ions with sulfate rejection above 99%. On the other hand, NF270 membrane achieved about 96% sulfate rejection, 91 – 94% rejection of the divalent cations and less than 70% rejection of monovalent ions. NF90 and NF270 membranes have isoelectric point (IEP) of 4.2 and 2.8, respectively [79]. Because these crossflow tests were conducted at pH of 5.6 ± 0.1, which is above the IEPs of both these membranes, negative surface charge contributed to high sulfate rejection [165, 178, 179]. Along with high sulfate rejection, cations would also have to be rejected to balance the electroneutrality on both sides of the membrane [99]. Hence, cations are efficiently rejected in accordance to their diffusion coefficients and Stokes radii [97], so that the rejection order of cations was $R(Mg^{+2}) > R(Ca^{+2}) > R(Na^{+})$. In addition, NF90 has smaller effective pore size than NF270 membrane [88, 95, 113], which explains better rejection of monovalent ions by NF90 membrane. NF90 was previously shown to achieve higher rejection of calcium and magnesium [79, 95], boron and total dissolved solids [90] and nitrate [96] compared to NF270. It should also be noted that sulfate rejection achieved in the crossflow module (Figure 5.7) was much higher than in the dead–end module (Figure 5.6 (a)). It is argued that the shear force in the dead–end module is high and in the direction of flow, which may force the ions to shed hydration water (i.e., dehydrate) and permeate through the membrane as compared to the parallel flow in the crossflow module [46].

Also, feed concentration in the dead–end module increases with time, thereby increasing the concentration polarization at the feed side and reducing the rejection of inorganic species with time. Although concentration polarization is also present in the case of a crossflow module, it is mitigated by the shear force caused by the horizontal feed flow, so that the rejection efficiency is less impacted than in the case of a dead–end module [180].

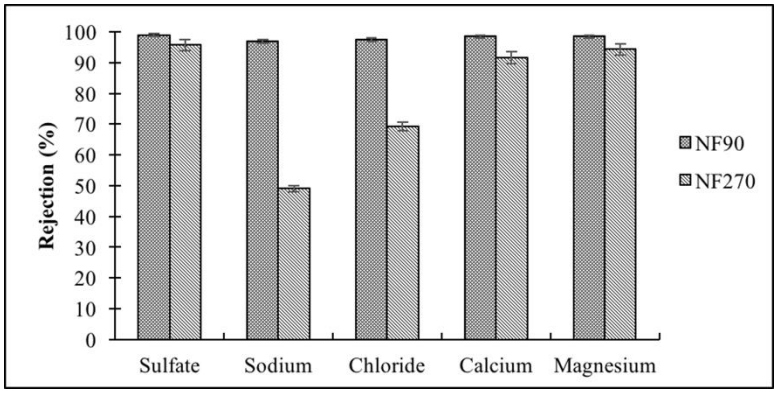

Figure 5.7. Ion rejection by NF90 and NF270 with AMD II solution in a crossflow module

Results in Figure 5.7 clearly favor the use of NF90 membrane over NF270 for AMD treatment. Figure 5.8 shows rejection of various ions and permeate flux with NF90 membrane over the test period of four hours in the crossflow module using real AMD B. This membrane was able to achieve > 99% rejection of sulfate, while the rejection of divalent cations and monovalent ions was > 98% and > 88%, respectively. The observed performance is in agreement with the studies using synthetic AMD II (Figure 5.7). As seen from Figure 5.8 (b), the average permeate flux of 2.7 LMH/bar was virtually constant over the entire test period, which suggests that no appreciable scaling/fouling occurred under the experimental conditions used in this test with real AMD.

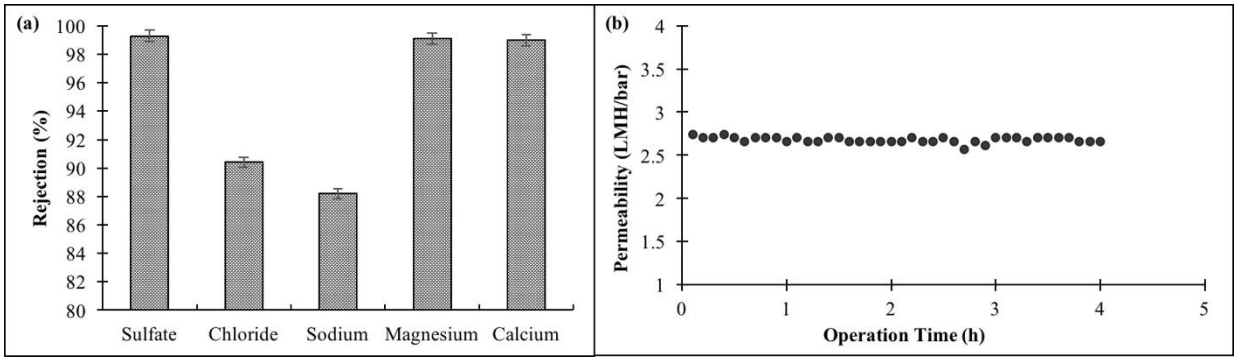

Figure 5.8. (a) Ion rejection and (b) permeate flux for NF90 membrane with AMD B in a crossflow module

5.3.2 Pilot–scale study

Based on these laboratory studies, NF90 membrane was selected for pilot–scale testing using real AMD A. Table 5.4 shows average composition of UF permeate that was blended with a portion of NF reject to achieve higher concentration of sulfate in the NF influent stream. Each value shown in Table 5.4 is an average of six samples collected after 20, 54, 89, 135, 170 and 193 hours of the pilot–scale operation.

Table 5.4. Chemical characteristics of different streams in the pilot–scale system

Streams	pH	Concentration (mg/l)				
		TDS	Sulfate	Chloride	Calcium	Magnesium
UF Permeate	7.2 ± 0.3	1,250 ± 55	780 ± 25	61 ± 2	101 ± 7	22 ± 2
NF Influent	5.5 ± 0	2,672 ± 296	1,732 ± 86	140 ± 14	218 ± 21	45 ± 5
NF Reject	4.6 ± 0.6	6,233 ± 484	3,941 ± 287	323 ± 43	490 ± 56	100 ± 12
NF Permeate	5.1 ± 0.8	38.3 ± 11.6	7.4 ± 2	13.5 ± 4	1.1 ± 0.3	0.3 ± 0.1
Rejection (%)	-	98.6	99.6	90.4	99.5	99.4

Rejection of sulfate, chloride, calcium, magnesium, selenium and nickel achieved in the pilot–scale system is shown in Figure 5.9 while TDS and TOC removal is shown in Figure 5.10.

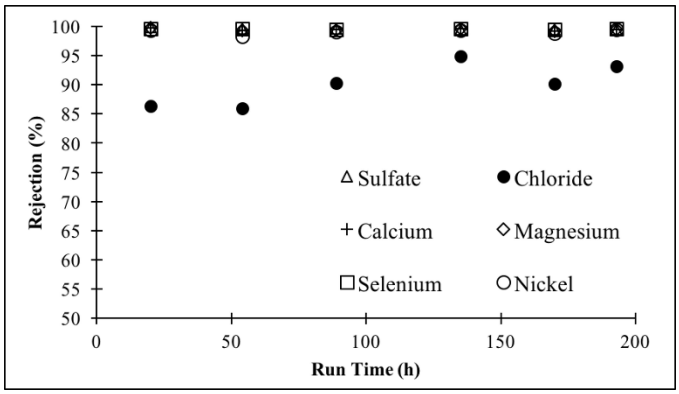

Figure 5.9. Rejection of sulfate, chloride, calcium, magnesium, selenium and nickel by NF90 in a pilot–scale test

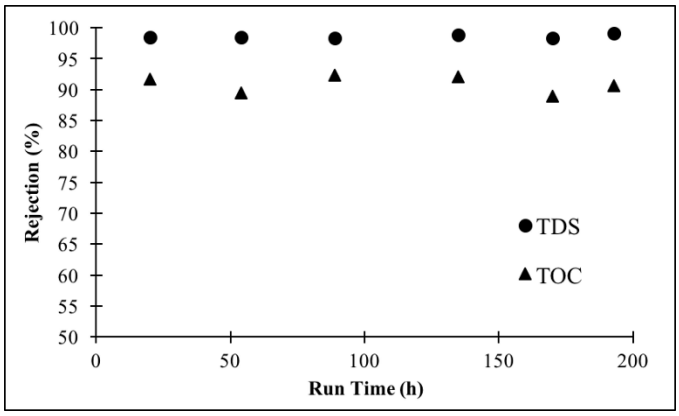

Figure 5.10. TDS and TOC rejection by NF90 in pilot–scale test

The pilot plant was successfully operated for over 200 hours while achieving stable sulfate rejection of more than 99% over the entire period of study. In addition, more than 99% removal of calcium and magnesium was also achieved together with over 98% TDS removal. Other studies have also reported 95 to > 99% sulfate rejection along with 90 – 99% rejection of metal ions when treating AMD with NF membranes but at laboratory–scale [16, 17, 165, 167]. Ion rejection observed in laboratory–scale experiments corresponds very well to those observed in

the pilot–scale test. Divalent and monovalent ion rejection of > 98% and > 88%, respectively was observed in the laboratory–scale crossflow tests while in case of pilot–scale, rejections observed were > 99% and 90%, respectively. This agreement highlights the importance of the laboratory–scale screening protocol and the crossflow tests. In addition, it is also important to note that the NF90 membrane also achieved an average of 90% rejection of chloride ions. NF90 is a tight polyamide membrane and hence can reject even the smaller monovalent ions effectively [1]. Water recovery of 57% was achieved during the pilot–scale operation, which adds credit to this study that demonstrated very high rejection of ions along with high water recovery that is comparable to full–scale operation. Mass balance calculations for all ionic species were close to 100% (data not shown) indicating requisite pilot–scale monitoring and high quality analytical measurements.

Trace and minor elements were also measured during the pilot–scale study to evaluate the feasibility of extending the results of this study to other applications. Among the trace elements analyzed in this study, selenium and nickel were present at an average concentration of 95 ± 8.4 μg/l, 155 ± 17.6 μg/l and 2.83 ± 0.7 mg/l respectively. Even at such low concentrations, the NF system was able to reject > 99% selenium (permeate concentration of 0.46 ± 0.07 μg/l) and > 98% nickel (permeate concentration of 1.13 ± 0.67 μg/), which confirms a very good potential for the removal of trace constituents of interest for reusing AMD for many other applications. Figure 5.10 shows that average TOC removal of 90% (permeate concentration of 0.26 ± 0.09 mg/) was also achieved by the pilot–scale system, confirming that the NF90 membrane is also capable of efficiently rejecting both small ions and large organic molecules at very dilute concentrations.

5.3.3 Fouling analysis

Fouling analysis of the membranes used in the pilot–scale study was carried out by monitoring the pressure drop across the NF system and conducting the clean water permeability tests with the spiral would NF modules used in the pilot–scale system in combination with chemical equilibrium calculations using PHREEQC (Version 3.1.7, USGS) software package.

As seen in Figure 5.11, the pressure drop across the NF system during the pilot plant operation experienced some fluctuation initially but stabilized at about 1.7 bar after 50 hours of operation and remained constant for the remainder of the pilot plant operation. This low and stable pressure drop suggests that almost no membrane fouling occurred during the pilot plant operation (pressure drop increase of 10 – 15% suggests the need for membrane cleaning [57]).

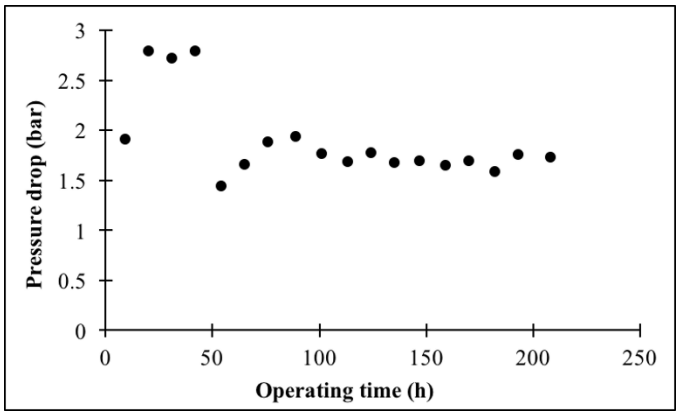

Figure 5.11. Pressure drop across the pilot–scale NF system

After the completion of pilot–scale study, permeability test with DI water was conducted separately on the first and fourth NF module connected in series. The inlet feed pressure for these tests was adjusted to 10 bar, which is identical to the value used in pilot–scale study. However, feed flow rate of only 2.1 GPM could be achieved in the laboratory–scale testing

because of pump limitations. Under these conditions, a permeate flow rate of 0.7 GPM was measured for both NF modules. Because the NF modules were connected in series with the reject of the preceding module serving as the feed for the next module, the fourth module would have seen the most concentrated feed and hence would be the most vulnerable to fouling/scaling. However, a constant and equal permeate flow rate was measured for both module in these permeability tests, which confirms that no measurable fouling of NF membranes occurred during the 208 hours of pilot–scale operation.

Thermodynamic calculations with PHREEQC chemical speciation software were also used to predict the saturation index (SI) for the salts that might precipitate during the pilot plant operation. These calculations revealed that none of the potential inorganic precipitates would form under the NF feed stream experimental conditions in the pilot–scale system (i.e., feed composition and pH). Gypsum ($CaSO_4.2H_2O$) had a slightly positive SI (i.e., 0.06) considering NF reject stream composition and pH. However, the pressure drop monitoring across the NF system (Figure 5.11) and DI permeability tests support the conclusion that gypsum scales did not form in sufficient quantity to cause a change in membrane performance. Al-Zoubi et al.[17] reported no membrane fouling even for a highly concentrated synthetic AMD with a SI of 0.16 for gypsum. In addition, Colburn et al. [181] report no fouling/scaling issues with gypsum even at high calcium and sulfate concentrations, which they claim was because the formed gypsum particulates did not adhere to the membrane surface on account of the convective crossflow. Also, PHREEQC simulations suggest that $Fe(OH)_3$ (SI = 4.58) and Geothite (FeOOH, SI = 10.47) would have precipitated during the pilot–scale study if iron had not been removed in the pre–treatment step. Fouling by iron scales has been reported to impact the membrane permeate

flux [115], which thereby emphasizes the importance of pre–treatment for the removal of iron in a full–scale system.

5.3.4 AMD reusability

The pilot plant operated in this study recovered two separate streams (i.e., NF permeate ad NF reject/concentrate) from highly contaminated AMD stream. NF permeate had TDS < 50 mg/l with a sulfate concentration < 10 mg/l while calcium and magnesium were present at an average of about 1 mg/l and 0.3 mg/l respectively. The permeate quality exceeds the drinking water standard in terms of the TDS, TOC and individual ions [182, 183] and represents a new source of fresh water. This stream could be used for a number of different applications, like makeup water for cooling in power plants [184], irrigation [185, 186], dairy industry [187], construction industry, creating artificial wetlands and enhancing natural wetlands [188], groundwater replenishment and salt water intrusion control [189]. The NF reject/concentrate had TDS of about 6,500 mg/l with a very high sulfate concentration of 4,000 mg/l. This represents a viable source of sulfate for treating the produced and flowback water from unconventional gas industry to remove the scale causing cations (i.e. barium, strontium) by sulfate precipitation to enable its reuse for hydraulic fracturing. Barium and strontium are present in produced waters at concentrations as high as 6,000 and 12,000 mg/l, respectively [130] and the fast sulfate precipitation kinetics [190, 191] is particularly suitable for the recovery of huge quantities of these impaired waters. In addition to barium and strontium precipitation, the barite sludge has also been reported to co–precipitate radium resulting in > 99% radium removal [174], which ensures permanent sequestration of naturally occurring radioactive materials (NORM) from the radiogenic waters produced in Marcellus Shale region.

5.4 CONCLUSIONS

This study was designed to optimize and validate the use of nanofiltration membranes for treatment of AMD at full–scale to produce two streams: treated water stream that can serve as a substitute for fresh water in industrial applications and a concentrated sulfate stream that is ideally suited for use in produced water treatment for sulfate precipitation to control divalent cations in the finished water and enable its reuse for hydraulic fracturing of subsequent wells.

Laboratory–scale screening of eight commercially available NF membranes was performed with synthetic AMD solutions in a dead–end module and two membranes, i.e., NF90 and NF270, were selected for testing with real AMD solution based on sulfate rejection and permeate flux. These membranes were also tested in the crossflow module where NF90 membrane performed better than NF270 membrane in terms of rejection of all ions of interest. Hence, NF90 membrane was selected for pilot–scale study.

The NF90 membrane exhibited impressive performance in the pilot–scale system by achieving very high removal of sulfate from the real AMD. The sulfate concentration in the feed solution of about 1,700 mg/l was reduced to less than 10 mg/l, representing more than 99% sulfate removal during 208 hours of continuous operation. In addition, more than 99% rejection of calcium, magnesium, nickel and selenium was observed in the pilot–scale tests with total dissolved solids and total organic carbon rejection of 98% and 90%, respectively. The NF system also achieved about 90% chloride removal which points towards a potential benefit in conditioning water for use in industries that are sensitive to corrosion issues.

The pre–treatment comprised of aeration, sedimentation, bag filtration and ultrafiltration used in the pilot–scale study was highly effective in removing iron from the feed stream to facilitate stable operation of the NF system over the 208–hour period. A steady–state water

recovery of 57% was achieved with the feed pressure of 10 bar and feed flow rate of 3.5 GPM during the entire pilot plant operation. Chemical equilibrium calculations indicate a very small degree of gypsum supersaturation but a constant pressure drop of about 1.7 bar during pilot–scale testing and DI water permeability tests on used NF modules confirmed that no measurable fouling/scaling occurred with this particular AMD. Thus, the goal of producing two valuable product streams, one of high quality (NF permeate with TDS < 50 mg/l) and the other with high sulfate concentration (NF reject with a sulfate concentration of about 4,000 mg/l, which can be used to recover flowback and produced water), was successfully accomplished in this study.

In addition, laboratory–scale experiments clearly indicate that testing in a dead–end module can only be used for relative comparison of NF membranes while the crossflow system facilitates a detailed process study to optimize NF performance. The performance of NF membrane in a crossflow laboratory–scale system compares well with that observed in the pilot–scale system, which confirms the scalability of membrane filtration process and further emphasizes the value of laboratory–scale tests in a crossflow module to predict full–scale system performance.

6.0 COMPARISON OF CERAMIC AND POLYMERIC NANOFILTRATION MEMBRANES FOR TREATMENT OF ABANDONED COAL MINE DRAINAGE

This work has been published as:

S.S. Wadekar, R.D. Vidic, Comparison of ceramic and polymeric nanofiltration membranes for treatment of abandoned coal mine drainage, Desalination, (2018), 440 (2018) 135-145.

Performance of ceramic and polymeric nanofiltration membranes for treatment of abandoned mine drainage from a coal mine was investigated in this study. The increase in permeate recovery improved ion rejection but reduced the permeability for both membranes. Arsenic was poorly rejected by both membranes with maximum rejection being 33% for the polymeric membrane. Fouling occurred at 75% permeate recovery and was dominated by gypsum scales. Chemical cleaning improved permeability but reduced ion rejection indicating a slight increase in the effective membrane pore size for both membranes. When feed pH was adjusted to 4, ion rejection increased for the ceramic membrane and decreased for the polymeric membrane due to impacts on the charge of the active layer. Addition of antiscalant improved ion rejection for both membranes, especially for arsenic whose rejection improved by at least 141%, but resulted in about 40% decrease in permeability for both membranes and was attributed to the formation of a more complex and gel–like scale. A tighter polymeric nanofiltration membrane

achieved more than 99% rejection of all multivalent ions to meet all drinking water standards except for arsenic, which has to be removed prior to nanofiltration step.

6.1 INTRODUCTION

Membrane technology has been increasingly applied in wastewater treatment and desalination applications over the last few decades. Use of polymeric microfiltration (MF), ultrafiltration (UF), nanofiltration (NF) and reverse osmosis (RO) membranes has been growing exponentially owing to their wide set of separation characteristics for different applications [62]. Ceramic membranes have recently been gaining prominence due to better resistance to fouling, easier cleaning, lower maintenance, better thermal resistance and greater mechanical strength [36, 37]. Ceramic NF membranes are commonly made using the sol–gel technique with Al_2O_3, ZrO_2 or TiO_2 as the active layer, with the latter two preferred due to greater stability [38]. Ceramic membranes are typically available with molecular weight cut–off (MWCO) close to ~ 1000 Da and have been applied to remove organic molecules and natural organic matter (NOM) [39, 40]. Newer manufacturing techniques like atmospheric pressure atomic layer deposition (APALD) [41] and DNA template technology [42] are being studied to manufacture ceramic NF membranes with MWCO below 500 Da that could effectively reject multivalent ions. This study was designed to compare ceramic and polymeric NF membranes for treatment of abandoned or acid mine drainage (AMD) from a coal mine in terms of ion rejection and fouling behavior.

AMD has been a major environmental concern over the past five decades as it is a highly contaminated stream with high acidity (pH 2 – 4), high sulfate concentration (0.1 – 20 g/L) and presence of potentially toxic elements (PTEs) such as Al, As, Ca, Cd, Cu, Fe, Mg, Mn,

Ni, Pb and Se [16]. Most of these contaminants occur from the natural oxidation of sulfide minerals like pyrite (FeS_2), chalcocite (Cu_2S) and mackinawite (FeS) when in contact with water and oxygen [17, 165]. Because the conventional AMD treatment with limestone addition cannot achieve requisite effluent standards [20], other techniques for sulfate removal, including sulfate reducing bacteria [161] or cation exchange resin [162] have been investigated; however, these techniques are not widely accepted as they depend on the external carbon source and have high cost, respectively. Polymeric NF membranes have been investigated to achieve effluent standards [16, 17, 23, 76, 116, 156, 167] or even drinking water standards [116]. Commercially available NF membranes can reject > 95% sulfate with real AMD [156] and their performance depends on pH, temperature, operational conditions and feed quality [76, 167]. Two recent studies successfully tested polymeric NF membranes at pilot–scale and offered information on operational and maintenance costs [114, 192] and concluded that AMD pre–treatment is essential prior to the use of NF membranes to treat AMD.

Ceramic NF membranes have been previously tested with simple synthetic solutions of NaCl, KCl and Na_2SO_4 [38, 193]. Chen et al. [193] found that ceramic NF membrane with a MWCO of 900 Da rejected 10% chloride and about 40% sulfate in addition to effectively rejecting various dyes. Gestel et al. [38] found that the rejection of simple monovalent and divalent ions was minimal at the iso–electric point (IEP) or point of zero charge (PZC) of the membrane. 85% rejection of NaCl and 95% rejection of Na_2SO_4 was reported at low and high pH.

Fouling has been a major concern with membrane treatment [55, 58, 107, 130, 194] and chemical cleaning is typically applied when the permeability decreases by about 10% or when the pressure drop increases by about 10 – 15% [58]. Therefore, it is critically important

to understand both performance and fouling characteristics of ceramic NF membranes to ensure optimal performance for any application.

This study compared the performance and fouling characteristics of ceramic and polymeric NF membranes for AMD treatment. The performance was characterized by ion rejection and permeability as a function of permeate recovery rates. Fouling and fouling mitigation strategies were investigated in terms of the type of foulants and the effects of pH adjustment and antiscalant addition on performance of the ceramic and polymeric NF membranes. The efficiency of chemical cleaning procedures for recovery of membrane performance was also evaluated in this study.

6.2 EXPERIMENTAL

6.2.1 Membranes and AMD

Ceramic nanofiltration membrane prototype (MWCO of ~500 Da) comprised of fused alumina and active surface layer of amorphous titania (TiO_2) and was provided by Cerahelix (Orono, ME). DNA template technology was used to make linear and identical pores with typical size of 1 nm [195]. Polypiperazine amide membrane (NF270) with MWCO of ~200 – 300 Da (Dow Filmtech, Edina, MN) and polyamide membrane (TS80) with MWCO of ~150 Da (Trisep, Goleta, CA) were also used in this study. Pore radii of 0.87 ± 0.02 nm and 0.71 ± 0.02 nm for NF270 and TS80 membranes, respectively have been measured using the membrane potential technique [1]. Water permeability tests were conducted with deionized (DI) water obtained from MilliQ water system (Millipore, Billerica, MA). Dilute NaOH, HCl and $Na_2SO_4.10H_2O$ were

purchased from Fisher Scientific (Pittsburgh, PA). Antiscalant RL9004 used for fouling mitigation was purchased from ChemTreat (Glen Allen, VA). Dilute NaOH and HCl were used for pH adjustment.

AMD was collected from a site in southwestern Pennsylvania. The actual AMD had about 60 mg/L of total dissolved iron, which had to be removed before nanofiltration to prevent severe fouling. Hence, 20 – 24 h of aeration followed by filtration through 0.22 μm membrane preceded all NF tests. The composition of AMD post aeration and microfiltration is given in Table 6.1.

Table 6.1. Characteristics of AMD post aeration and microfiltration

Ions	Concentration
Sulfate (mg/L)	645.9 ± 2.5
Chloride (mg/L)	97.8 ± 1.9
Sodium (mg/L)	108.9 ± 4.2
Calcium (mg/L)	151.8 ± 2.1
Magnesium (mg/L)	29.7 ± 1.1
Potassium (mg/L)	4.3 ± 1.6
Manganese (mg/L)	1.2 ± 0.6
Strontium (mg/L)	1.7 ± 0.3
Barium (μg/L)	76.7 ± 4.1
Aluminum (μg/L)	50.5 ± 1.2
Nickel (μg/L)	38.5 ± 4.9
Arsenic (μg/L)	70.0 ± 6.4
Selenium (μg/L)	55.2 ± 3.9
Total iron (mg/L)	< 0.02
pH	7.8 ± 0.2

6.2.2 Module and experiments

All NF experiments with polymeric membranes were carried out in the laboratory–scale test cell SEPA–CFII (GE Osmonics, Minnetonka, MN) with a usable membrane area of 140 cm^2 [6]. Pristine polymeric membrane used for each experiment was immersed in DI water for at least 24 h to ensure complete wetting of membrane pores. Each polymeric membrane was first exposed to DI feed pressure of 50 bar for 1 h to ensure no compaction effects during testing and

DI water permeability was measured at experimental pressures for membrane integrity testing. Ceramic membrane tests were conducted in the same system except that the SEPA–CFII module was replaced with the housing designed for a single channel tubular membrane with diameter of 6 mm and length of 500 mm (total nominal membrane area of 100 cm^2). Unlike polymeric membranes, no compaction of ceramic membranes was necessary prior to testing with AMD.

Assessment of recovery rate: The first step in this study included the assessment of the effect of permeate recovery rate (i.e., 0%, 50% and 75%) on membrane performance followed by fouling analysis. The feed tank was filled with 20L of AMD and was allowed to stabilize for 2 h with total recirculation when samples corresponding to 0% recovery were collected. The system was monitored for the next 24 h to collect transient permeability and conductivity rejection data at 0% recovery. After that, 10L of permeate was collected to achieve a 50% recovery rate. The ceramic membrane was then chemically cleaned and the polymeric membranes were replaced. Permeate samples were collected after 2 h of stabilization in total recirculation mode and transient permeability and conductivity rejection data were monitored for the next 24 h. After that, 5L of additional permeate (i.e., a total of 15L permeate) was removed from the system and membranes were either cleaned (ceramic) or replaced (polymeric) prior to collecting samples for 75% recovery after 2 h of stabilization period with total recirculation. Transient permeability and conductivity rejection data was also collected over the next 24 h.

Fouling analysis: Only one ceramic membrane was available and hence it had to be chemically cleaned prior to testing new process parameters. Unlike the ceramic membrane, a new polymeric membrane was employed each time since the used membrane underwent destructive analysis by scanning electron microscopy (SEM, JEOL JSM6510, Peabody, MA) and energy dispersive X–ray spectroscopy (EDS) to characterize the fouling layer.

Assessment of chemical cleaning: The effect of chemical cleaning on membrane performance was evaluated using chemical cleaning procedures shown in Table 6.2. The performance data were compared at 75% AMD recovery to evaluate the efficiency of chemical cleaning.

Fouling mitigation strategies: Two fouling mitigation strategies, namely pH adjustment and antiscalant addition, were evaluated in this study. Membrane performance with no antiscalant addition or pH adjustment at 75% AMD recovery was compared with that when feed pH was adjusted to 4 or when 15 mg/L of antiscalant was added to the feed. In each case, the membrane was stabilized for 2 h followed by permeate sample collection to determine ion rejections and then measurement of transient permeability and conductivity data over the next 24 h period.

All experiments were conducted at a constant pressure of 35 bar, temperature of 25 ± 1°C and feed flow rate of 5.68 LPM unless otherwise indicated. This feed flow rate corresponds to a crossflow velocity of 1.16 m/s with the flat sheet polymeric membranes and 3.35 m/s with the tubular ceramic membrane. The rejection of various ions was calculated as:

$$\text{R (\%)} = \frac{c_i^{feed} - c_i^{permeate}}{c_i^{feed}} \times 100$$

where, R is the observed rejection and c_i^{feed} and $c_i^{permeate}$ are the concentrations of ion 'i' in the bulk feed and the bulk permeate, respectively. Al, Ba, Ca, K, Mg, Mn, Na and Sr were analyzed using Inductively Coupled Plasma–Optical Emission Spectroscopy (ICP–OES) (Model 5100, Agilent Technologies, Santa Clara, CA) and Se, As, and Ni were analyzed using Inductively Coupled Plasma–Mass Spectroscopy (ICP–MS) (Model 7700x with HEHe–mode octopole reaction cell, Agilent, Santa Clara, CA). Operating conditions for the ICP–MS were

optimized daily via the autotune function of the Agilent MassHunter software using 1000:1 diluted Agilent tuning solutions [196]. All anions were analyzed using ion chromatography (IC) (Dionex ICS–1100, Sunnywale, CA) with the IonPac AS22 carbonate eluent anion–exchange column after suitable dilutions with DI water. Total iron concentration was measured using HACH method 8008 with FerroVer powder pillows (measurement range = 0.02 – 3.00 mg/L). All experiments to assess the recovery rate, effect of chemical cleaning and those with synthetic solutions were performed in duplicates. All the remaining experiments were performed only once because: (1) real AMD was available in limited quantities for testing, (2) the standard deviations for the experiments run in duplets were very small (maximum of ± 0.25 LMH/bar for permeability and ± 0.3% for ionic rejection) and (3) only one ceramic NF membrane was available for testing.

Table 6.2. Chemical cleaning steps employed for testing the cleaning efficiency with ceramic and polymeric (NF270) membrane

Steps	Ceramic membrane	Polymeric (NF270) membrane
1	Flush out process water	Flush out process water
2	High flowrate DI water flush – 5 L	High flowrate DI water flush – 5 L
3	High flowrate flushing with NaOH (pH 10) – 5 L	Low flowrate flushing with 0.1% wt NaOH (pH 11) – 5 L
4	High flowrate recirculation with NaOH (pH 10) – 15 min	Soaking in 0.1% wt NaOH (pH 11, no pumping used) – 1 h
5	High flowrate flushing with citric acid – 5 L	High flowrate recirculation with 0.1% wt NaOH (pH 11) – 15 min
6	High flowrate recirculation with citric acid – 15 min	Low flowrate flushing with 0.1% wt HCl (pH 2) – 5 L
7	Again, high flowrate recirculation with citric acid – 15 min	Soaking in 0.1% wt HCl (pH 2, no pumping used) – 1 h
8	DI water flush – 5 L	High flowrate recirculation with 0.1% wt HCl (pH 2) – 15 min
9	High flowrate DI water recirculation – 15 min	DI water flush – 5 L
10	DI water flush – 5 L	High flowrate DI water recirculation – 15 min
11	–	DI water flush – 5 L

High and low flow rates correspond to 9.46 and 1.89 LPM feed flow rates respectively. No feed pressure was applied during any cleaning procedure.

6.3 RESULTS AND DISCUSSION

6.3.1 Effect of feed sulfate concentration on membrane performance

Sulfate is the major contaminant in AMD that can be present at concentrations as high as 20 g/L. Hence, the effect of sulfate concentration on the rejection and permeability was first tested with synthetic solution containing 500 – 10,000 mg/L sulfate prepared using $Na_2SO_4 \cdot 10H_2O$ in DI water. Figure 6.1 shows sulfate rejection and permeability with increasing sulfate concentration for ceramic and NF270 membranes. As can be seen in Figure 6.1 (a), sulfate rejection increased very slightly or did not change in the case of NF270 membrane but it increased from 17 to 68% with increasing sulfate concentration for the ceramic NF membrane. Adsorption of sulfate on the active layer of ceramic NF membrane that enhanced transport resistance due to increased electrostatic interactions might be one of the major mechanisms to explain more than 3–fold increase in sulfate rejection. The permeability decreased from 2.5 to 1.4 LMH/bar in the case of ceramic and from 12.8 to 9.1 LMH/bar for NF270 membrane (Figure 6.1 (b)). This can be attributed to the increase in the feed osmotic pressure, which increased from 0.13 to 2.58 bar (neglecting concentration polarization) with an increase in sulfate concentration from 500 to 10,000 mg/L. The polymeric membrane achieved effective rejection of sulfate even at very high feed concentrations. It also achieved higher permeability than the ceramic membrane in spite of having a slightly lower MWCO. Such behavior may be due to the thickness of active layers of the two membranes with thicker active layer for maintaining the mechanical integrity of the ceramic membrane resulting in increased mass transport resistance.

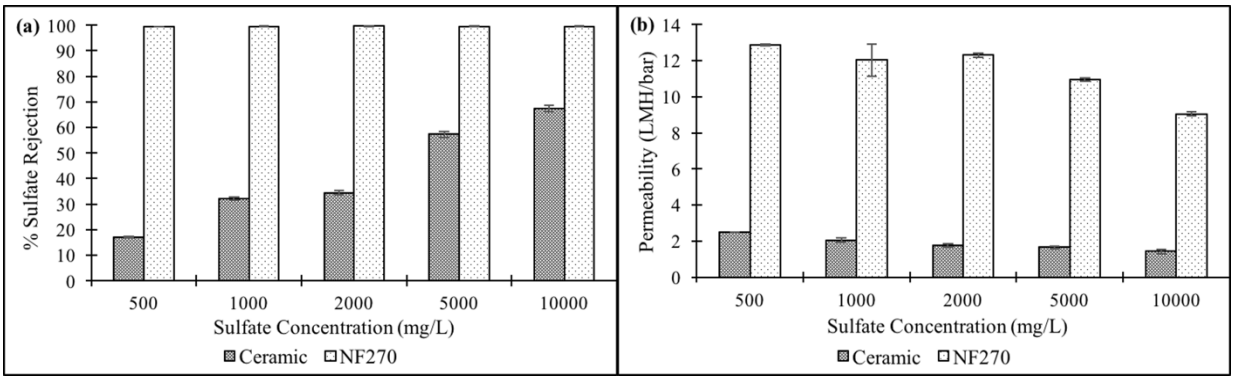

Figure 6.1. Sulfate rejection and permeability of polymeric (NF270) and ceramic membranes with synthetic solution. Experimental feed pressure = 30 bar

6.3.2 Influence of permeate recovery on ion rejection

Full scale NF membrane treatment plants typically operate at 50 – 75% permeate recovery [116, 197] and recoveries of 0%, 50% and 75% were chosen in this study to investigate the effect of feed concentration on ion rejection and permeability of ceramic and polymeric NF membranes.

Figure 6.2 shows the rejection of all ions as a function of permeate recovery using real AMD as feed. Rejection of all ionic species increased with an increase in recovery rate in the case of the ceramic membrane (i.e., Figure 6.2 (a)). Rejection of divalent cations ranged between 55 – 67% at the highest recovery rate (i.e., 75%). The observed rejection order of $Mg^{2+} \approx Ni^{2+} > Mn^{2+} > Sr^{2+} > Ca^{2+} > Ba^{2+}$ can be explained by the diffusion coefficients and Stokes radii of these divalent cations. The diffusion coefficient for these ions are in the order $Ba^{2+} > Ca^{2+} > Sr^{2+} > Mn^{2+} > Mg^{2+} > Ni^{2+}$ where lower diffusion coefficient corresponds to larger Stokes radii and results in better rejection [47]. Greater rejection of sulfate (i.e., 49.4 – 62.8%) than chloride (i.e., 5.4 – 6.7%) can be explained by the necessity to maintain electroneutrality on both sides of the

membrane [99, 147] and larger Stokes radii and lower diffusivity of sulfate compared to chloride [47]. The rejection of all monovalent ions (i.e., sodium, potassium and chloride) along with aluminum, arsenic and selenium was always below 50% with minimum rejection for chloride (i.e., 5.4 – 6.7%), indicating that the ceramic membrane offered minimal resistance to monovalent ions.

In the case of NF270, rejection of all ionic species except the monovalent ions changed slightly or did not change with an increase in permeate recovery (i.e., Figure 6.2 (b)). Marginal increase was measured as compared to that with the ceramic membrane (e.g., the overall conductivity rejection with NF270 membrane increased from 91.2 to 92.5%). The increase in rejection with increasing feed concentration in the case of polymeric membranes is typically attributed to the preferential permeation of like charged ions, thereby adding resistance for the transport of solute through the membrane [138, 158].

NF270 is a semi–aromatic NF membrane and the charge effects (Donnan exclusion) contribute to the overall ionic separation along with steric exclusion effects [1], especially at the ionic strength of 0.027 M used in this study. The increase in feed concentration eliminates charge effects (they are typically screened out at ionic strength above 0.1 M [1]) and the rejection of monovalent ions decreases. Chloride rejection, for instance, decreased from 61 to 44% with increase in permeate recovery from 0 to 75%, which is partially also the result of electroneutrality requirements on both sides of the membrane because the rejection of sulfate ions increased as explained above. In addition to achieving > 97% rejection of sulfate, Ba, Ca, Mg, Mn, Na, Ni and Sr, NF270 membrane also achieved 95 – 96.1% rejection of Se, whose release to environment from mining, oil refineries, manufacturing and agricultural drainage has been a major concern [198].

NF270 rejected 33% of arsenic while the ceramic membrane only achieved 20% arsenic rejection at 75% recovery. Such low rejections suggest that arsenic might be present as an uncharged species. As (III) present as H_3AsO_3 below its pKa = 9.22 is poorly rejected by NF membranes [199, 200] while the rejection of As (III) and As (V) is influenced by Donnan (charge) exclusion [157].

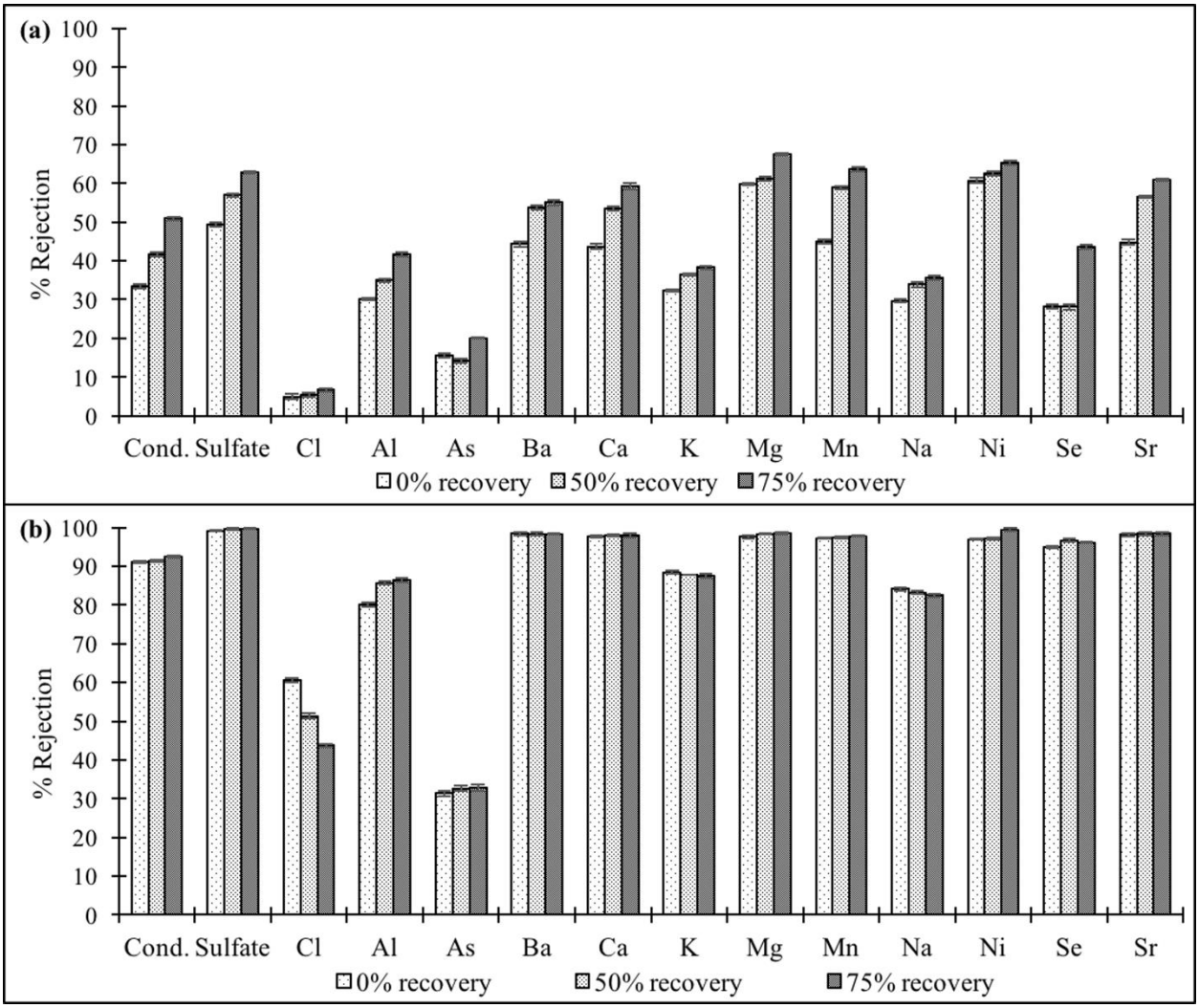

Figure 6.2. Ion rejections with (a) Ceramic and (b) NF270 membranes as a function of increasing recovery rates with real AMD

It is important to note that even though the two membranes had similar nominal pore sizes, NF270 membrane achieved much higher rejections compared to the ceramic membrane. This provides significant evidence that charge (Donnan) exclusion might be a dominant separation mechanism in addition to size exclusion and dielectric exclusion phenomenon [64, 201]. Thus, active layer surface modification of the ceramic membrane to introduce charged groups could help to improve the overall rejection of ionic species under the conditions that were investigated in this study.

6.3.3 Membrane fouling

To evaluate membrane fouling, filtration experiments were carried out for 24 h in total recirculation mode while monitoring the transient permeability and the feed and permeate conductivity. Figure 6.3 shows the measured transient permeability and overall conductivity rejection over 24 h for the ceramic and NF270 membranes at different permeate recoveries.

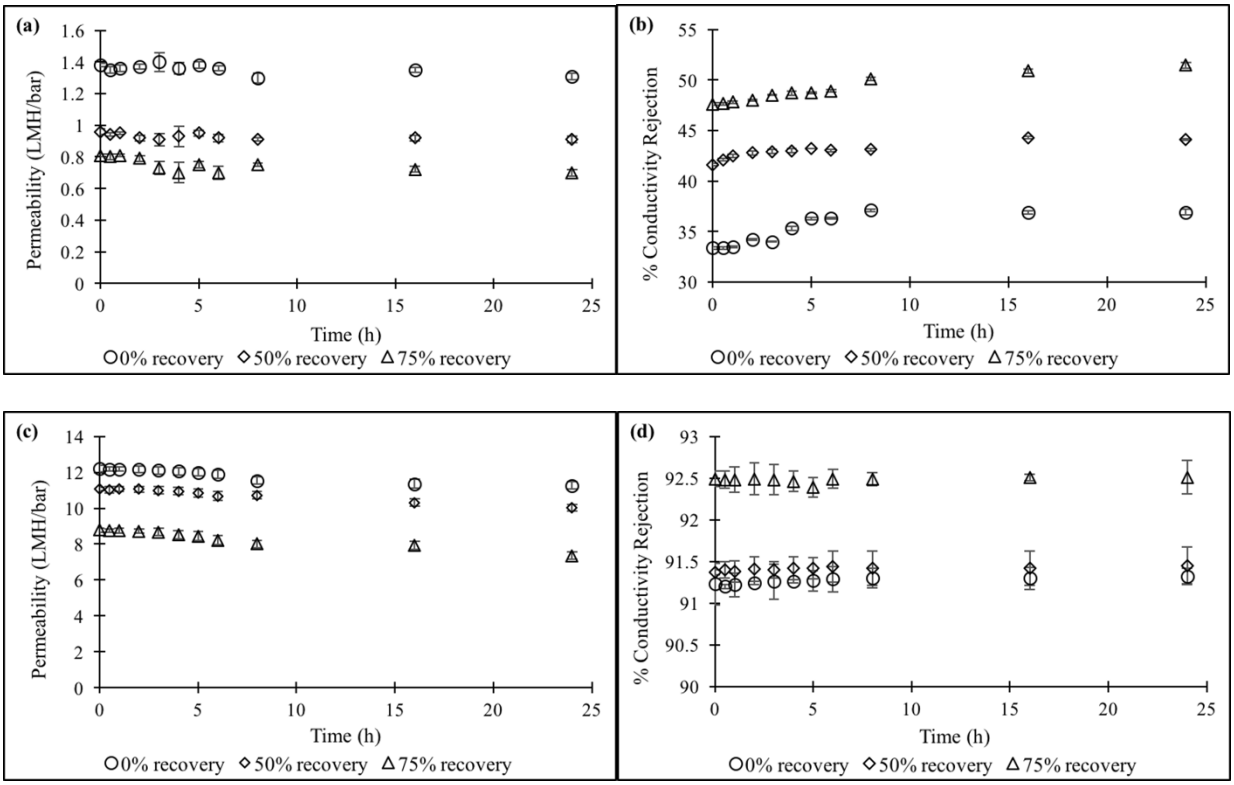

Figure 6.3. Permeability ((a) and (c) for ceramic and NF270 membrane, respectively) and overall conductivity rejection ((b) and (d) for ceramic and NF270 membrane, respectively) as a function of permeate recovery with real AMD over 24 h

Maximum decrease in permeability was observed at 75% recovery for both membranes. Ceramic membrane permeability decreased by 13.6% (i.e., from 0.81 ± 0.01 LMH/bar to 0.70 ± 0.03 LMH/bar, Figure 6.3 (a)) while NF270 permeability decreased by 16.2% (i.e., from 8.78 ± 0.11 LMH/bar to 7.36 ± 0.23 LMH/bar, Figure 6.3 (c)). The conductivity rejection on the other hand remained unchanged in the case of NF270 membrane (i.e., < 0.1%, Figure 6.3 (d)) or increased as much as 8% in the case of ceramic membrane (i.e., from 47.62% ± 0.12% to 51.45% ± 0.28% at 75% recovery, Figure 6.3 (b)). The increase in rejection with a decrease in permeability suggests that scaling/fouling has occurred in these tests.

At these conditions, thermodynamic equilibrium calculations (PHREEQC version 3.1.7, USGS) indicate that $BaSO_4$, $CaSO_4.2H_2O$ (gypsum), $KAl_3(SO_4)_2(OH)_2$ and $Al(OH)_3$ scales may be formed on the feed side. The scales that were formed on the membrane surface at 75% recovery in tests with the polymeric NF270 membrane were analyzed (Figure 6.4) for morphology and elemental composition using SEM and EDS respectively. Figure 6.4 indicates non-homogeneous scale with distinct crystal structures. Gypsum was identified as the most dominant component and the average elemental analysis of the scale from five different areas by EDS revealed the following composition: O = 52.76 ± 5.7%, S = 21.44 ± 4.2% and Ca = 25.8 ± 6.1% and Mn = 1.62 ± 0.1%.

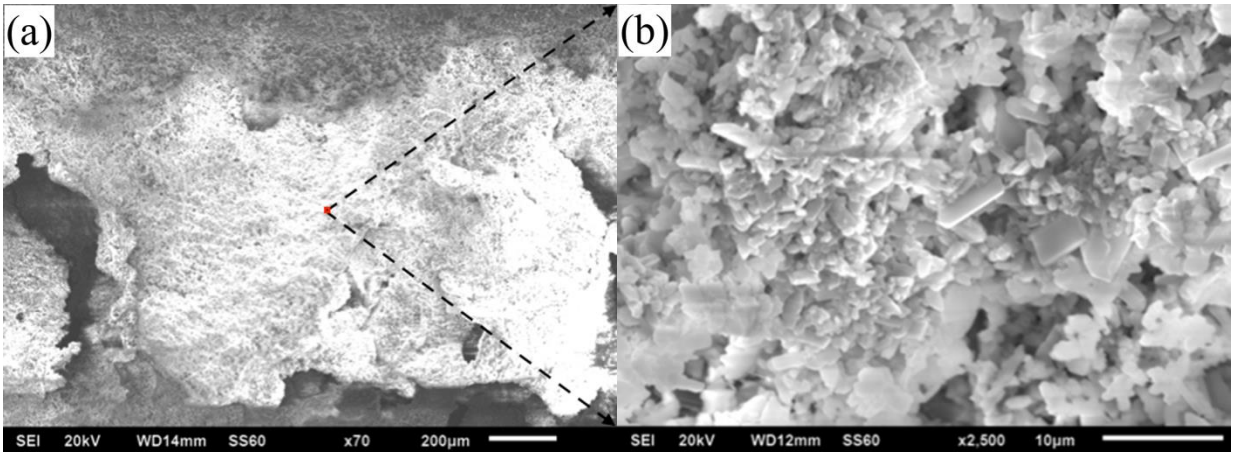

Figure 6.4. SEM micrograph of scales formed on NF270 membrane after 24 h of testing at 75% recovery rate with real AMD (a) at 70X magnification and (b) at 2,500X magnification

6.3.4 Impact of chemical cleaning on membrane performance

Chemical cleaning procedures shown in Table 6.2 were applied after 24 h of filtration in total recirculation mode at 75% permeate recovery of real coal mine drainage. Figure 6.5

compares ionic rejection while Figure 6.6 compares permeability for pristine and chemically cleaned membranes. The rejection of all ions after chemical cleaning decreased (except arsenic rejection by ceramic membrane) while the permeability increased for both membranes. Overall conductivity rejection in the case of ceramic membrane decreased by about 18% while it decreased by only 0.4% in the case of NF270 membrane. The order of rejection of various ions remained the same as shown in Section 6.3.2 and can be explained by the diffusion coefficients and Stokes radii of these ions. Increased permeability and decreased ion rejection indicate that the membrane pores might be slightly enlarged by the chemical cleaning step. Enhanced electrostatic repulsion between the carboxylic groups with acidic and basic cleaning agents is expected to affect the pore size of the polymeric membrane, thereby affecting the performance [105]. Increase in permeability with caustic cleaning has been reported for NF270 membrane [102]. Even though the overall conductivity rejection decreased only slightly in the case of NF270 membrane, the decrease in rejection of monovalent ions and arsenic was not insignificant (i.e., chloride rejection decreased by 8.2% while that of arsenic decreased by about 6%). The smallest changes in pore dimensions would be most reflected in the rejection of monovalent ions, which provides further evidence for the proposed slight enlargement of NF270 membrane pores by chemical cleaning. Unlike, chemical cleaning of polymeric membranes, cleaning of ceramic NF membranes has not yet been completely explored. In this study, conductivity rejection decreased from 51 to 42% for the ceramic membrane, which indicates that chemical cleaning affected the physicochemical characteristics of the active layer of the ceramic membrane. Contrary to all other ions, rejection of arsenic by the ceramic membrane increased from 20 to 37.9%. It has been shown that the rejection of arsenic can be approximately quantified by its accumulation through adsorption on the membrane surface [141], which is dependent on the

membrane surface roughness. Hence, it can be concluded that the surface roughness of the ceramic membrane was affected during the chemical cleaning step, which led to this unexpected increase in rejection of arsenic as compared to other ions.

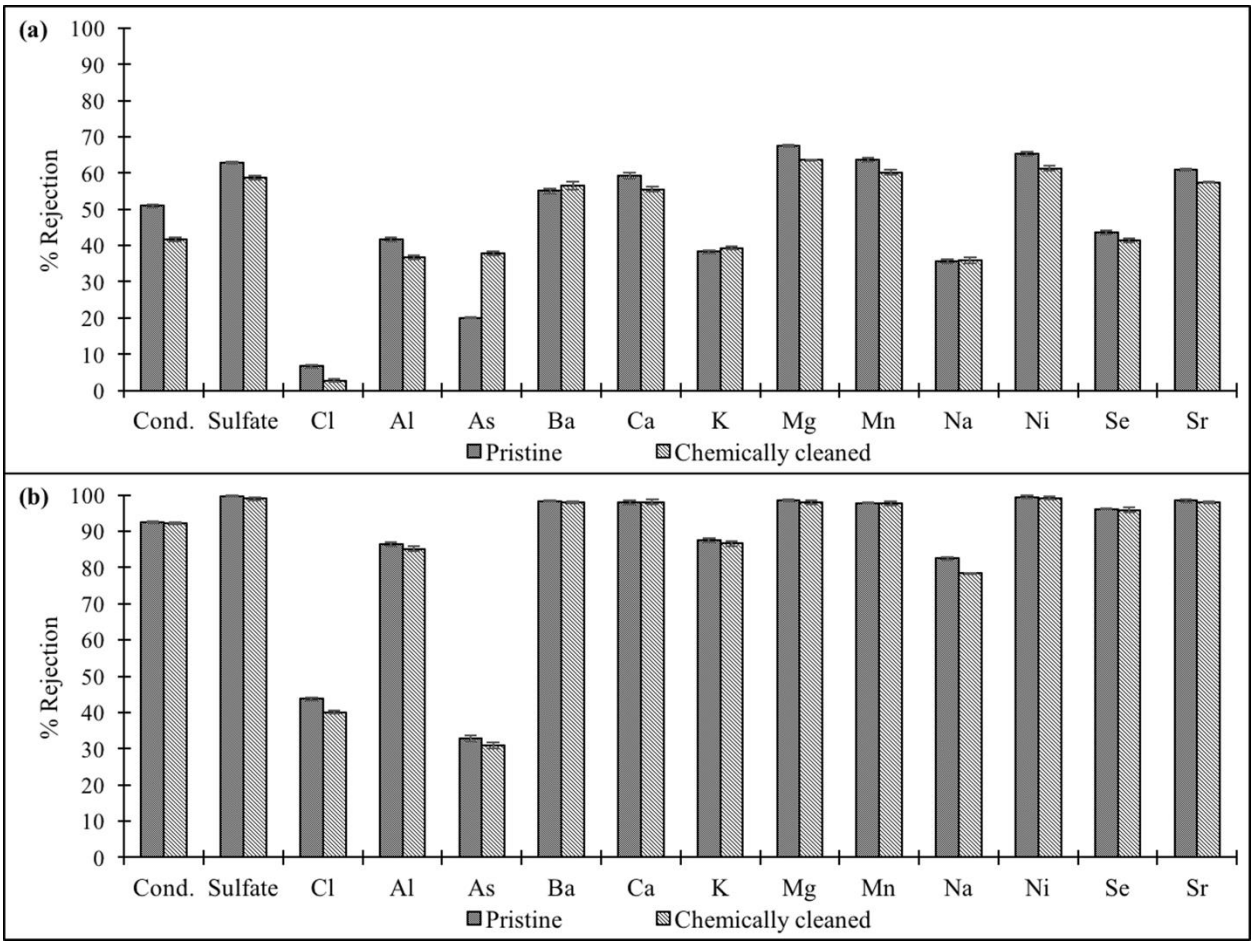

Figure 6.5. Ion rejections with (a) Ceramic and (b) NF270 membranes pre– and post–chemical cleaning with real AMD at 75% recovery rate

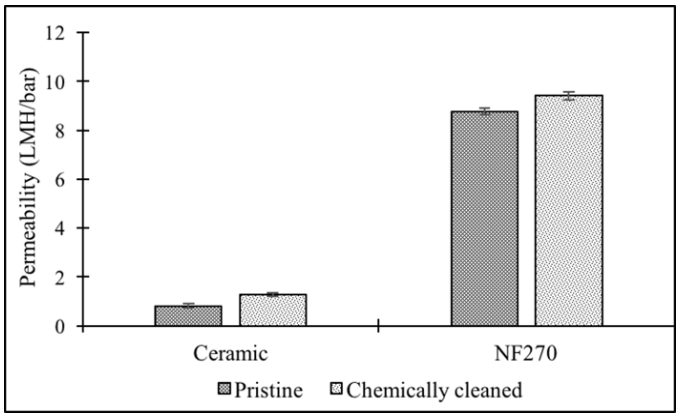

Figure 6.6. Permeability of ceramic and NF270 membranes pre– and post–chemical cleaning with real AMD at 75% recovery rate

6.3.5 Fouling mitigation strategies

Fouling of nanofiltration membranes has been a major concern [30, 202] and was also observed with the AMD selected for this study. Bertrand et al. reported that chemical cleaning had to be used every 6 – 8 weeks in a full–scale NF membrane plant treating highly sulfated and hard water despite a pre–treatment step to remove calcium and reduce $CaSO_4$ fouling, which was identified as the major foulant [116]. Sulfate and calcium concentrations reached 2,500 and 665 mg/L, respectively at 75% recovery with AMD used in this study, which are similar to those reported for the full–scale plant in [116].

Two fouling mitigation strategies, namely pH adjustment and addition of antiscalant were investigated in this study. The feed pH was adjusted to 4 to investigate pH adjustment as a fouling mitigation strategy and to understand NF performance in the case of AMD with low pH. Figure 6.7 shows ionic rejections and Figure 6.8 shows permeability with pH adjustment and antiscalant addition as compared to unaltered feed conditions.

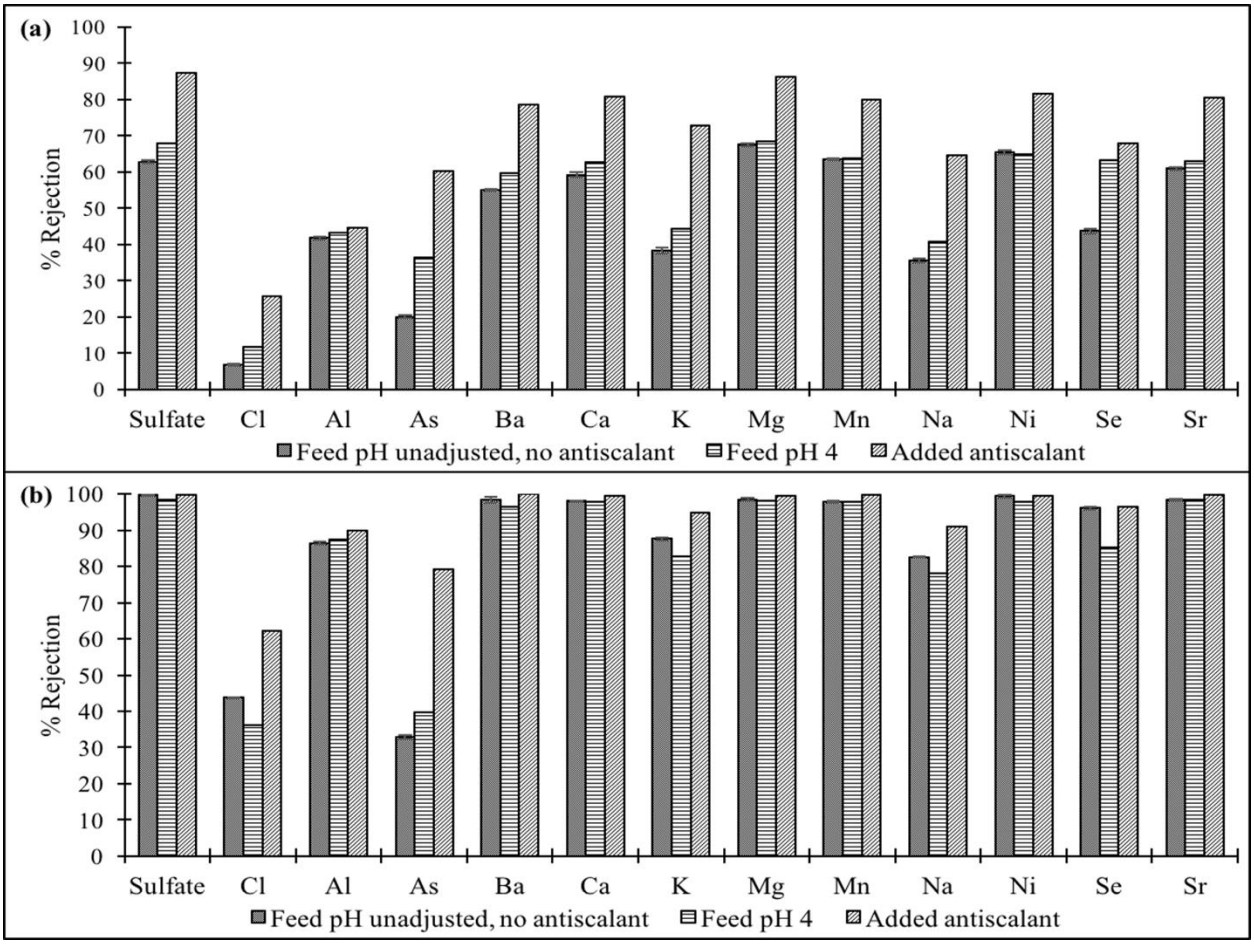

Figure 6.7. Ionic rejections with (a) Ceramic and (b) NF270 membranes due to pH adjustment and antiscalant addition with real AMD at 75% recovery rate

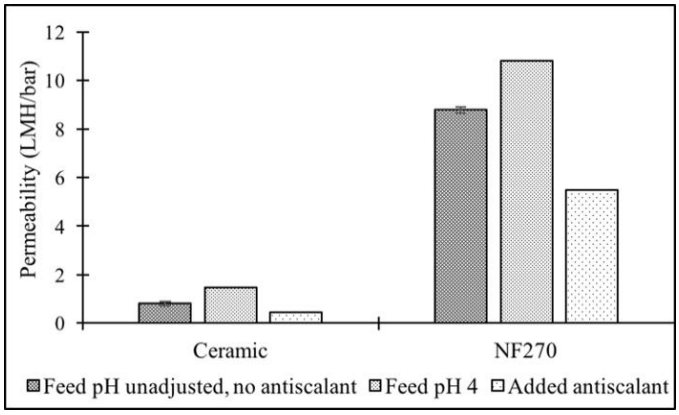

Figure 6.8. Permeability of ceramic and NF270 membranes due to pH adjustment and antiscalant addition with real AMD at 75% recovery rate

Rejection of all ions increased or remained constant in the case of ceramic membrane and decreased or remained constant for the polymeric NF270 membrane when the feed pH was adjusted to 4 (Figure 6.7). The order of rejection of various ions remained the same as shown in Section 3.2 and can be explained by their diffusion coefficients and Stokes radii. Largest increase in ion rejection in the case of ceramic membrane was observed for selenium (45%) and arsenic (81.5%). Along with this increase in ion rejection, the permeability also increased from 0.8 to 1.5 LMH/bar for the ceramic NF membrane (Figure 6.8). Usually, an increase in rejection is accompanied with a decrease in permeability, which is explained by the increase in the feed side osmotic pressure thereby decreasing the driving force. However, a contradictory observation was made with the ceramic membrane. Because size exclusion cannot explain the changes in the ionic rejection, it can be concluded that charge (Donnan) exclusion contributed to ionic rejection at low pH. Membrane manufacturer indicated an isoelectric point (IEP) for the active titania layer of the ceramic NF membrane between 6 – 7, which means that the active layer is positively charged at pH 4. This positive surface charge would lead to an increased rejection of cations, which would also increase the rejection of anions in order to maintain electroneutrality on both sides of the membrane. Gestel et al. [38] also reported an increased rejection for divalent and monovalent salts at lower pH with a ceramic NF membrane. However, it is not clear what mechanism is responsible for the increased rejection of arsenic (III), which is present as uncharged H_3AsO_3 at pH 4 [199].

In the case of polymeric NF270 membrane, rejection of all ionic species except arsenic decreased slightly or remained constant (about 17% for chloride, 5% for monovalent cations and less than 2% for divalent ions) at pH 4 (Figure 6.7). NF270 has an IEP of 2.8 – 3 [79, 90] and the zeta potential at pH 4 is only slightly negative compared to a very high negative

value at pH = 7.8 [1]. Therefore, the contribution of charge (Donnan) exclusion decreases with a pH decrease, which can explain the decrease in the observed ion rejection. Decrease in ion rejection was accompanied by a corresponding increase in permeability from 8.8 to 10.8 LMH/bar (Figure 6.8) and can be explained partly by the decrease in the feed–side osmotic pressure and also by the possible increase in the effective pore size of NF270 membrane at pH 4.

Irrespective of the membrane type, arsenic rejection increased with a decrease in the feed pH to 4. Urase et al. [199] reported a decrease in arsenic rejection with decreasing pH but Al-Rashdi et al. [141] reported an increase in arsenic (III) rejection with decreasing pH. The increased arsenic rejection observed in this study might be attributed to its increased deposition/adsorption on the membrane surface [141].

Addition of antiscalant increased the rejection of all ions by the ceramic membrane (Figure 6.7) with a maximum increase observed for chloride (≈282%) and arsenic (≈200%), followed by 80 – 90% increase for sodium and potassium. Also, an average of 30% increase in rejection of Ba, Ca and sulfate was observed in these experiments while the rejection of all other ions increased by about 15 – 20%. The increase in rejection due to antiscalant addition in the case of NF270 membrane was marginal (≈0 – 2%) except for the smaller ions (i.e., sodium and potassium rejection increasing by about 9% and that of chloride by about 72%). However, a large increase in the rejection of arsenic (i.e., 141%) was observed when antiscalant was added to the feed. This overall increase in rejection was accompanied by a corresponding decrease in permeability as seen in Figure 6.8. Permeability decreased by 43% for the ceramic NF membrane (0.81 to 0.46 LMH/bar) and by 38% for NF270 membrane (8.78 to 5.47 LMH/bar) with addition of antiscalant.

The antiscalant used in this study was a polymer of 2–phosphono–1,2,4–butane tri–carboxylic acid. This tri–carboxylic acid deprotonates at pH of 7.8 and contributes to enhanced charge exclusion and increased rejection of ionic species. However, the large antiscalant molecules also reduced membrane permeability. The SEM images (Figure 6.9) of the polymeric NF270 membrane after 24 h of testing with AMD at 75% permeate recovery with added antiscalant reveal the scale that appears to be more gel–like and compact as compared to that formed without the use of antiscalant (Figure 6.4). Average elemental composition of the scale based on EDS analysis at 5 different locations is: O = 38.2 ± 4.8%, C = 31.5 ± 6.3%, Ca = 20.8 ± 4.3%, P = 5.4 ± 1%, Mg = 1.9 ± 0.2%, S = 1.5 ± 0.2%, Mn = 0.8 ± 0.2%. This indicates that a complex scale is formed on the membrane surface consisting of the tri-carboxylic acid (i.e., carbon and phosphorus) along with sulfate and divalent cations calcium, magnesium and manganese. Scale formation improved the rejection of monovalent ions and uncharged As (III) species by both membranes but at the expense of reduced permeability.

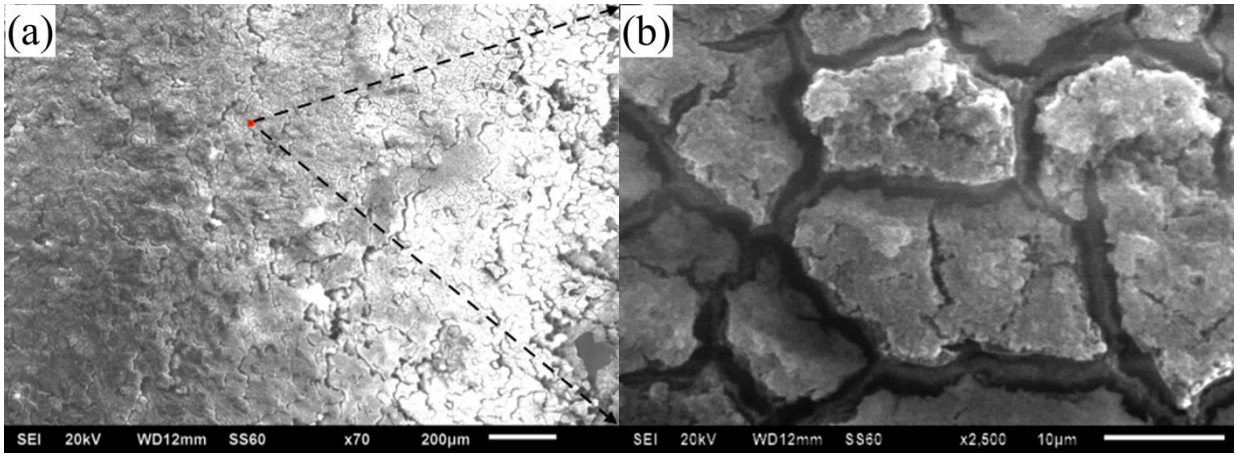

Figure 6.9. SEM micrograph of scales formed on NF270 membrane after 24 h of testing at 75% recovery rate with real AMD + antiscalant (a) at 70X magnification and (b) at 2,500X magnification

Figure 6.10 shows the permeability at 75% recovery over a 24 h period with two fouling mitigation strategies. Adjusting the feed pH to 4 worked very well not only in terms of improving the permeability but also in terms of keeping it fairly constant over a 24 h period. For instance, the permeability of ceramic membrane decreased by 3.4% (from 1.47 to 1.42 LMH/bar) while it decreased by 2.8% (from 10.81 to 10.5 LMH/bar) in the case of NF270 membrane. However, when antiscalant was used as a fouling mitigation strategy, the permeability of ceramic membrane decreased by about 32.6% (from 0.46 to 0.31 LMH/bar) and by 27.3% (5.5 to 4 LMH/bar) for NF270 membrane. This huge decrease in permeability within 24 h can be attributed to the gel–like and compact scale formed on the membrane surface as shown in Figure 6.9. The complexity of the antiscalant action depends on three most important factors: threshold effect, metal ion sequestration capacity and particle dispersion capacity [194]. However, it is very difficult to predict which type of antiscalant would work well and how much of it would be required. For full–scale plant operation, intensive pilot–scale tests are performed to determine the best antiscalant and the optimum dose. Such investigation was outside the scope of this study.

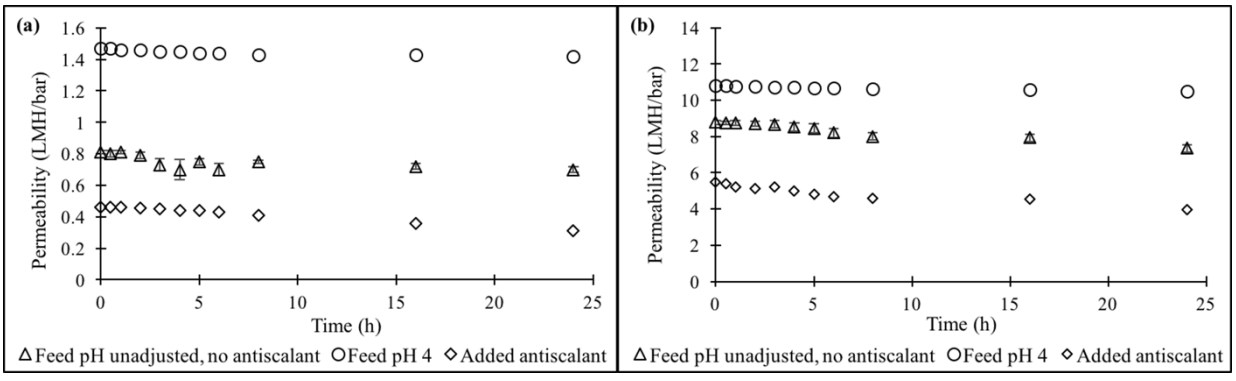

Figure 6.10. Transient permeability of (a) Ceramic and (b) NF270 membranes over 24 h period with pH adjustment and antiscalant addition as fouling mitigation strategies with real AMD at 75% recovery rate

Overall, feed pH adjustment to 4 as a fouling mitigation step worked well. It led to an increase in both ion rejection and permeability for the ceramic membrane. With NF270 membrane, the rejection of monovalent ions decreased along with a marginal decrease in the rejection of the multivalent ions but the permeability increased by 22.7%. Lower feed pH appears to be an attractive option for longer term flux behavior, which is particularly relevant for many acidic streams from abandoned coal mines.

6.3.6 Achieving drinking water standards

This study also investigated the ability of the NF permeate to meet drinking water standards when using real AMD as feed. Since the ceramic and NF270 are relatively loose NF membranes, a tighter NF membrane, namely TS80, was investigated with the same AMD at 0%, 50% and 75% recovery rates. Table 6.3 shows the permeate quality at different recovery rates for all three NF membranes where gray color filled boxes indicate the concentrations above the drinking water standards [134].

TS80 membrane is a tight polyamide NF membrane with a MWCO of ~150 Da and pore radius of 0.71 ± 0.02 nm [1]. It was able to achieve > 98% overall conductivity rejection with multivalent ions being rejected above 99% except for arsenic, which was rejected close to 70%. Among the monovalent ions, sodium and potassium were rejected at about 97% while the rejection of chloride was close to 90%. Such high ion rejection by TS80 membrane has been previously reported and explained by the dominant steric exclusion mechanism [1, 113]. High ion rejections were accompanied by reduced permeability (i.e., 4.3 – 3.8 LMH/bar) compared to the NF270 membrane, which can be largely explained by lower MWCO and pore size of the TS80 membrane [1].

Table 6.3. Permeate quality for ceramic, NF270 and TS80 membranes at 0%, 50% and 75% recovery rates

Ions	Drinking Water Level	Permeate Quality Ceramic 0%	Ceramic 50%	Ceramic 75%	NF270 0%	NF270 50%	NF270 75%	TS80 0%	TS80 50%	TS80 75%
Permeability (LMH/bar)*		1.38	0.96	0.81	12.2	11.1	8.8	4.85	4.3	3.78
SO_4 (mg/L)	250[2]	287	355	482	4.7	5.3	21	0.8	0.8	1
Cl (mg/L)	250[2]	63.6	64.3	65.6	26.1	50.2	89.7	5.62	11.2	25.4
Al (µg/L)	50–200[2]	45	55.3	57	10.5	12.1	15.7	7.8	4.2	2.7
As (µg/L)	10[1]	49.6	53.8	39.8	31.3	32.7	32.8	24	36	56
Ba (µg/L)	2,000[1]	44.8	54.8	71.5	< 1	< 1	< 1	< 1	< 1	< 1
Ca (mg/L)	100–300[3]	91.8	108.6	140.6	4.0	6.6	13.1	0.13	0.08	0.31
K (mg/L)	-	3.1	3.7	4.5	0.55	1.1	2.0	0.06	0.20	0.42
Mg (mg/L)	10[4]	26.1	29.7	39.2	1.26	1.72	3.71	0.03	0.03	0.12
Mn (µg/L)	50[2]	1100	1200	1500	50	80	170	1	1	3
Na (mg/L)	30–60[3]	75.8	90.4	109	19.2	32.9	57.0	3.42	7.6	15.7
Ni (µg/L)	100[1]	17.1	74	117	1.54	3.47	1.7	2.55	2.51	2.05
Se (µg/L)	50[1]	37.1	41	32.5	3.0	4.0	8.0	< 1	< 1	< 1
Sr (µg/L)	1,500[5]	948	1107	1409	31	51	106.7	< 1	< 1	< 1

*Permeability measured at time = 0 min post 2 h stabilization period.
[1]Primary Maximum Contaminant Level (P-MCL) by EPA [134].
[2]Secondary Maximum Contaminant Level (S-MCL) by EPA.
[3]Taste threshold by EPA.
[4]Taste threshold by [203].
[5]Health reference level set by EPA. There is no current drinking water standard set at this time [135].

As seen from Table 6.3, TS80 was able to achieve drinking water standards for all ions except arsenic, whose regulatory level is 10 μg/L. The permeate from ceramic membrane violated these standards for many different ions but the permeate from NF270 membrane was in violation only in the case of manganese at 50% and 75% recovery in addition to arsenic. It is obvious that arsenic has to be removed in a separate treatment step as none of the membranes could meet the drinking water standard for arsenic. If manganese can also be removed before the NF step, a relatively looser (i.e., NF270) membrane could be utilized instead of the tight (i.e., TS80) membrane because it will provide higher permeate flux (permeability with NF270 was 5 LMH/bar higher than with TS80 membrane at 75% recovery). Addition of antiscalant resulted in a dramatic increase in arsenic rejection and the permeate concentrations at 75% recovery for the ceramic and NF270 membranes were measured at 17.2 and 16 μg/L, respectively. These concentrations are only slightly above the allowable limits for drinking water. Hence, it is reasonable to expect that the addition of antiscalant with a tighter membrane like TS80 could bring the arsenic concentration in the permeate below the allowable limit. However, increased rejection would be accompanied by a loss in permeability by membrane fouling as observed in the case of the ceramic and NF270 membranes and hence would not be recommended. Even though the drinking water standards were not met by any of the NF membranes, the permeate stream could be used for a number of non-potable applications including irrigation [186, 204], construction industry, make-up cooling water in power plants [184], enhancing natural wetlands [188] and saltwater intrusion control [189].

6.4 CONCLUSIONS

This study compared performance and fouling characteristics of ceramic and a polymeric nanofiltration membranes for treatment of abandoned mine drainage from an actual site in southwestern Pennsylvania. Several potentially toxic elements including aluminum, arsenic, barium, iron, manganese, nickel, selenium and strontium were present in the AMD along with about 650 mg/L of sulfate. Also, about 60 mg/L total iron was present, which had to be removed by aeration and microfiltration prior to testing AMD with the NF membranes to avoid severe membrane fouling.

Both ceramic and polymeric membranes were screened with increasing concentrations of sulfate in the synthetic feed to determine their capacity to reject sulfate as the major constituent in AMD. NF270 membrane achieved > 99% rejection in all cases while the rejection increased more than 3–fold for the ceramic NF membrane (i.e., from 17.2 to 67.5%) when the sulfate feed concentration increased from 500 to 10,000 mg/L. In addition, NF270 membrane also achieved higher permeability than the ceramic NF membrane (i.e., 12.9 – 9.1 LMH/bar vs. 2.5 – 1.44 LMH/bar) in all cases.

The impact of permeate recovery on ion rejection and permeability of both membranes was tested with real AMD at recoveries of up to 75%. Ion rejection increased with an increase in percent recovery, with NF270 achieving higher rejection than the ceramic membrane for all ions under all experimental conditions. NF270 rejected more than 96% of all multivalent ions while the ceramic membrane achieved rejections between 55 – 67%. Arsenic was not effectively rejected by either membrane (i.e., NF270 achieved 33% rejection and ceramic membrane achieved 20% rejection). Fouling of both membranes occurred at 75% permeate

recovery over the 24 h period. The fouling layer consisted mostly of gypsum, which was in agreement with the thermodynamic predictions.

The efficiency of chemical cleaning techniques specified by manufacturers were tested for their ability to restore permeability and ion rejection after membrane fouling. The permeability increased and ion rejection decreased after chemical cleaning indicating a slight enlargement of the effective membrane pores for both membranes. pH adjustment and addition of antiscalant were investigated as fouling mitigation strategies for the scaling that occurred at 75% recovery. Interestingly, feed pH adjustment to 4 caused an increase in ion rejection by the ceramic membrane and a decrease in ion rejection in the case of NF270 membrane. Such behavior can be explained by the changes in the charge characteristics of these membranes. Addition of antiscalant to the feed increased rejection of all ions by both membranes and was particularly significant for monovalent ions and arsenic. Arsenic rejection by ceramic and polymeric membrane increased by about 200 and 141%, respectively. This increase in rejection, however, occurred with a significant decrease in permeability of 43 and 38% for ceramic and NF270 membranes, respectively. The gel–like and compact scale formed on the membrane surface consisting of the tri–carboxylic acid (i.e., carbon and phosphorus) along with sulfate and divalent cations calcium, magnesium and manganese was identified as the main reason for the decrease in permeability and an increase in ion rejection, especially in the case of arsenic that is present as an uncharged species at these feed conditions.

This study also investigated a relatively tight NF membrane (i.e., TS80) for the possibility of producing the permeate from AMD that can serve as a drinking water source. TS80 membrane achieved > 98% rejection of overall conductivity with > 99% rejection of all multivalent ions. The only exception was arsenic, which was present in the permeate above the

allowable drinking water level. The permeate from the ceramic membrane was in violation of these standards for many different ions but the permeate from NF270 membrane was in violation only in the case of manganese (at 50% and 75% recovery) and arsenic (at all recovery rates). The use of antiscalant increased arsenic rejection and its addition in the case of TS80 membrane could help to meet the drinking water standard; however, the issue of intensive fouling observed with the use of antiscalant makes this approach infeasible. It is obvious that arsenic has to be removed in a separate treatment step as none of the membranes evaluated in this study could meet the drinking water standard. If manganese can also be removed before the NF step, a relatively looser (i.e., NF270) membrane could be utilized instead of the tighter (i.e., TS80) membrane because it will provide higher permeability.

7.0 CONCLUSIONS AND FUTURE OUTLOOK

7.1 CONCLUSIONS

In summary, the overall aim of the work presented in this thesis was to improve the understanding of nanofiltration processes so that the technical knowledge obtained could help contribute to solutions addressing the world water crisis. The work had a total of five subparts: (1) To examine the influence of active layers on separation potentials of nanofiltration membranes for inorganic ions, (2) To investigate the impact of chemical cleaning on physicochemical characteristics and ion rejection by nanofiltration membranes, (3) To gain insights into the removal of barium and strontium ions using nanofiltration membrane by experimental and modeling analysis, (4) Optimization of nanofiltration membranes at laboratory–scale and then testing at pilot–scale for complete recovery of abandoned mine drainage, and (5) Comparing ceramic and polymeric nanofiltration membranes for the treatment of abandoned mine drainage. A brief of the conclusions obtained in each of these areas is as follows:

(1) Chapter 2.0 contributes significantly to understanding the separation mechanisms of two types of commonly used nanofiltration membranes with a view of realizing new potential applications. We first analyzed the active layer chemistries of four commercially available

nanofiltration membranes with two different active layer chemistries: polyamide (1,3–benzenediamine (m-phenylenediamine) (MPD) with trimesoyl chloride (TMC) and poly(piperazineamide) (piperazine (PIP) with TMC) to prove that these membranes were representative of the respective categories with no coatings or modification of the active layer. Effective membrane pore size and zeta potential characterization of the four membranes suggested that poly(piperazineamide) membranes had relatively larger pore sizes and that they were more electronegative for all feed compositions tested. Crossflow rejection experiments at low and high ionic strength feed suggested that Donnan (charge) exclusion was significant for poly(piperazineamide) membranes and that these membranes should be preferred in applications requiring partial ion removal (e.g., dairy industry) or charged based separations (e.g., charged organic separations), while polyamide membranes should be considered in desalination applications since steric exclusion was the most dominant separation potential. Qualitative analysis suggests that the contribution of dielectric exclusion to overall rejection by polyamide membranes would be more significant than that for poly(piperazineamide) membranes. This study offered additional insights into how the separation potentials of polyamide and poly(piperazineamide) active layer chemistries vary even with a very small difference in the effective membrane pore size.

(2) The impact of chemical cleaning on physicochemical characteristics and separation performance of nanofiltration membranes was determined to be dependent on the type of active layer chemistry in Chapter 3.0. ATR–FTIR and XPS analysis indicated no chemical changes to the membrane active layers after chemical cleaning with HCl or NaOH. The active layer thicknesses of the membranes selected for this study decreased in the order NF90

> TS80 > TS40 > NF270. The degree of crosslinking in the active layer was higher for NF90 membrane than TS80 membrane (PA membranes) and that for TS40 membrane was higher than NF270 membrane (PP membranes). Membrane cleaning with HCl did not have significant impact on zeta potential while cleaning with NaOH further reduced zeta potentials for membranes with high concentration of carboxylic acid groups on the surface (i.e., TS80, TS40 and NF270). The effective pore radii of all membranes increased as a result of chemical cleaning and poly(piperazineamide) membranes were more affected than polyamide membranes. HCl cleaning resulted in larger effective membrane pore radii for all membranes by 3 – 5%. Cleaning with NaOH had a much more pronounced impact on the effective pore radii and an increase of as high as 23% was observed for a PP membrane (NF270) after exposure for 18 h. This study offered evidence that NaOH can cause increased swelling of the active layer with an increase in cleaning time and this was particularly evident for poly(piperazineamide) membranes. The PP membranes are particularly vulnerable when it comes to regaining the permeability and rejection characteristics of pristine membrane if NaOH is used as a cleaning solution. Ion rejection test with single salt (1 mM Na_2SO_4) and a mixture of salts (1 mM Na_2SO_4 + 1 mM $MgCl_2$ + 1 mM $CaCl_2$) revealed that rejection of all ions decreased after chemical cleaning. Rejection of sulfate for poly(piperazineamide) membranes decreased only slightly despite a fairly significant increase in the effective pore radii, which can be explained by their dependence on charge exclusion mechanism for ion rejection that was actually enhanced by a decrease in zeta potential by NaOH cleaning. The impact of the increased effective pore radii was readily seen in the rejection of monovalent ions when the feed was adjusted to a mixture of salts. The 23% increase in the effective pore radii for the NF270 membrane after NaOH cleaning for 18

h lead to a decrease of 25, 36, 53 and 62% rejection of magnesium, calcium, sodium and chloride ions, respectively. At the same time, only a 7% decrease in the rejection of sulfate ions was observed, which could be explained by the 16% decrease in zeta potential. The changes in permeability due to chemical cleaning were in agreement with the changes in rejection (i.e., a decrease in ion rejection corresponded to an increase in membrane permeability). The effective pore radii measured using the membrane potential technique correlated well with DI water permeability for all membranes before and after cleaning. The importance of charge exclusion in rejection of inorganic ions was highlighted by the observed differences in rejection and permeability values when testing these membranes post cleaning with NaOH for 9 and 18 h. This study significantly contributed to help understand the lesser known effects of chemical cleaning of the rejection behavior of inorganic ions and its dependence on the physicochemical characteristics and separation potentials of two commonly used active layers of nanofiltration membranes.

(3) A polyamide nanofiltration membrane (NF90) was investigated for the rejection of barium and strontium ions from single salt solutions at relevant process conditions in Chapter 4.0. Analysis of the zeta potential of NF90 membrane at varying concentrations of barium and strontium revealed that neither of these ions specifically adsorbed onto the membrane surface as the iso–electric point of the membrane did not change even with a hundred–fold increase in solute concentration. Combining these results with the observed rejection performance at different feed pH lead to a conclusion that electrostatic effects and H^+ rejection did not contribute to rejection of these cations and that size exclusion was the dominant separation mechanism. Increase in the effective pore size by conformal changes to the polyamide active

skin layer were responsible for the marginal decrease in the observed rejection (≈ 1 – 2%) with increasing pH for both barium and strontium ions. Concentration polarization modulus decreased with increase in crossflow velocity, decrease in feed pressure and increase in bulk feed concentration because of increase in shear mass transfer rate, decrease in permeate convection and increase in feed osmotic pressure, respectively. The permeate flux increased with increase in feed pressure but ion rejection stabilized at around 15 – 20 bar for both barium and strontium. Hence, feed pressure of 20 bar and crossflow velocity of 1.16 m/s are recommended as optimal operating conditions based on the observed ion rejection and concentration polarization modulus. Spiegler–Kedem model fitted very well with the experimental data. The concentration dependent model transport parameters (i.e., permeability and reflection coefficient for solute) indicate that both barium and strontium were equally rejected by the NF90 membrane at all conditions. Maximum rejection of 99.5% and minimum of 92% indicate exceptional performance of NF90 membrane while achieving appreciable permeability between 3.9 – 5.9 LMH/bar.

(4) The study presented in Chapter 5.0 was designed to optimize and validate the use of nanofiltration membranes for treatment of AMD at full–scale to produce two streams: treated water stream that can serve as a substitute for fresh water in industrial applications and a concentrated sulfate stream that is ideally suited for use in produced water treatment for sulfate precipitation to control divalent cations in the finished water and enable its reuse for hydraulic fracturing of subsequent wells. Laboratory–scale screening of eight commercially available NF membranes was performed with synthetic AMD solutions in a dead–end module and two membranes, i.e., NF90 and NF270, were selected for testing with real AMD

solution based on sulfate rejection and permeate flux. These membranes were also tested in the crossflow module where NF90 membrane performed better than NF270 membrane in terms of rejection of all ions of interest. Hence, NF90 membrane was selected for pilot–scale study. NF90 membrane exhibited impressive performance in the pilot–scale system by achieving very high removal of sulfate from the real AMD. The sulfate concentration in the feed solution of about 1,700 mg/l was reduced to less than 10 mg/l, representing more than 99% sulfate removal during 208 hours of continuous operation. In addition, more than 99% rejection of calcium, magnesium, nickel and selenium was achieved in the pilot–scale tests with total dissolved solids and total organic carbon rejection of 98% and 90%, respectively. The NF system also achieved about 90% chloride removal which points towards a potential benefit in conditioning water for use in industries that are sensitive to corrosion issues. The pretreatment steps of aeration, sedimentation, bag filtration and ultrafiltration used in the pilot–scale study were highly effective in removing iron from the feed stream to facilitate stable operation of the NF system over the 208–hour period. A steady–state water recovery of 57% was achieved with the feed pressure of 10 bar and feed flow rate of 3.5 GPM during the entire pilot plant operation. Chemical equilibrium calculations indicate a very small degree of gypsum supersaturation but a constant pressure drop of about 1.7 bar during pilot–scale testing and DI water permeability tests on used NF modules confirmed that no measurable fouling/scaling occurred with this particular AMD. Thus, the goal of producing two valuable product streams, one of high quality (NF permeate with TDS < 50 mg/l) and the other with high sulfate concentration (NF reject with a sulfate concentration of about 4,000 mg/l, which can be used to recover flowback and produced water), was successfully accomplished in this study. In addition, laboratory–scale experiments clearly indicate that

testing in a dead–end module can only be used for relative comparison of NF membranes while the crossflow system facilitates a detailed process study to optimize NF performance. The performance of NF membrane in a crossflow laboratory–scale system compares well with that observed in a pilot–scale system, which confirms the scalability of membrane filtration process and further emphasizes the value of laboratory–scale tests in a crossflow module to predict full–scale system performance.

(5) The study in Chapter 6.0 compared the performance and fouling characteristics of a ceramic and a polymeric nanofiltration membrane for treatment of abandoned coal mine drainage from an actual site in southwestern Pennsylvania. Several potentially toxic elements including aluminum, arsenic, barium, iron, manganese, nickel, selenium and strontium were present in the AMD along with about 650 mg/L of sulfate. Also, about 60 mg/L total iron was present, which had to be removed by aeration and microfiltration prior to testing AMD with the NF membranes to avoid severe membrane fouling. Both ceramic and polymeric membranes were screened with increasing concentrations of sulfate in the synthetic feed to determine their capacity to reject sulfate as the major constituent in AMD. NF270 membrane achieved > 99% rejection in all cases while the rejection increased more than 3–fold for the ceramic NF membrane (i.e., from 17.2 to 67.5%) when the sulfate feed concentration increased from 500 to 10,000 mg/L. In addition, NF270 membrane also achieved higher permeability than the ceramic NF membrane (i.e., 12.9 – 9.1 LMH/bar vs. 2.5 – 1.44 LMH/bar) in all cases. The impact of permeate recovery on ion rejection and permeability of both membranes was tested with real AMD at recoveries of up to 75%. Ion rejection increased with an increase in percent recovery, with NF270 membrane achieving higher rejection than the ceramic membrane for all ions under all experimental conditions. NF270

membrane rejected more than 96% of all multivalent ions while the ceramic membrane achieved rejections between 55 – 67%. Arsenic was not effectively rejected by either membrane (i.e., NF270 achieved 33% rejection and ceramic membrane achieved 20% rejection). Fouling of both membranes occurred at 75% permeate recovery over the 24 h period. The fouling layer consisted mostly of gypsum, which was in agreement with the thermodynamic predictions. The efficiency of chemical cleaning techniques specified by manufacturers were tested for their ability to restore permeability and ion rejection after membrane fouling. The permeability increased and ion rejection decreased after chemical cleaning indicating a slight enlargement of the effective membrane pores for both membranes. pH adjustment and addition of antiscalant were investigated as fouling mitigation strategies for the scaling that occurred at 75% recovery. Interestingly, feed pH adjustment to 4 caused an increase in ion rejection by the ceramic membrane and a decrease in rejection in the case of NF270 membrane. Such behavior can be explained by the changes in the charge characteristics of these membranes. Addition of antiscalant to the feed increased rejection of all ions by both membranes and was particularly significant for monovalent ions and arsenic. Arsenic rejection by ceramic and polymeric membrane increased by about 200 and 141%, respectively. This increase in rejection, however, occurred with a significant decrease in permeability of 43 and 38% for ceramic and NF270 membranes, respectively. The gel–like and compact scale formed on the membrane surface consisting of the phosphono tri–carboxylic acid (i.e., carbon and phosphorus) along with sulfate and divalent cations calcium, magnesium and manganese was identified as the main reason for the decrease in permeability and an increase in ion rejection, especially in the case of arsenic that is present as an uncharged species at these feed conditions. In addition, this

study also investigated a relatively tight NF membrane (i.e., TS80) for the possibility of producing the permeate from AMD that can serve as a drinking water source. TS80 membrane achieved > 98% rejection of overall conductivity with > 99% rejection of all multivalent ions. The only exception was arsenic, which was present in the permeate above the allowable drinking water level. The permeate from the ceramic membrane was in violation of these standards for many different ions but the permeate from NF270 membrane was in violation only in the case of manganese (at 50% and 75% recovery) and arsenic (at all recovery rates). The use of antiscalant increased arsenic rejection and its addition in the case of TS80 membrane could help to meet the drinking water standard; however, the issue of intensive fouling observed with the use of antiscalant makes this approach infeasible. It is obvious that arsenic had to be removed in a separate treatment step as none of the membranes evaluated in this study could meet the drinking water standard. If manganese can also be removed before the NF step, a relatively looser (i.e., NF270) membrane could be utilized instead of the tighter (i.e., TS80) membrane because it will provide higher permeability.

7.2 KEY CONTRIBUTIONS

Chapter 2. Influence of active layers on separation potentials on NF membranes for inorganic ions

Key Results:

- Poly(piperazineamide) membranes have a slightly open structure (bigger pore size) as compared to polyamide membranes.
- Poly(piperazineamide) membranes are more negatively charged (lower zeta potential) than polyamide membranes.
- Polyamide NF membranes rely dominantly on size exclusion mechanism for ion rejection while for poly(piperazineamide) membranes both size and charge (Donnan) exclusion contribute to ion rejection.

Chapter 3. Influence of chemical cleaning on the physicochemical characteristics and ion rejection by nanofiltration membranes

Key Results:

- No changes in elemental composition measured with HCl (at pH 2) or NaOH (at pH 12) cleaning.
- Effective pore radii of all membranes increased post chemical cleaning and poly(piperazineamide) membranes were more affected than polyamide membranes. Time dependent changes were measured with poly(piperazineamide) membranes with NaOH cleaning.
- Poly(piperazineamide) membranes achieved high rejection of sulfate even with a 23% increase in the effective pore radii with NaOH cleaning owing to their dependence on charge exclusion mechanism in addition to size exclusion.

Chapter 4. Insights into the rejection of barium and strontium by nanofiltration membrane from experimental and modeling analysis

Key Results:

- Barium and strontium ions did not specifically adsorb at the membrane surface.
- Size exclusion was the dominant separation mechanism. Electrostatic effects and H^+ rejection did not influence rejection of barium and strontium.
- Spiegler–Kedem model fitted very well with the experimental data and a concentration dependent equation was developed to approximate the rejection of barium and strontium over the concentration range of 0.36 – 36.4 mM.

Chapter 5. Laboratory and pilot–scale nanofiltration treatment of abandoned mine drainage for the recovery of products suitable for industrial reuse

Key Results:

- Laboratory–scale screening of eight commercially available polymeric NF membranes was performed and NF90 membrane was selected based on optimized rejection and permeability.
- Pilot–scale study comprised of aeration, bag filtration, UF and NF. >98% TDS and >90% TOC was removed with no fouling at 57% water recovery.
- Reusability of AMD was established by using both the permeate (TDS<50 mg/L) for industrial processes, irrigation and reject (sulfate – 4000 mg/L) for treating produced and flowback water to remove the scale causing cations by sulfate precipitation to enable its reuse for hydraulic fracturing.

Chapter 6. Comparison of ceramic and polymeric nanofiltration membranes for treatment of abandoned coal mine drainage

Key Results:

- Polymeric NF membrane achieved both better rejection and permeability than the ceramic NF membrane in all cases.
- At 75% recovery, fouling was dominated by gypsum precipitation and arsenic was not rejected effectively in any case.
- Addition of antiscalant formed a gel–like and compact scale owing to complex interactions between calcium, magnesium, manganese and the phosphono tri–carboxylic acid antiscalant molecules.

7.3 FUTURE OUTLOOK

The work presented in this thesis has successfully answered very interesting questions, which have also raised many more other questions and research directions to be explored.

It was successfully shown in Chapter 2.0 that steric exclusion is the dominant separation mechanism for polyamide membranes and that poly(piperazineamide) membranes depended on both steric and Donnan exclusion for ion rejection. This points towards the use of poly(piperazineamide) membranes for potential applications involving the selective separation of charged species. Since commercial membranes were used in this study, nanofiltration membrane fabrication to further study the dependence of Donnan exclusion mechanism and the related changes in ion rejection and permeability with poly(piperazineamide) active layer thickness, surface modifications, etc. would be essential to enhance the use of these membranes for applications involving selective separation of charged species. *(Experimental)*

Chapter 3.0 confirmed that ion rejection decreased and permeability increased for both polyamide and poly(piperazineamide) nanofiltration membranes owing to conformal changes in the active layer structure as explained by the increased effective pore radii with no changes observed in the elemental composition of the active layer after chemical cleaning. Interestingly, poly(piperazineamide) membranes were affected more and time dependent changes were observed with NaOH cleaning. Usual industrial chemical cleaning procedures employ an acid cleaning step post alkali cleaning, which helps in regaining the lost membrane performance characteristics. The time dependent behavior observed with poly(piperazineamide) membranes indicates that difficulties could be observed with regaining membrane performance in the case of poly(piperazineamide) membranes and is subject to further enquiry. Insights related to the degree

of membrane performance regained would be instrumental in extending the average membrane life. *(Experimental, pilot–scale)*

Effective removal of barium and strontium ions with the polyamide membrane was shown in Chapter 4.0 and the role of steric exclusion was highlighted. All tests were run with single salt solutions. Elucidating the dependence of membrane performance on feed chemistry would be interesting given the relevance to actual scenario. *(Experimental)*

Chapter 6.0 showed the comparison of polymeric and ceramic NF membranes for treatment of abandoned mine drainage and polymeric membrane achieved both higher rejection and permeability than the ceramic nanofiltration membrane. This illustrates the need for improving ceramic nanofiltration membranes that have superior mechanical characteristics as compared to the currently used polymeric membranes. As of today, only a handful of ceramic nanofiltration membranes are commercially available partly because of the unavailability of competing fabrication technologies to make ceramic nanofiltration membranes with low molecular weight cut-off's. There exists a plethora of fundamental (mechanism of separation, specific ion rejection, permeability, impact of chemical cleaning) as well as applied (pilot–scale testing) aspects that are yet to be explored and can provide valuable contributions for the development of ceramic nanofiltration membranes. *(Experimental, Modeling, pilot–scale)*

Another interesting aspect observed in Chapter 6.0 was the compact gel–like scale formed with the use of antiscalant during treatment of abandoned mine drainage at 75% recovery. Understanding the complex interactions of calcium and sulfate ions with the phosphono tri–carboxylic acid groups on the antiscalant molecules could provide valuable insights for the development of newer antiscalants that are much more effective with high concentrations of calcium ions. *(Experimental)*

In conclusion, this thesis has successfully provided novel insights into understanding the separation mechanisms of two commonly used active layers of polymeric nanofiltration membranes as well as treatment of abandoned mine drainage using ceramic and polymeric nanofiltration membranes. It is hoped that this evaluation will be a valuable contribution in the bid to improve the crisis related to the global need for safe drinking water.

APPENDIX A

A.1 SUPPORTING INFORMATION FOR CHAPTER 2.0

A.1.1 Results and discussion for ATR–FTIR section

Among various observed peaks in Figure 2.2, those at ∼1584, ∼1503, ∼1486, 1385 – 1365, 1350 – 1280, ∼1235, 1180 – 1145 and ∼830 cm^{-1} are common for all four membranes (i.e., NF90, TS80, NF270 and TS40). These peaks can be attributed to the common polysulfone support layer. Kwon and Leckie [118] have attributed the peaks at ∼1584, ∼1503 and ∼1486 cm^{-1} to the aromatic in–plane ring bend stretching vibration. The peaks in the range of 1385 – 1365 cm^{-1} are due to the C–H symmetric vibration and those in the 1350 – 1280 and 1180 – 1145 cm^{-1} range are due to the asymmetric SO_2 stretching vibration and symmetric vibration, respectively. Also, the prominent peaks at ∼1235 and 830 cm^{-1} are due to C–O–C stretching vibration in polysulfone and in–phase out–of–plane hydrogen deformation of para–substituted phenyl groups [205].

A.1.2 Membrane pore size measurement

Measurement of pore size is based on the membrane potential that is created between two half–cells of the same electrolyte(s) at identical temperature and hydrostatic pressure but at different concentrations. The difference between the electric potential in the bulk solution of the higher concentration and that in the bulk solution of the lower concentration half–cell is called the membrane potential. The steric, electric and dielectric exclusion (SEDE) model, which is an improved version of the Teorell–Meyer–Sievers (TMS) model is used to describe the membrane potential that can be used to determine the pore sizes of NF membranes. It has been shown that the diffusion potential (high concentration limit of the membrane potential) in solutions of single binary electrolyte is only affected by the membrane pore size and does not depend on either the dielectric constant inside the pores or the membrane fixed charge [67, 80, 206]. Thus, membrane potential measurements carried out at high concentrations with binary electrolyte are used to assess the pore sizes of NF membranes.

Since a full theoretical description of the SEDE model is available elsewhere [68, 80, 99], just a brief description of the equations used for the calculation of pore size (expression for membrane potential at high concentration of binary electrolyte) is given below. The apparatus for the measurement of the membrane potentials is shown in Figure A.1 and all the equations are listed in Table A.1.

Within the scope of SEDE and TMS models, the membrane potential ($\Delta\psi_m$) can be shown as the sum of two components, namely the difference in the Donnan potentials at opposite membrane/external solution interfaces ($\Delta\psi_D^{\Delta x} - \Delta\psi_D^0$) and the diffusion potential ($\Delta\psi_{diff}$) arising from the membrane pores as shown in Eq 1 [207]. However, the membrane potential for binary

electrolyte at high concentrations equals only the contribution from diffusion potential while the Donnan potential contribution is zero, which is shown in Eq 2. In the formalism of the SEDE model, the diffusion and membrane potential reads as shown in Eq 3. For the sake of simplifying Eq 3, the concentration of electrolyte in the high concentration half–cell is chosen to be twice the concentration of electrolyte in the lower concentration half–cell (Eq 4). Also, within the scope of the SEDE model, the partitioning coefficient accounts for steric effects, the Donnan exclusion and the dielectric exclusion and can be calculated as shown in Eq 5. Escoda et al. [80] have shown that at high salt concentration, $\Delta\psi_D^{\Delta x} = \Delta\psi_D^0$ and $k_i^0 = k_i^{\Delta x}$. Thus, writing Eq 5 for both membrane interfaces (int = 0 and Δx) and considering the electrolyte concentrations in the bulk phase at these interfaces (Eq 4), we can derive Eq 6 that describes the ratio of the concentration of ion 'i' at the interface between the membrane and the most diluted solution to its concentration at the interface between the membrane and the most concentrated solution equal to half (both inside the membrane and in the bulk). Combining Eq 6 and Eq 3 gives the final expression for the membrane potential developed at high concentration of single salt (MA) as shown in Eq 7.

$\Delta\psi_{cell}$ can be measured using two half–cell membrane potential measurement setup (Figure A.1) and $\Delta\psi_m$ can be calculated using Eq 8, which considers the concentration potential resulting from the difference in solution concentrations. Knowing the membrane potential ($\Delta\psi_m$), effective pore radius of the membrane can be calculated by iteration using Eq 7 and the equation for the steric hindrance factor (K_i).

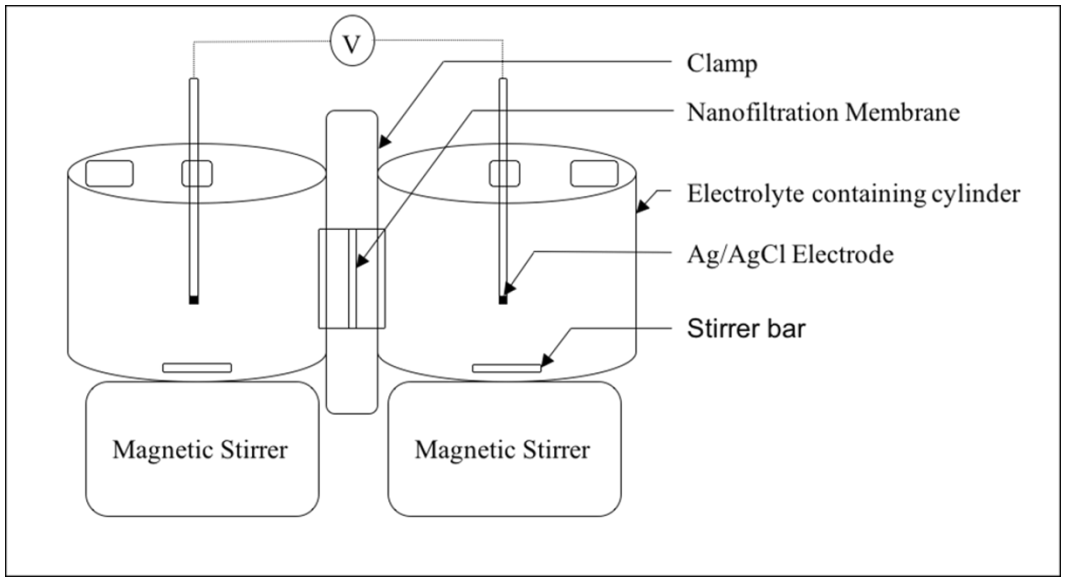

Figure A.1. Apparatus for measurement of effective membrane pore radii

Table A.1. SEDE model equations for binary electrolyte at high concentration to calculate the pore size of membrane

Equations	Eq #
$\Delta\psi_m = (\Delta\psi_D^{\Delta x} - \Delta\psi_D^0) + \Delta\psi_{diff}$	1
$\Delta\psi_m = \Delta\psi_{diff}$	2
$\Delta\psi_m = -\frac{k_B T}{e}\left(\frac{\sum_i K_i D_i z_i \left(C_i^{\Delta x} - C_i^0\right)}{\sum_i K_i D_i z_i^2 \left(C_i^{\Delta x} - C_i^0\right)}\right) \ln\left(\frac{\sum_i K_i D_i z_i^2 C_i^0}{K_i D_i z_i^2 C_i^{\Delta x}}\right)$	3
$c_i^0 = 2c_i^{\Delta x}$	4
$\frac{C_i^{int}}{c_i^{int}} = k_i^{int} \exp\left(-\frac{z_i e \Delta\psi_D^{int}}{k_B T}\right)$	5
$\frac{C_i^{\Delta x}}{C_i^0} = \frac{c_i^{\Delta x}}{c_i^0} = \frac{1}{2}$	6
$\Delta\psi_m = -\frac{k_B T}{e}\left(\frac{K_{M^+} D_{M^+} - K_{A^-} D_{A^-}}{K_{M^+} D_{M^+} + K_{A^-} D_{A^-}}\right) \ln(2)$	7
$\Delta\psi_m = \Delta\psi_{cell} - \frac{k_B T}{e} \ln(2)$	8
Δx and 0 refer to the interface between the membrane and the most diluted solution and the interface between the membrane and the most concentrated solution respectively. Superscript 'int' stands for Δx and 0 depending on the interface that is considered.	

Table A.1. (Continued)

C_i^{int} and c_i^{int} refer to the concentration of ion 'i' inside the membrane and in the bulk respectively.

k_B = Boltzman constant, T = Temperature, e = Electron charge

K_i, D_i, z_i = Hindrance diffusion factor accounting for effect of finite ion and pore sizes, diffusion coefficient at infinite dilution and valence of ion 'i' respectively.

Where, considering cylindrical pores, $K_i = \frac{6\pi}{K_{i,t}}$

$$K_{i,t} = \frac{9}{4}\pi^2\sqrt{2}(1-\lambda_i)^{-5/2}\left[1 + \sum_{n=1}^{2} a_n(1-\lambda_i)^n\right] + \sum_{n=0}^{4} a_{n+3}\lambda_i^n$$

with $a_1 = -\frac{73}{60}, a_2 = \frac{77.293}{50.400}, a_3 = -22.5083, a_4 = -5.6117, a_5 = -0.3363,$ $a_6 = -1.216$ *and* $a_7 = 1.647$

where $\lambda_i = r_i/r_p$, r_i is the Stokes radius of ion 'i' and r_p is the membrane pore radius.

k_i^{int} is a function of the interaction energies due to the Born dielectric effect and image forces.

A.1.3 Additional ion rejection experiments

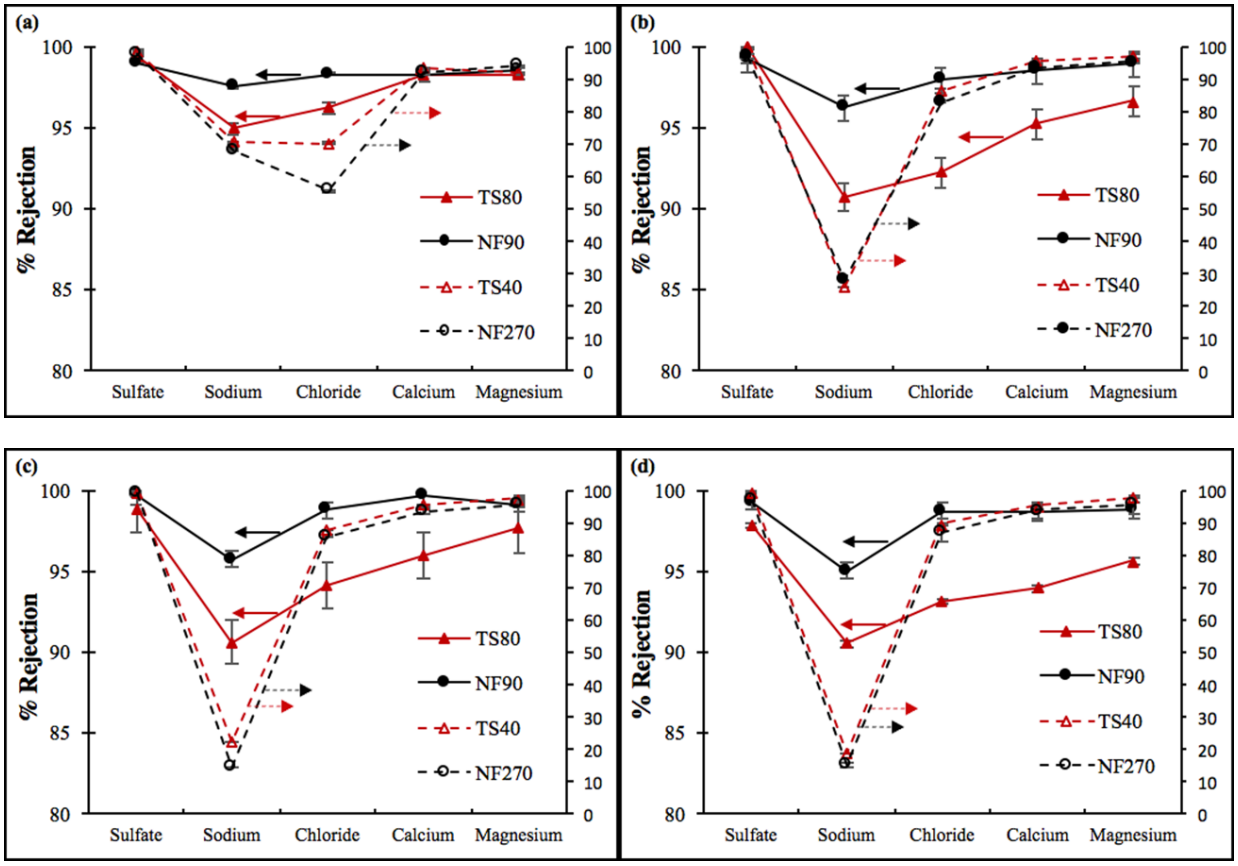

Figure A.2. Rejection of ionic species with feed solutions: (a) 96 mg/l sulfate + 24 mg/l magnesium + 40 mg/l calcium (b) 650 mg/l sulfate + 200 mg/L magnesium + 1000 mg/l calcium, (c) 650 mg/L sulfate + 1000 mg/L magnesium + 200 mg/l calcium and (d) 650 mg/L sulfate + 1000 mg/L magnesium + 1000 mg/L calcium

Figure A.2 provides additional evidence for the impact of separation potentials of active layers (i.e. polyamide/fully aromatic and poly(piperazineamide)/semi–aromatic) on the rejection performance of nanofiltration membranes. Results on Figure A.2 (a) were obtained using dilute feed ionic strength (i.e., 96 mg/l sulfate + 24 mg/l magnesium + 40 mg/l calcium) where both Donnan (charge) and steric effects would contribute to ion rejection [98]. Polyamide membranes achieved > 98% rejection of calcium and magnesium ions while poly(piperazineamide)

membranes achieved 91 – 93% rejection of these cations. Also, polyamide membranes achieved > 94% rejection of sodium and chloride ions in each case while the rejection of these ions by poly(piperazineamide) membranes ranged between 60 – 70%. This further provides evidence that poly(piperazineamide) membranes achieved lower ion rejection despite having more electronegative surfaces than polyamide membranes and clearly supports that the steric rejection potential can be more dominant than Donnan potential in the overall rejection by a particular membrane. Such behavior suggests that the contribution of charge effects (Donnan potential) towards ion rejection by polyamide membranes is weak.

Rejection of divalent ions (i.e., sulfate, magnesium and calcium) changed only slightly (3.5% or less) for both PA and PP membranes at high feed ionic strength (i.e., Figure A.2 (b), (c) & (d)). However, the rejection of sodium and chloride ions was affected by the elevated ion concentrations in the feed as compared to those achieved with dilute feed (i.e., Figure A.1 (a)). The decrease in the rejection of sodium with an increase in feed concentration was significant for PP membranes where it decreased by at least 35% while it changed by 5% or less for PA membranes. This decrease in rejection for poly(piperazineamide) membranes occurs when the Donnan separation potential has been screened out and is no longer assisting the separation, which suggests that Donnan potential contributed significantly to separation at dilute feed conditions for PP membranes.

These additional experiments support the conclusion that rejection by polyamide membranes is predominantly dependent on the pore size effects (i.e., size exclusion) and that the contribution of Donnan (charge) effects is rather weak. On the other hand, increase in the ionic strength of the feed solution when the Donnan exclusion effects are negligible due to charge screening strongly influenced ion rejection by poly(piperazineamide) membranes, which

confirmed that the Donnan (charge) exclusion contributes significantly to the performance of poly(piperazineamide) membranes in addition to steric hindrance.

A.1.4 Schematic of the crossflow NF filtration system

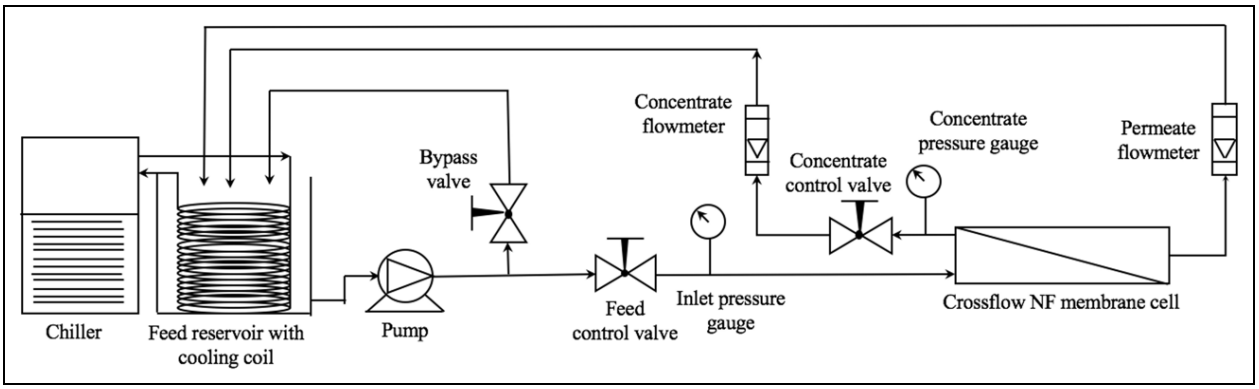

Figure A.3. Schematic of the crossflow NF filtration system

A.1.5 Ionic diffusivity and Stokes radii of ions used in this study

Table A.2. Ionic diffusivity [47] and Stokes radii of ions used in this study

Ions	Diffusivities (10^{-9} m^2/s)	Stokes Radii (nm)
SO_4^{-2}	1.065	0.229
Cl^-	2.032	0.12
Na^+	1.334	0.183
Mg^{+2}	0.706	0.345
Ca^{+2}	0.792	0.307

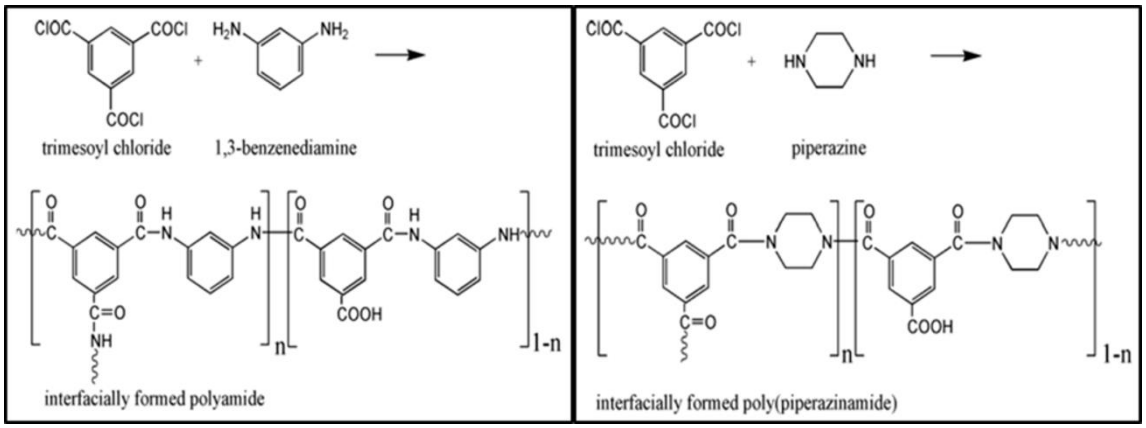

Figure A.4. Reaction schemes for synthesis of polyamide TFC NF membranes. Fully aromatic based on trimesoyl chloride (TMC) and 1,3-benzenediamaine (MPD) (*left*), Semi-aromatic based on trimesoyl chloride (TMC) and piperazine (PIP) (*right*) *[63]*

A.2 SUPPORTING INFORMATION FOR CHAPTER 3.0

A.2.1 SEM characterization

Membrane surface and cross section were characterized using SEM and the average overall membrane and the support thickness were measured (Table A.3). Each value shown in Table A.3 represents an average of more than 9 measurements made with 3 membrane samples. The poly(piperazineamide) membranes (i.e., NF270 and TS40) were relatively smooth as compared to polyamide membranes (i.e., NF90 and TS80) and hence were hard to focus with the SEM (Figure A.5). Also, cross section view showed similar average polysulfone support layer thickness for all the four membranes tested (Figure A.6 and Table A.3).

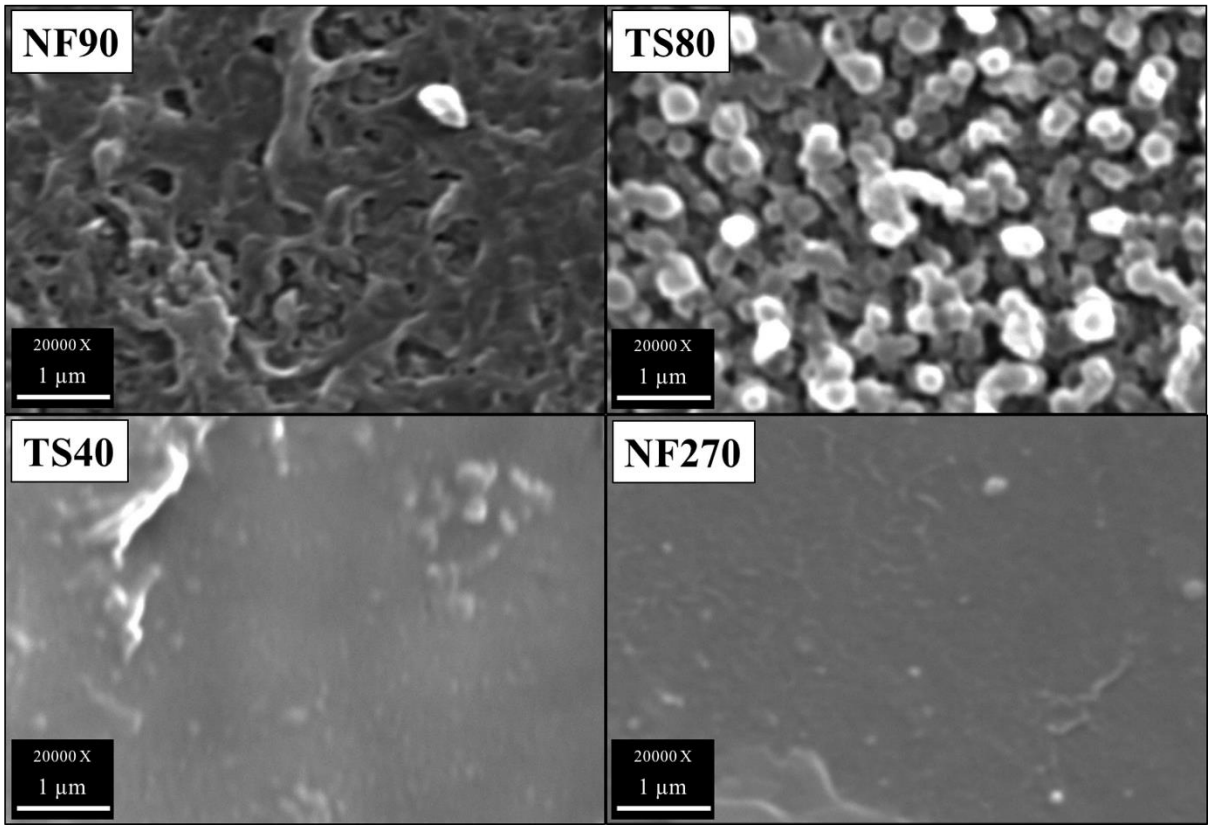

Figure A.5. SEM characterization of NF membrane surfaces at 20,000X magnification.

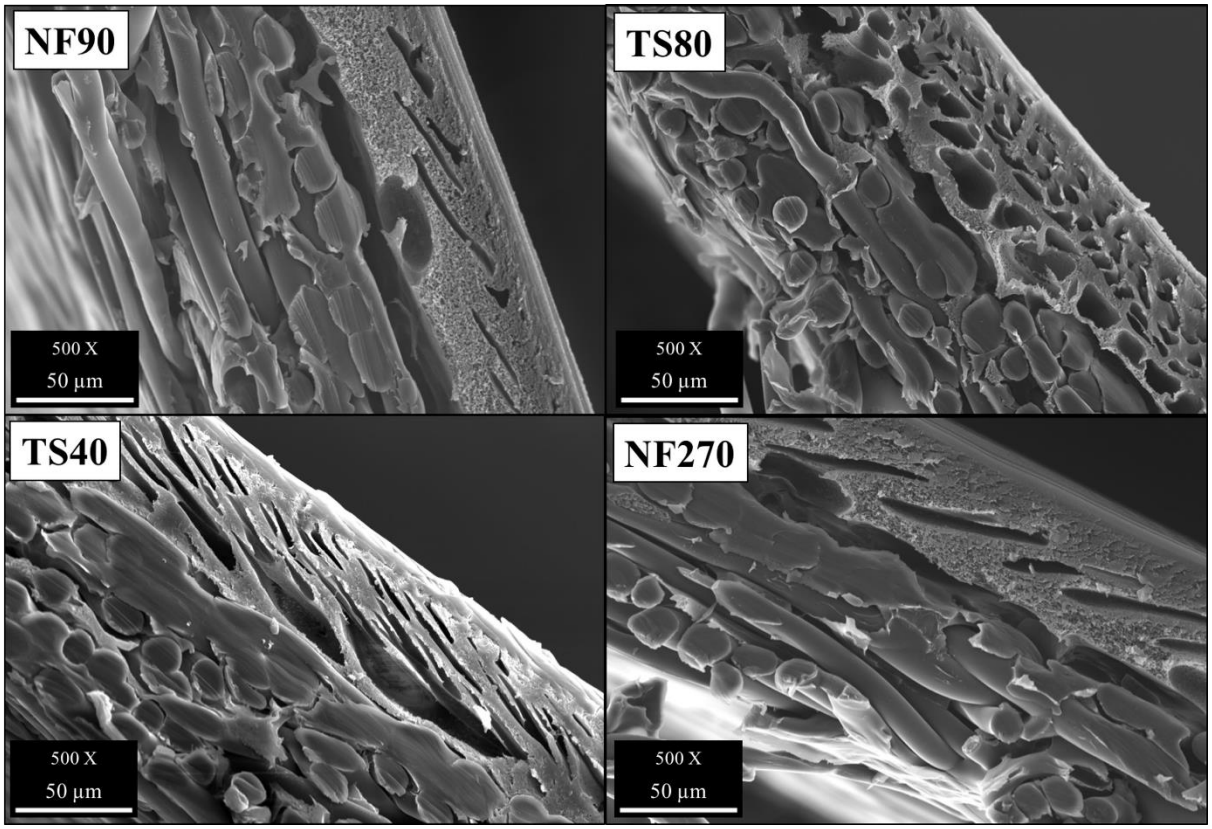

Figure A.6. SEM characterization of NF membrane cross section at 500X magnification.

Table A.3. Characteristics of membranes used in this study.

Membranes	Fully Aromatic (FA)		Semi–Aromatic (SA)	
	NF90	TS80	NF270	TS40
Active layer	Polyamide	Polyamide	Poly(piperazine–amide)	Poly(piperazine–amide)
MWCO	~200[a]	~150[b]	~200–300[c]	~200[b]
Effective mean pore radii (nm)[d]	0.68 ± 0.02	0.71 ± 0.02	0.87 ± 0.02	0.8 ± 0.03
Polysulfone support layer thickness (µm)	55.8 ± 1.9	57.3 ± 5.8	57.5 ± 3.5	58.2 ± 2.7
Overall membrane thickness (µm)	140.9 ± 2.2	136.7 ± 2.5	142 ± 1.8	145.4 ± 6.6

Active layer thicknesses: NF90 > TS80 > TS40 > NF270; a[79], b[76], [c]Provided by manufacturer, d[1]

A.2.2 XPS characterization

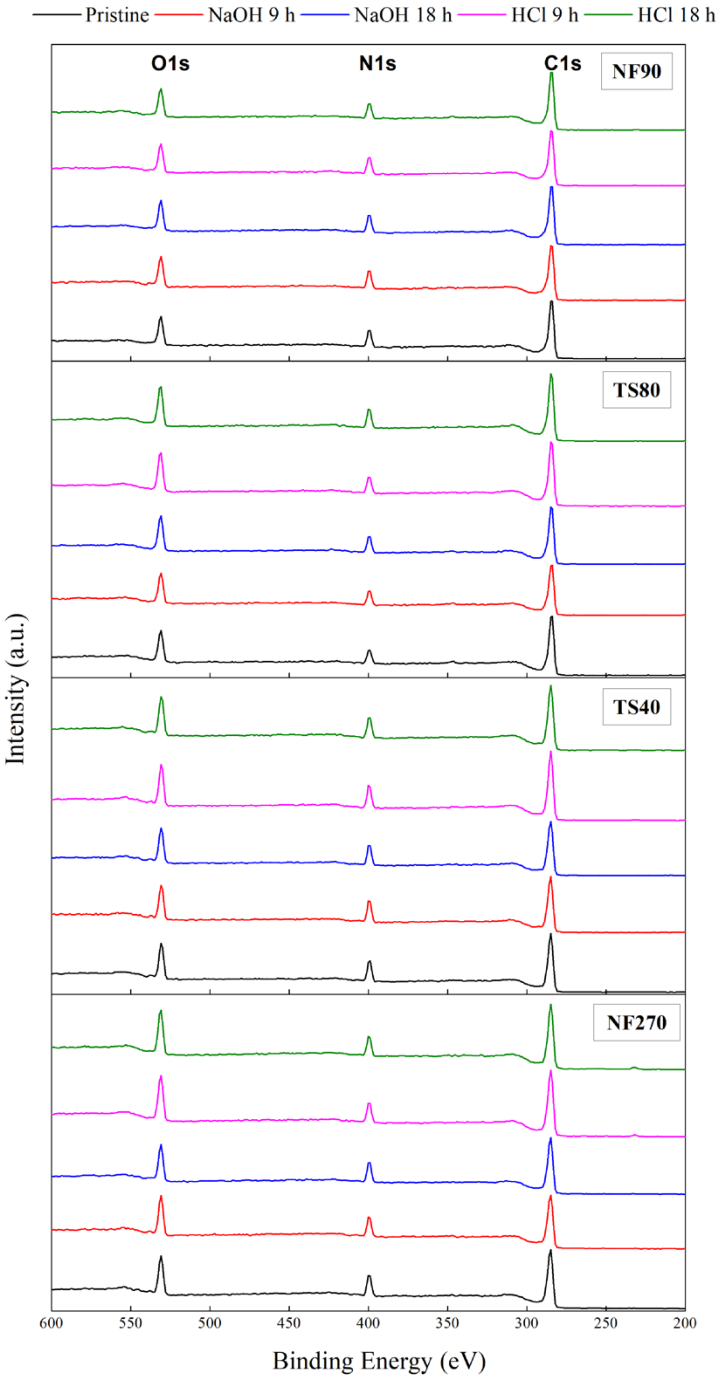

a

Figure A.7. Survey spectra showing O (1s), N (1s) and C (1s) peaks using XPS for all four tested membranes pre– and post–chemical cleaning

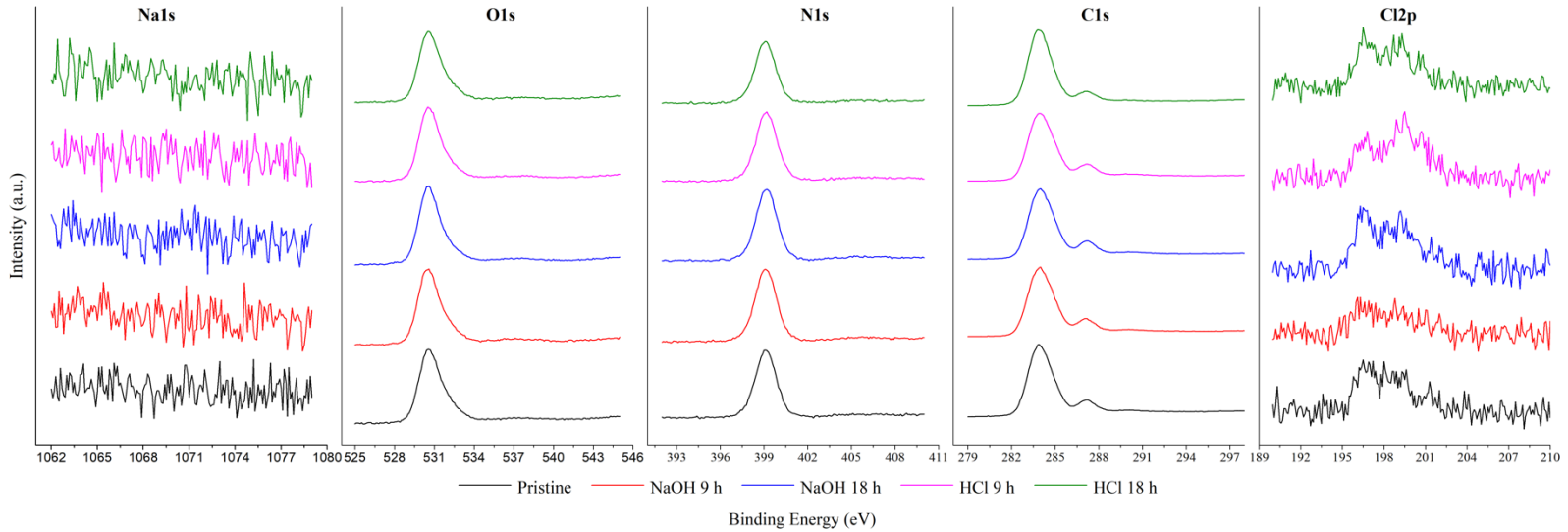

Figure A.8. High resolution peaks for Na (1s), O (1s), N (1s), C (1s) and Cl (2p) using XPS for NF90 membrane pre– and post–chemical cleaning. Peaks for Na (1s) were not detected and that for Cl (2p) were not quantifiable. Identical characteristics were observed with TS80, NF270 and TS40 membranes

A.3 SUPPORTING INFORMATION FOR CHAPTER 4.0

A.3.1 Zeta potential analysis

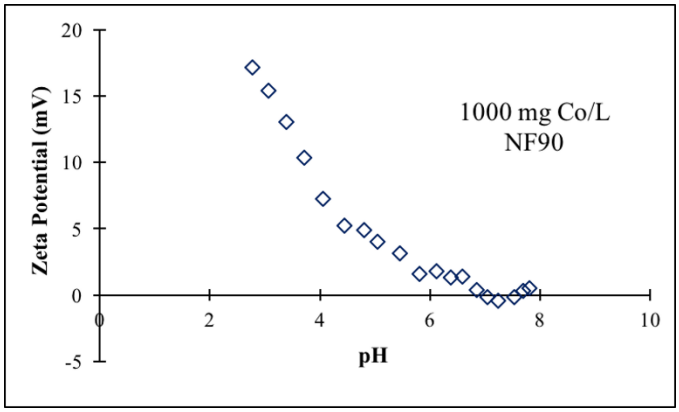

Figure A.9. Zeta potential analysis with 1000 mg Co/L with NF90 membrane

A.3.2 Influence of crossflow velocity on ion rejection

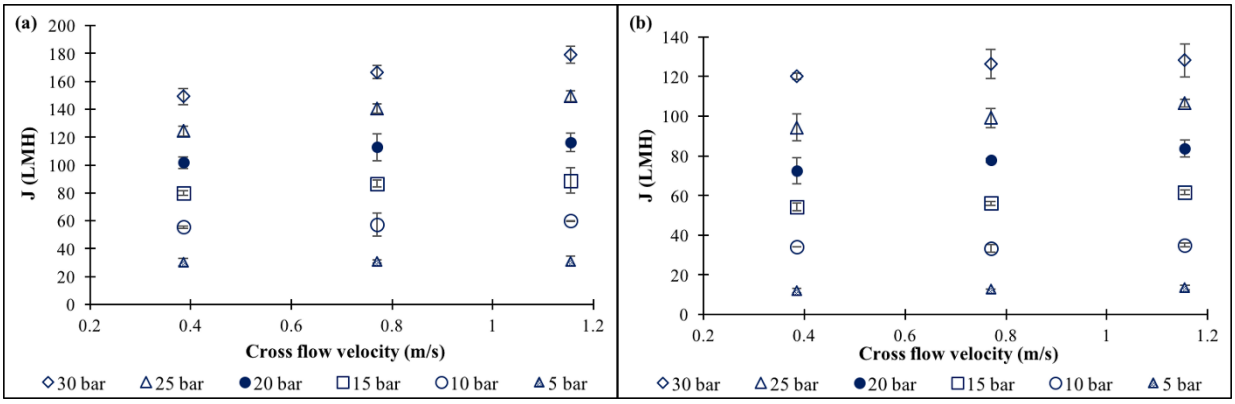

Figure A.10. Permeate flux as a function of feed crossflow velocity for (a) 0.36 mM and (b) 36.4 mM strontium chloride feed concentration (Experimental conditions: Feed pH = 5.6 ± 0.2, T = 23 ± 1°C)

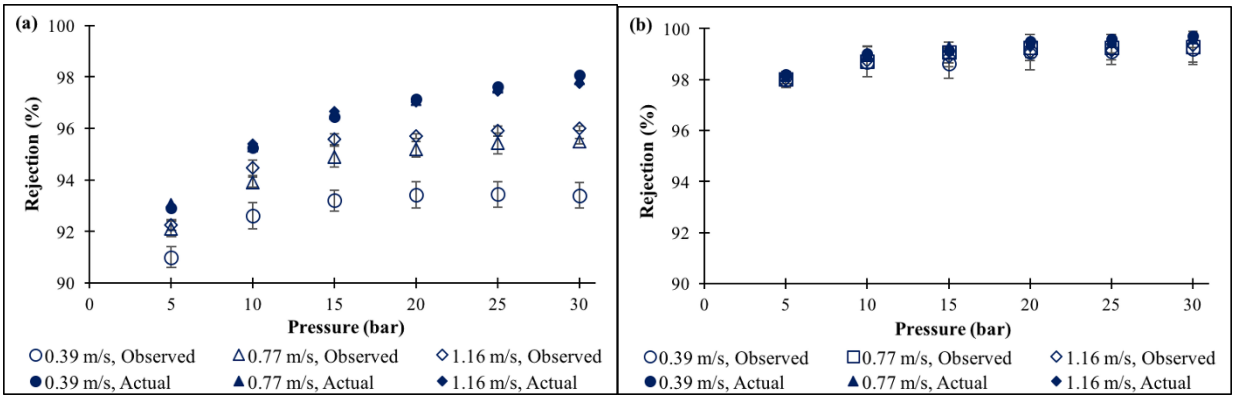

Figure A.11. Impact of operating feed pressure on the observed and actual (intrinsic) ion rejection for (a) 0.36 mM and (b) 36.4 mM strontium chloride concentration (Experimental conditions: Feed pH = 5.6 ± 0.2, T = 23 ± 1°C)

A.3.3 Influence of feed pressure and concentration on ion rejection

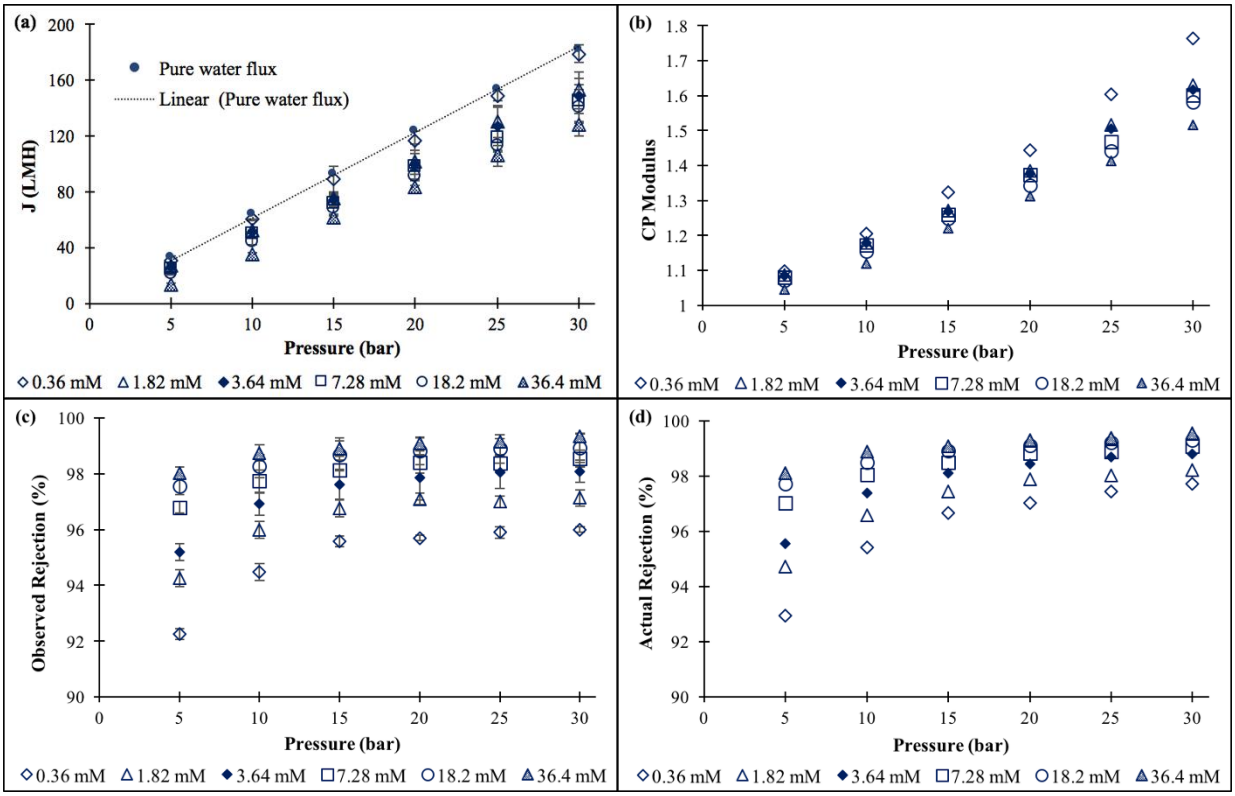

Figure A.12. Impact of operating feed pressure on (a) permeate flux, (b) CP modulus, (c) observed rejection, and (d) actual (intrinsic) rejection for strontium chloride. (Experimental conditions: Feed crossflow velocity = 1.16 m/s, pH = 5.6 $\pm$ 0.2, T = 23 $\pm$ 1°C)

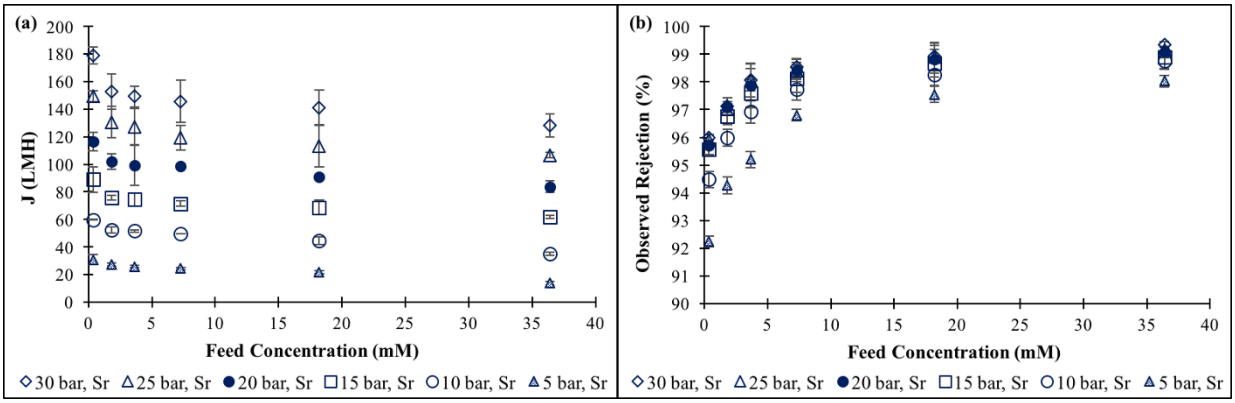

Figure A.13. Impact of feed strontium chloride concentration on (a) permeate flux and (b) observed ion rejection.

(Experimental conditions: Feed crossflow velocity = 1.16 m/s, pH = 5.6 ± 0.2, T = 23 ± 1°C)

BIBLIOGRAPHY

[1] S.S. Wadekar, R.D. Vidic, Influence of Active Layer on Separation Potentials of Nanofiltration Membranes for Inorganic Ions, Environmental Science & Technology, 51 (2017) 5658-5665.

[2] S.S. Wadekar, T. Hayes, O.R. Lokare, D. Mittal, R.D. Vidic, Laboratory and Pilot-Scale Nanofiltration Treatment of Abandoned Mine Drainage for the Recovery of Products Suitable for Industrial Reuse, Industrial & Engineering Chemistry Research, 56 (2017) 7355-7364.

[3] S.S. Wadekar, R.D. Vidic, Comparison of ceramic and polymeric nanofiltration membranes for treatment of abandoned coal mine drainage, Desalination, 440 (2018) 135-145.

[4] S.S. Wadekar, R.D. Vidic, Insights into the rejection of barium and strontium by nanofiltration membrane from experimental and modeling analysis, Journal of Membrane Science, (2018) *(under review).*

[5] S.S. Wadekar, Y. Wang, O.R. Lokare, R.D. Vidic, Influence of chemical cleaning on the physicochemical characteristics and ion rejection by thin film composite nanofiltration membranes, Journal of Membrane Science, (2018) *(under review).*

[6] S.S. Wadekar, R.D. Vidic, Optimization of abandoned mine drainage treatment by commercially available nanofiltration membranes, in: Proceedings of the 2017 American Water Works Association (AWWA)–American Membrane Technology Association (AMTA) Membrane Technology Conference and Exposition, Long Beach, California, 2017.

[7] S.S. Wadekar, R.D. Vidic, Effect of repetitive chemical cleaning on the performance of polymeric nanofiltration membranes, in: Proceedings of the 2018 American Water Works Association (AWWA)–American Membrane Technology Association (AMTA) Membrane Technology Conference and Exposition, West Palm Beach, Florida, 2018.

[8] G. Wade Miller, Integrated concepts in water reuse: managing global water needs, Desalination, 187 (2006) 65-75.

[9] United Nations, GLASS Report, UN-Water Global Annual Assessment of Sanitation and Drinking Water, (2010) http://apps.who.int/iris/bitstream/handle/10665/254999/9789241512190-eng.pdf?sequence=1 (accessed 03/18/2018).

[10] R.F. Service, Desalination Freshens Up, Science, 313 (2006) 1088-1090.

[11] World Health Organization, Guidelines for Drinking Water Quality: Third Edition, Incorporating the First and Second Addenda, Geneva, (2008), http://www.who.int/water_sanitation_health/dwq/fulltext.pdf (accessed 03/18/2018).

[12] M. Elimelech, W.A. Phillip, The Future of Seawater Desalination: Energy, Technology, and the Environment, Science, 333 (2011) 712-717.

[13] M.A. Shannon, P.W. Bohn, M. Elimelech, J.G. Georgiadis, B.J. Marinas, A.M. Mayes, Science and technology for water purification in the coming decades, Nature, 452 (2008) 301-310.

[14] M. Mullett, R. Fornarelli, D. Ralph, Nanofiltration of mine water: impact of feed pH and membrane charge on resource recovery and water discharge, Membranes, 4 (2014) 163-180.

[15] B. Dold, Basic concepts in environmental geochemistry of sulfidic mine-waste management, INTECH Open Access Publisher, 2010.

[16] H. Al-Zoubi, A. Rieger, P. Steinberger, W. Pelz, R. Haseneder, G. Härtel, Nanofiltration of acid mine drainage, Desalination and Water Treatment, 21 (2010) 148-161.

[17] H. Al-Zoubi, A. Rieger, P. Steinberger, W. Pelz, R. Haseneder, G. Härtel, Optimization study for treatment of acid mine drainage using membrane technology, Separation Science and Technology, 45 (2010) 2004-2016.

[18] A. Akcil, S. Koldas, Acid Mine Drainage (AMD): causes, treatment and case studies, Journal of Cleaner Production, 14 (2006) 1139-1145.

[19] Pennsylvania Water Shed Project http://pennsylvaniawatersheds.org/our-work/abandoned-mine-drainage/ (accessed 02/18/2016).

[20] R.S. Hedin, G.R. Watzlaf, R.W. Nairn, Passive treatment of acid mine drainage with limestone, Journal of Environmental Quality, 23 (1994) 1338-1345.

[21] S. Santomartino, J.A. Webb, Estimating the longevity of limestone drains in treating acid mine drainage containing high concentrations of iron, Applied Geochemistry, 22 (2007) 2344-2361.

[22] G.S. Simate, S. Ndlovu, Acid mine drainage: Challenges and opportunities, Journal of Environmental Chemical Engineering, 2 (2014) 1785-1803.

[23] A. Rieger, P. Steinberger, W. Pelz, R. Haseneder, G. Härtel, Mine water treatment by membrane filtration processes-Experimental investigations on applicability, Desalination and Water Treatment, 6 (2009) 54-60.

[24] C. Binnie, M. Kimber, G. Smethurst, Basic water treatment, Royal society of chemistry, 2002.

[25] S. Loeb, S. Sourirajan, Sea Water Demineralization by Means of an Osmotic Membrane, Saline Water Conversion—II, AMERICAN CHEMICAL SOCIETY, 1963, pp. 117-132.

[26] L.F. Greenlee, D.F. Lawler, B.D. Freeman, B. Marrot, P. Moulin, Reverse osmosis desalination: Water sources, technology, and today's challenges, Water Research, 43 (2009) 2317-2348.

[27] P. Eriksson, Nanofiltration extends the range of membrane filtration, Environmental Progress, 7 (1988) 58-62.

[28] B. Van der Bruggen, C. Vandecasteele, Removal of pollutants from surface water and groundwater by nanofiltration: overview of possible applications in the drinking water industry, Environmental Pollution, 122 (2003) 435-445.

[29] R.J. Peterson, Composite reverse-osmosis and nano-filtration membranes, Journal of Membrane Science, 83 (1993) 81-150.

[30] A.W. Mohammad, Y.H. Teow, W.L. Ang, Y.T. Chung, D.L. Oatley-Radcliffe, N. Hilal, Nanofiltration membranes review: Recent advances and future prospects, Desalination, 356 (2015) 226-254.

[31] S. Veríssimo, K.V. Peinemann, J. Bordado, Influence of the diamine structure on the nanofiltration performance, surface morphology and surface charge of the composite polyamide membranes, Journal of Membrane Science, 279 (2006) 266-275.

[32] Y. Li, Y. Su, Y. Dong, X. Zhao, Z. Jiang, R. Zhang, J. Zhao, Separation performance of thin-film composite nanofiltration membrane through interfacial polymerization using different amine monomers, Desalination, 333 (2014) 59-65.

[33] A.L. Ahmad, B.S. Ooi, A.W. Mohammad, J.P. Choudhury, Composite Nanofiltration Polyamide Membrane: A Study on the Diamine Ratio and Its Performance Evaluation, Industrial & Engineering Chemistry Research, 43 (2004) 8074-8082.

[34] B.B. Vyas, P. Ray, Preparation of nanofiltration membranes and relating surface chemistry with potential and topography: Application in separation and desalting of amino acids, Desalination, 362 (2015) 104-116.

[35] J. Jegal, S.G. Min, K.H. Lee, Factors affecting the interfacial polymerization of polyamide active layers for the formation of polyamide composite membranes, Journal of Applied Polymer Science, 86 (2002) 2781-2787.

[36] T. Van Gestel, C. Vandecasteele, A. Buekenhoudt, C. Dotremont, J. Luyten, B. Van der Bruggen, G. Maes, Corrosion properties of alumina and titania NF membranes, Journal of Membrane Science, 214 (2003) 21-29.

[37] Y.S. Lin, I. Kumakiri, B.N. Nair, H. Alsyouri, Microporus inorganic membranes, Separation and Purification Methods, 31 (2002) 229-379.

[38] T. Van Gestel, C. Vandecasteele, A. Buekenhoudt, C. Dotremont, J. Luyten, R. Leysen, B. Van der Bruggen, G. Maes, Salt retention in nanofiltration with multilayer ceramic TiO_2 membranes, Journal of Membrane Science, 209 (2002) 379-389.

[39] W. Puthai, M. Kanezashi, H. Nagasawa, T. Tsuru, Development and permeation properties of SiO_2-ZrO_2 nanofiltration membranes with a MWCO of <200, Journal of Membrane Science, 535 (2017) 331-341.

[40] T. Fujioka, S.J. Khan, J.A. McDonald, L.D. Nghiem, Nanofiltration of trace organic chemicals: A comparison between ceramic and polymeric membranes, Separation and Purification Technology, 136 (2014) 258-264.

[41] R. Shang, A. Goulas, C.Y. Tang, X. de Frias Serra, L.C. Rietveld, S.G.J. Heijman, Atmospheric pressure atomic layer deposition for tight ceramic nanofiltration membranes: Synthesis and application in water purification, Journal of Membrane Science, 528 (2017) 163-170.

[42] K.D. Bishop, T.J. Kirkmann, Inorganic structure for molecular separations, US Patent 20090131244 A1, 2013.

[43] S. Choi, Z. Yun, S. Hong, K. Ahn, The effect of co-existing ions and surface characteristics of nanomembranes on the removal of nitrate and fluoride, Desalination, 133 (2001) 53-64.

[44] A.I. Schäfer, A.G. Fane, T.D. Waite, Nanofiltration: principles and applications, Elsevier, Oxford, UK, 2005.

[45] C. Bartels, R. Franks, S. Rybar, M. Schierach, M. Wilf, The effect of feed ionic strength on salt passage through reverse osmosis membranes, Desalination, 184 (2005) 185-195.

[46] B. Tansel, J. Sager, T. Rector, J. Garland, R.F. Strayer, L. Levine, M. Roberts, M. Hummerick, J. Bauer, Significance of hydrated radius and hydration shells on ionic permeability during nanofiltration in dead end and cross flow modes, Separation and Purification Technology, 51 (2006) 40-47.

[47] R.C. Weast, M.J. Astle, W.H. Beyer, CRC handbook of chemistry and physics, CRC press Boca Raton, FL, 1988.

[48] L. Li, J. Dong, T.M. Nenoff, Transport of water and alkali metal ions through MFI zeolite membranes during reverse osmosis, Separation and Purification Technology, 53 (2007) 42-48.

[49] W.M. Deen, Hindered transport of large molecules in liquid-filled pores, AIChE Journal, 33 (1987) 1409-1425.

[50] A.E. Yaroshchuk, Non-steric mechanisms of nanofiltration: superposition of Donnan and dielectric exclusion, Separation and Purification Technology, 22-23 (2001) 143-158.

[51] T. Luxbacher, The ZETA Guide: Principles of the Streaming Potential Technique, Anton Paar, (2014).

[52] R. Rautenbach, A. Gröschl, Separation potential of nanofiltration membranes, Desalination, 77 (1990) 73-84.

[53] A.E. Yaroshchuk, Dielectric exclusion of ions from membranes, Advances in colloid and interface science, 85 (2000) 193-230.

[54] A. Yaroshchuk, M.L. Bruening, E.E. Licón Bernal, Solution-Diffusion–Electro-Migration model and its uses for analysis of nanofiltration, pressure-retarded osmosis and forward osmosis in multi-ionic solutions, Journal of Membrane Science, 447 (2013) 463-476.

[55] A. Al-Amoudi, R.W. Lovitt, Fouling strategies and the cleaning system of NF membranes and factors affecting cleaning efficiency, Journal of Membrane Science, 303 (2007) 4-28.

[56] B. Van der Bruggen, M. Mänttäri, M. Nyström, Drawbacks of applying nanofiltration and how to avoid them: A review, Separation and Purification Technology, 63 (2008) 251-263.

[57] DOW FILMTECH MEMBRANES, Cleaning Procedures for DOW FILMTECH FT30 Elements, Tech Fact, http://msdssearch.dow.com/PublishedLiteratureDOWCOM/dh_060a/0901b8038060a66f.pdf?filepath=liquidseps/pdfs/noreg/609-23010.pdf&fromPage=GetDoc.

[58] A.S. Al-Amoudi, A.M. Farooque, Performance restoration and autopsy of NF membranes used in seawater pretreatment, Desalination, 178 (2005) 261-271.

[59] R. Liikanen, J. Yli-Kuivila, R. Laukkanen, Efficiency of various chemical cleanings for nanofiltration membrane fouled by conventionally-treated surface water, Journal of Membrane Science, 195 (2002) 265-276.

[60] S. Siavash Madaeni, T. Mohamamdi, M. Kazemi Moghadam, Chemical cleaning of reverse osmosis membranes, Desalination, 134 (2001) 77-82.

[61] X. Li, J. Li, X. Fu, R. Wickramasinghe, J. Chen, Chemical cleaning of PS ultrafilters fouled by the fermentation broth of glutamic acid, Separation and Purification Technology, 42 (2005) 181-187.

[62] G.M. Geise, H.-S. Lee, D.J. Miller, B.D. Freeman, J.E. McGrath, D.R. Paul, Water purification by membranes: The role of polymer science, Journal of Polymer Science Part B: Polymer Physics, 48 (2010) 1685-1718.

[63] C.Y. Tang, Y.-N. Kwon, J.O. Leckie, Effect of membrane chemistry and coating layer on physiochemical properties of thin film composite polyamide RO and NF membranes: I. FTIR and XPS characterization of polyamide and coating layer chemistry, Desalination, 242 (2009) 149-167.

[64] A. Szymczyk, Mechanistic modeling of transport in nanofiltration, Encyclopedia of Membrane Science and Technology, (2013).

[65] L.D. Nghiem, A.I. Schäfer, M. Elimelech, Pharmaceutical Retention Mechanisms by Nanofiltration Membranes, Environmental Science & Technology, 39 (2005) 7698-7705.

[66] J. Schaep, C. Vandecasteele, A.W. MOHAMMAD, W.R. Bowen, Analysis of the salt retention of nanofiltration membranes using the Donnan–Steric partitioning pore model, Separation science and Technology, 34 (1999) 3009-3030.

[67] Y. Lanteri, A. Szymczyk, P. Fievet, Influence of Steric, Electric, and Dielectric Effects on Membrane Potential, Langmuir, 24 (2008) 7955-7962.

[68] Y. Lanteri, P. Fievet, A. Szymczyk, Evaluation of the steric, electric, and dielectric exclusion model on the basis of salt rejection rate and membrane potential measurements, Journal of Colloid and Interface Science, 331 (2009) 148-155.

[69] R.J. Petersen, J.E. Cadotte, Thin film composite reverse osmosis membranes, Handbook of industrial membrane technology, (1990) 307-348.

[70] C.Y. Tang, Y.-N. Kwon, J.O. Leckie, Effect of membrane chemistry and coating layer on physiochemical properties of thin film composite polyamide RO and NF membranes: II. Membrane physiochemical properties and their dependence on polyamide and coating layers, Desalination, 242 (2009) 168-182.

[71] O. Coronell, B.J. Mariñas, X. Zhang, D.G. Cahill, Quantification of Functional Groups and Modeling of Their Ionization Behavior in the Active Layer of FT30 Reverse Osmosis Membrane, Environmental Science & Technology, 42 (2008) 5260-5266.

[72] O. Coronell, M.I. González, B.J. Mariñas, D.G. Cahill, Ionization Behavior, Stoichiometry of Association, and Accessibility of Functional Groups in the Active Layers of Reverse Osmosis and Nanofiltration Membranes, Environmental Science & Technology, 44 (2010) 6808-6814.

[73] O. Coronell, B.J. Mariñas, D.G. Cahill, Accessibility and Ion Exchange Stoichiometry of Ionized Carboxylic Groups in the Active Layer of FT30 Reverse Osmosis Membrane, Environmental Science & Technology, 43 (2009) 5042-5048.

[74] V. Freger, Nanoscale heterogeneity of polyamide membranes formed by interfacial polymerization, Langmuir, 19 (2003) 4791-4797.

[75] O. Coronell, B.J. Mariñas, D.G. Cahill, Depth Heterogeneity of Fully Aromatic Polyamide Active Layers in Reverse Osmosis and Nanofiltration Membranes, Environmental Science & Technology, 45 (2011) 4513-4520.

[76] H.M. Krieg, S.J. Modise, K. Keizer, H.W.J.P. Neomagus, Salt rejection in nanofiltration for single and binary salt mixtures in view of sulphate removal, Desalination, 171 (2005) 205-215.

[77] P.C. Singer, W. Stumm, Acidic Mine Drainage: The Rate-Determining Step, Science, 167 (1970) 1121-1123.

[78] D.B. Johnson, K.B. Hallberg, Acid mine drainage remediation options: a review, Science of The Total Environment, 338 (2005) 3-14.

[79] G. Artuğ, I. Roosmasari, K. Richau, J. Hapke, A Comprehensive Characterization of Commercial Nanofiltration Membranes, Separation Science and Technology, 42 (2007) 2947-2986.

[80] A. Escoda, Y. Lanteri, P. Fievet, S. Déon, A. Szymczyk, Determining the Dielectric Constant inside Pores of Nanofiltration Membranes from Membrane Potential Measurements, Langmuir, 26 (2010) 14628-14635.

[81] N.K. Saha, S.V. Joshi, Performance evaluation of thin film composite polyamide nanofiltration membrane with variation in monomer type, Journal of Membrane Science, 342 (2009) 60-69.

[82] D.J. Skrovanek, S.E. Howe, P.C. Painter, M.M. Coleman, Hydrogen bonding in polymers: infrared temperature studies of an amorphous polyamide, Macromolecules, 18 (1985) 1676-1683.

[83] G. Socrates, Infrared characteristic Group Frequencies, Wiley-Interscience, (1994).

[84] N.-W. Oh, Jegal, J. and Lee, K.-H., Preparation and characterization of nanofiltration composite membranes using polyacrylonitrile (PAN). I. preparation and modification of PAN supports, J. Appl. Polym. Sci., 80 (2001) 1854–1862.

[85] R. Lo, A. Bhattacharya, B. Ganguly, Probing the selective salt rejection behavior of thin film composite membranes: A DFT study, Journal of Membrane Science, 436 (2013) 90-96.

[86] V. Freger, Swelling and Morphology of the Skin Layer of Polyamide Composite Membranes: An Atomic Force Microscopy Study, Environmental Science & Technology, 38 (2004) 3168-3175.

[87] N. Hilal, H. Al-Zoubi, N.A. Darwish, A.W. Mohammad, Characterisation of nanofiltration membranes using atomic force microscopy, Desalination, 177 (2005) 187-199.

[88] L.D. Nghiem, A.I. Schäfer, M. Elimelech, Removal of Natural Hormones by Nanofiltration Membranes: Measurement, Modeling, and Mechanisms, Environmental Science & Technology, 38 (2004) 1888-1896.

[89] W.R. Bowen, A.W. Mohammad, Characterization and Prediction of Nanofiltration Membrane Performance—A General Assessment, Chemical Engineering Research and Design, 76 (1998) 885-893.

[90] K.L. Tu, L.D. Nghiem, A.R. Chivas, Coupling effects of feed solution pH and ionic strength on the rejection of boron by NF/RO membranes, Chemical Engineering Journal, 168 (2011) 700-706.

[91] A.E. Childress, M. Elimelech, Effect of solution chemistry on the surface charge of polymeric reverse osmosis and nanofiltration membranes, Journal of Membrane Science, 119 (1996) 253-268.

[92] A.E. Childress, M. Elimelech, Relating Nanofiltration Membrane Performance to Membrane Charge (Electrokinetic) Characteristics, Environmental Science & Technology, 34 (2000) 3710-3716.

[93] M.R. Teixeira, M.J. Rosa, M. Nyström, The role of membrane charge on nanofiltration performance, Journal of Membrane Science, 265 (2005) 160-166.

[94] J.-H. Tay, J. Liu, D. Delai Sun, Effect of solution physico-chemistry on the charge property of nanofiltration membranes, Water Research, 36 (2002) 585-598.

[95] N. Hilal, H. Al-Zoubi, N.A. Darwish, A.W. Mohammad, Nanofiltration of Magnesium Chloride, Sodium Carbonate, and Calcium Sulphate in Salt Solutions, Separation Science and Technology, 40 (2005) 3299-3321.

[96] A. Santafé-Moros, J. Gozálvez-Zafrilla, J. Lora-García, Performance of commercial nanofiltration membranes in the removal of nitrate ions, Desalination, 185 (2005) 281-287.

[97] D.-X. Wang, M. Su, Z.-Y. Yu, X.-L. Wang, M. Ando, T. Shintani, Separation performance of a nanofiltration membrane influenced by species and concentration of ions, Desalination, 175 (2005) 219-225.

[98] J.M.M. Peeters, J.P. Boom, M.H.V. Mulder, H. Strathmann, Retention measurements of nanofiltration membranes with electrolyte solutions, Journal of Membrane Science, 145 (1998) 199-209.

[99] A. Szymczyk, P. Fievet, Investigating transport properties of nanofiltration membranes by means of a steric, electric and dielectric exclusion model, Journal of Membrane Science, 252 (2005) 77-88.

[100] A. Parsegian, Energy of an ion crossing a low dielectric membrane: solutions to four relevant electrostatic problems, Nature, 221 (1969) 844-846.

[101] N. Porcelli, S. Judd, Chemical cleaning of potable water membranes: A review, Separation and Purification Technology, 71 (2010) 137-143.

[102] A. Simon, J.A. McDonald, S.J. Khan, W.E. Price, L.D. Nghiem, Effects of caustic cleaning on pore size of nanofiltration membranes and their rejection of trace organic chemicals, Journal of Membrane Science, 447 (2013) 153-162.

[103] A. Simon, W.E. Price, L.D. Nghiem, Effects of chemical cleaning on the nanofiltration of pharmaceutically active compounds (PhACs), Separation and Purification Technology, 88 (2012) 208-215.

[104] A. Simon, Impact of chemical cleaning on the rejection of trace organic contaminants by nanofiltration membranes, (2013).

[105] A. Simon, W.E. Price, L.D. Nghiem, Influence of formulated chemical cleaning reagents on the surface properties and separation efficiency of nanofiltrationmembranes, Journal of membrane science, 432 (2013) 73-82.

[106] M. Nilsson, G. Trägårdh, K. Östergren, Influence of temperature and cleaning on aromatic and semi-aromatic polyamide thin-film composite NF and RO membranes, Separation and Purification Technology, 62 (2008) 717-726.

[107] A. Al-Amoudi, P. Williams, A.S. Al-Hobaib, R.W. Lovitt, Cleaning results of new and fouled nanofiltration membrane characterized by contact angle, updated DSPM, flux and salts rejection, Applied Surface Science, 254 (2008) 3983-3992.

[108] A. Al-Amoudi, P. Williams, S. Mandale, R.W. Lovitt, Cleaning results of new and fouled nanofiltration membrane characterized by zeta potential and permeability, Separation and Purification Technology, 54 (2007) 234-240.

[109] T. Fujioka, S.J. Khan, J.A. McDonald, L.D. Nghiem, Rejection of trace organic chemicals by a nanofiltration membrane: the role of molecular properties and effects of caustic cleaning, Environmental Science: Water Research & Technology, 1 (2015) 846-854.

[110] K.L. Tu, A.R. Chivas, L.D. Nghiem, Chemical cleaning effects on properties and separation efficiency of an RO membrane, (2015).

[111] M. Kallioinen, T. Sainio, J. Lahti, A. Pihlajamäki, H. Koivikko, J. Mattila, M. Mänttäri, Effect of extended exposure to alkaline cleaning chemicals on performance of polyamide (PA) nanofiltration membranes, Separation and Purification Technology, 158 (2016) 115-123.

[112] A. Szymczyk, P. Fievet, Ion transport through nanofiltration membranes: the steric, electric and dielectric exclusion model, Desalination, 200 (2006) 122-124.

[113] S.S. Wadekar, R.D. Vidic, Role of active layer in the performance of aromatic and semi-aromatic nanofiltration membranes for water purification, in: Advanced Membrane Technology VII, USA Eds, ECI Symposium Series, Cork, Ireland, 2016.

[114] S.S. Wadekar, T. Hayes, O.R. Lokare, D. Mittal, R.D. Vidic, Laboratory and Pilot-Scale Nanofiltration Treatment of Abandoned Mine Drainage for the Recovery of Products Suitable for Industrial Reuse, Industrial & Engineering Chemistry Research, (2017).

[115] A.S. Al-Amoudi, Factors affecting natural organic matter (NOM) and scaling fouling in NF membranes: a review, Desalination, 259 (2010) 1-10.

[116] S. Bertrand, I. Lemaitre, E. Wittmann, Performance of a nanofiltration plant on hard and highly sulphated water during two years of operation, Desalination, 113 (1997) 277-281.

[117] V. Freger, J. Gilron, S. Belfer, TFC polyamide membranes modified by grafting of hydrophilic polymers: an FT-IR/AFM/TEM study, Journal of Membrane Science, 209 (2002) 283-292.

[118] Y.-N. Kwon, J.O. Leckie, Hypochlorite degradation of crosslinked polyamide membranes: II. Changes in hydrogen bonding behavior and performance, Journal of Membrane Science, 282 (2006) 456-464.

[119] A.S. Gorzalski, C. Donley, O. Coronell, Elemental composition of membrane foulant layers using EDS, XPS, and RBS, Journal of Membrane Science, 522 (2017) 31-44.

[120] J.-y. Tian, Z.-l. Chen, Y.-l. Yang, H. Liang, J. Nan, G.-b. Li, Consecutive chemical cleaning of fouled PVC membrane using NaOH and ethanol during ultrafiltration of river water, Water Research, 44 (2010) 59-68.

[121] J.W. Moore, S. Ramamoorthy, Heavy metals in natural waters: applied monitoring and impact assessment, Springer Science & Business Media, 2012.

[122] J.W. Patterson, Industrial wastewater treatment technology, Second edition, Butterworth Publishers, Stoneham, MA, USA, 1985.

[123] S.-R. Lim, J.M. Schoenung, Human health and ecological toxicity potentials due to heavy metal content in waste electronic devices with flat panel displays, Journal of Hazardous Materials, 177 (2010) 251-259.

[124] Independent Statistics & Analysis, U.S. Energy Information Administration, www.eia.gov (accessed 01/14/2018).

[125] R.D. Vidic, S.L. Brantley, J.M. Vandenbossche, D. Yoxtheimer, J.D. Abad, Impact of Shale Gas Development on Regional Water Quality, Science, 340 (2013).

[126] S.M. Olmstead, L.A. Muehlenbachs, J.-S. Shih, Z. Chu, A.J. Krupnick, Shale gas development impacts on surface water quality in Pennsylvania, Proceedings of the National Academy of Sciences, 110 (2013) 4962-4967.

[127] K.B. Gregory, R.D. Vidic, D.A. Dzombak, Water Management Challenges Associated with the Production of Shale Gas by Hydraulic Fracturing, Elements, 7 (2011) 181-186.

[128] L.O. Haluszczak, A.W. Rose, L.R. Kump, Geochemical evaluation of flowback brine from Marcellus gas wells in Pennsylvania, USA, Applied Geochemistry, 28 (2013) 55-61.

[129] W.L. Ellsworth, Injection-Induced Earthquakes, Science, 341 (2013).

[130] O.R. Lokare, S. Tavakkoli, S. Wadekar, V. Khanna, R.D. Vidic, Fouling in direct contact membrane distillation of produced water from unconventional gas extraction, Journal of Membrane Science, 524 (2017) 493-501.

[131] E.-D. Hwang, K.-W. Lee, K.-H. Choo, S.-J. Choi, S.-H. Kim, C.-H. Yoon, C.-H. Lee, Effect of precipitation and complexation on nanofiltration of strontium-containing nuclear wastewater, Desalination, 147 (2002) 289-294.

[132] S. Ding, Y. Yang, H. Huang, H. Liu, L.-a. Hou, Effects of feed solution chemistry on low pressure reverse osmosis filtration of cesium and strontium, Journal of Hazardous Materials, 294 (2015) 27-34.

[133] E. Gaubert, H. Barnier, A. Maurel, J. Foos, A. Guy, C. Bardot, M. Lemaire, Selective Strontium Removal from a Sodium Nitrate Aqueous Medium by Nanofiltration - Complexation, Separation Science and Technology, 32 (1997) 585-597.

[134] Environmental Protection Agency, United States, https://www.epa.gov/ (accessed 08//04/17).

[135] DrinkTap by the American Water Works Association, http://www.drinktap.org/water-info/whats-in-my-water/strontium.aspx (accessed 11/15/2017).

[136] L. Charerntanyarak, Heavy metals removal by chemical coagulation and precipitation, Water Science and Technology, 39 (1999) 135-138.

[137] C.-V. Gherasim, P. Mikulášek, Influence of operating variables on the removal of heavy metal ions from aqueous solutions by nanofiltration, Desalination, 343 (2014) 67-74.

[138] C.-V. Gherasim, K. Hancková, J. Palarčík, P. Mikulášek, Investigation of cobalt (II) retention from aqueous solutions by a polyamide nanofiltration membrane, Journal of Membrane Science, 490 (2015) 46-56.

[139] C.-V. Gherasim, J. Cuhorka, P. Mikulášek, Analysis of lead (II) retention from single salt and binary aqueous solutions by a polyamide nanofiltration membrane: Experimental results and modelling, Journal of Membrane Science, 436 (2013) 132-144.

[140] K.-H. Ahn, K.-G. Song, H.-Y. Cha, I.-T. Yeom, Removal of ions in nickel electroplating rinse water using low-pressure nanofiltration, Desalination, 122 (1999) 77-84.

[141] B. Al-Rashdi, D. Johnson, N. Hilal, Removal of heavy metal ions by nanofiltration, Desalination, 315 (2013) 2-17.

[142] Z.V.P. Murthy, A. Choudhary, Separation of cerium from feed solution by nanofiltration, Desalination, 279 (2011) 428-432.

[143] Z. Murthy, L.B. Chaudhari, Application of nanofiltration for the rejection of nickel ions from aqueous solutions and estimation of membrane transport parameters, Journal of hazardous materials, 160 (2008) 70-77.

[144] Y. Ku, S.-W. Chen, W.-Y. Wang, Effect of solution composition on the removal of copper ions by nanofiltration, Separation and Purification Technology, 43 (2005) 135-142.

[145] K. Spiegler, O. Kedem, Thermodynamics of hyperfiltration (reverse osmosis): criteria for efficient membranes, Desalination, 1 (1966) 311-326.

[146] S. Bandini, D. Vezzani, Nanofiltration modeling: the role of dielectric exclusion in membrane characterization, Chemical Engineering Science, 58 (2003) 3303-3326.

[147] B. Saliha, F. Patrick, S. Anthony, Investigating nanofiltration of multi-ionic solutions using the steric, electric and dielectric exclusion model, Chemical Engineering Science, 64 (2009) 3789-3798.

[148] L.A. Richards, B.S. Richards, A.I. Schäfer, Renewable energy powered membrane technology: salt and inorganic contaminant removal by nanofiltration/reverse osmosis, Journal of membrane science, 369 (2011) 188-195.

[149] J. Phattaranawik, R. Jiraratananon, A.G. Fane, C. Halim, Mass flux enhancement using spacer filled channels in direct contact membrane distillation, Journal of Membrane Science, 187 (2001) 193-201.

[150] A.R. Da Costa, A.G. Fane, D.E. Wiley, Spacer characterization and pressure drop modelling in spacer-filled channels for ultrafiltration, Journal of Membrane Science, 87 (1994) 79-98.

[151] K.S. Spiegler, O. Kedem, Thermodynamics of hyperfiltration (reverse osmosis): criteria for efficient membranes, Desalination, 1 (1966) 311-326.

[152] K.Y. Foo, B.H. Hameed, Insights into the modeling of adsorption isotherm systems, Chemical Engineering Journal, 156 (2010) 2-10.

[153] S. Kim, E.M.V. Hoek, Modeling concentration polarization in reverse osmosis processes, Desalination, 186 (2005) 111-128.

[154] S. Bouranene, P. Fievet, A. Szymczyk, M. El-Hadi Samar, A. Vidonne, Influence of operating conditions on the rejection of cobalt and lead ions in aqueous solutions by a nanofiltration polyamide membrane, Journal of Membrane Science, 325 (2008) 150-157.

[155] A. Garg, C.A. Cartier, K.J.M. Bishop, D. Velegol, Particle Zeta Potentials Remain Finite in Saturated Salt Solutions, Langmuir, 32 (2016) 11837-11844.

[156] T. Visser, S. Modise, H. Krieg, K. Keizer, The removal of acid sulphate pollution by nanofiltration, Desalination, 140 (2001) 79-86.

[157] A. Seidel, J.J. Waypa, M. Elimelech, Role of charge (Donnan) exclusion in removal of arsenic from water by a negatively charged porous nanofiltration membrane, Environmental Engineering Science, 18 (2001) 105-113.

[158] E.M. Vrijenhoek, J.J. Waypa, Arsenic removal from drinking water by a “loose” nanofiltration membrane, Desalination, 130 (2000) 265-277.

[159] S. Mehdipour, V. Vatanpour, H.-R. Kariminia, Influence of ion interaction on lead removal by a polyamide nanofiltration membrane, Desalination, 362 (2015) 84-92.

[160] N.C. Nguyen, S.-S. Chen, H.-T. Hsu, C.-W. Li, Separation of three divalent cations (Cu^{2+}, Co^{2+} and Ni^{2+}) by NF membranes from pHs 3 to 5, Desalination, 328 (2013) 51-57.

[161] D.H. Dvorak, R.S. Hedin, H.M. Edenborn, P.E. McIntire, Treatment of metal-contaminated water using bacterial sulfate reduction: Results from pilot-scale reactors, Biotechnology and bioengineering, 40 (1992) 609-616.

[162] P. Riveros, The extraction of Fe (III) using cation-exchange carboxylic resins, Hydrometallurgy, 72 (2004) 279-290.

[163] A. Bódalo, J.-L. Gómez, E. Gómez, G. León, M. Tejera, Reduction of sulphate content in aqueous solutions by reverse osmosis using cellulose acetate membranes, Desalination, 162 (2004) 55-60.

[164] M. Galiana-Aleixandre, A. Iborra-Clar, B. Bes-Piá, J. Mendoza-Roca, B. Cuartas-Uribe, M. Iborra-Clar, Nanofiltration for sulfate removal and water reuse of the pickling and tanning processes in a tannery, Desalination, 179 (2005) 307-313.

[165] C. Sierra, J.R.Á. Saiz, J.L.R. Gallego, Nanofiltration of Acid Mine Drainage in an Abandoned Mercury Mining Area, Water, Air, & Soil Pollution, 224 (2013) 1-12.

[166] J. Tanninen, S. Platt, A. Weis, M. Nyström, Long-term acid resistance and selectivity of NF membranes in very acidic conditions, Journal of membrane science, 240 (2004) 11-18.

[167] C.-M. Zhong, Z.-L. Xu, X.-H. Fang, L. Cheng, Treatment of acid mine drainage (AMD) by ultra-low-pressure reverse osmosis and nanofiltration, Environmental Engineering Science, 24 (2007) 1297-1306.

[168] B. Su, T. Wu, Z. Li, X. Cong, X. Gao, C. Gao, Pilot study of seawater nanofiltration softening technology based on integrated membrane system, Desalination, 368 (2015) 193-201.

[169] G. Ribera, L. Llenas, M. Rovira, J. de Pablo, X. Martinez-Llado, Pilot plant comparison study of two commercial nanofiltration membranes in a drinking water treatment plant, Desalination and water treatment, 51 (2013) 448-457.

[170] C. Bellona, J.E. Drewes, Viability of a low-pressure nanofilter in treating recycled water for water reuse applications: a pilot-scale study, Water Research, 41 (2007) 3948-3958.

[171] C.-Z. Liang, S.-P. Sun, B.-W. Zhao, T.-S. Chung, Integration of Nanofiltration Hollow Fiber Membranes with Coagulation–Flocculation to Treat Colored Wastewater from a Dyestuff Manufacturer: A Pilot-Scale Study, Industrial & Engineering Chemistry Research, 54 (2015) 11159-11166.

[172] C. He, T. Zhang, X. Zheng, Y. Li, R.D. Vidic, Management of Marcellus Shale Produced Water in Pennsylvania: A Review of Current Strategies and Perspectives, Energy Technology, 2 (2014) 968-976.

[173] S. Tavakkoli, O.R. Lokare, R.D. Vidic, V. Khanna, A techno-economic assessment of membrane distillation for treatment of Marcellus shale produced water, Desalination, 416 (2017) 24-34.

[174] C. He, T. Zhang, R.D. Vidic, Co-treatment of abandoned mine drainage and Marcellus Shale flowback water for use in hydraulic fracturing, Water Research, 104 (2016) 425-431.

[175] A.E. Childress, S.S. Deshmukh, Effect of humic substances and anionic surfactants on the surface charge and performance of reverse osmosis membranes, Desalination, 118 (1998) 167-174.

[176] R. Haddada, E. Ferjani, M.S. Roudesli, A. Deratani, Properties of cellulose acetate nanofiltration membranes. Application to brackish water desalination, Desalination, 167 (2004) 403-409.

[177] S.S. Deshmukh, A.E. Childress, Zeta potential of commercial RO membranes: influence of source water type and chemistry, Desalination, 140 (2001) 87-95.

[178] C. Mazzoni, L. Bruni, S. Bandini, Nanofiltration: Role of the Electrolyte and pH on Desal DK Performances, Industrial & Engineering Chemistry Research, 46 (2007) 2254-2262.

[179] Y.W. Ko, R.M. Chen, Ion rejection in single and binary mixed electrolyte systems by nanofiltration: effect of feed concentration, Separation Science and Technology, 42 (2007) 3071-3084.

[180] S. Bhattacharjee, J.C. Chen, M. Elimelech, Coupled model of concentration polarization and pore transport in crossflow nanofiltration, AIChE Journal, 47 (2001) 2733-2745.

[181] A.S. Colburn, N. Meeks, S.T. Weinman, D. Bhattacharyya, High Total Dissolved Solids Water Treatment by Charged Nanofiltration Membranes Relating to Power Plant Applications, Industrial & Engineering Chemistry Research, 55 (2016) 4089-4097.

[182] E. Hassinger, J. Watson, Drinking Water Standards, College of Agriculture and Life Sciences, University of Arizona (Tucson, AZ).

[183] W.H. Organization, Guidelines for drinking-water quality, World Health Organization, 2004.

[184] M.-K. Hsieh, H. Li, S.-H. Chien, J.D. Monnell, I. Chowdhury, D.A. Dzombak, R.D. Vidic, Corrosion control when using secondary treated municipal wastewater as alternative makeup water for cooling tower systems, Water Environment Research, 82 (2010) 2346-2356.

[185] L. Fewtrell, J. Bartram, Water Quality: Guidelines, Standards & Health, IWA publishing, 2001.

[186] N.R. Council, Soil and water quality: an agenda for agriculture, National Academies Press, 1993.

[187] B. Sarkar, P.P. Chakrabarti, A. Vijaykumar, V. Kale, Wastewater treatment in dairy industries — possibility of reuse, Desalination, 195 (2006) 141-152.

[188] T. Asano, Wastewater Reclamation and Reuse: Water Quality Management Library, CRC Press, 1998.

[189] J.E. Drewes, Ground water replenishment with recycled water—water quality improvements during managed aquifer recharge, Ground Water, 47 (2009) 502-505.

[190] C. He, M. Li, W. Liu, E. Barbot, R.D. Vidic, Kinetics and equilibrium of barium and strontium sulfate formation in Marcellus Shale flowback water, Journal of Environmental Engineering, 140 (2014) B4014001.

[191] T. Zhang, K. Gregory, R.W. Hammack, R.D. Vidic, Co-precipitation of radium with barium and strontium sulfate and its impact on the fate of radium during treatment of produced water from unconventional gas extraction, Environmental science & technology, 48 (2014) 4596-4603.

[192] A.O. Aguiar, L.H. Andrade, B.C. Ricci, W.L. Pires, G.A. Miranda, M.C.S. Amaral, Gold acid mine drainage treatment by membrane separation processes: An evaluation of the main operational conditions, Separation and Purification Technology, 170 (2016) 360-369.

[193] P. Chen, X. Ma, Z. Zhong, F. Zhang, W. Xing, Y. Fan, Performance of ceramic nanofiltration membrane for desalination of dye solutions containing NaCl and Na_2SO_4, Desalination, 404 (2017) 102-111.

[194] A. Plottu-Pecheux, B. Houssais, C. Democrate, D. Gatel, C. Parron, J. Cavard, Comparison of three antiscalants, as applied to the treatment of water from the River Oise, Desalination, 145 (2002) 273-280.

[195] Cerahelix, http://www.cerahelix.com/products/ (accessed 08/07/2017).

[196] C.W. Noack, K.M. Perkins, J.C. Callura, N.R. Washburn, D.A. Dzombak, A.K. Karamalidis, Effects of Ligand Chemistry and Geometry on Rare Earth Element Partitioning from Saline Solutions to Functionalized Adsorbents, ACS Sustainable Chemistry & Engineering, 4 (2016) 6115-6124.

[197] A. Gaid, G. Bablon, G. Turner, J. Franchet, J. Christophe Protais, Performance of 3 years' operation of nanofiltration plants, Desalination, 117 (1998) 149-158.

[198] M. Gui, J.K. Papp, A.S. Colburn, N.D. Meeks, B. Weaver, I. Wilf, D. Bhattacharyya, Engineered iron/iron oxide functionalized membranes for selenium and other toxic metal removal from power plant scrubber water, Journal of Membrane Science, 488 (2015) 79-91.

[199] T. Urase, J.-i. Oh, K. Yamamoto, Effect of pH on rejection of different species of arsenic by nanofiltration, Desalination, 117 (1998) 11-18.

[200] F.-f. Chang, W.-j. Liu, X.-m. Wang, Comparison of polyamide nanofiltration and low-pressure reverse osmosis membranes on As (III) rejection under various operational conditions, Desalination, 334 (2014) 10-16.

[201] A. Szymczyk, P. Fievet, C. Ramseyer, Dielectric constant of electrolyte solutions confined in a charged nanofiltration membrane, Desalination, 200 (2006) 125-126.

[202] A.S. Al-Amoudi, Factors affecting natural organic matter (NOM) and scaling fouling in NF membranes: A review, Desalination, 259 (2010) 1-10.

[203] B. Zoeteman, F. De Grunt, E. Köster, K. Smit, P. Punter, Taste assessment of individual salts in water: methodology and preliminary findings by a selected national panel, Chemical Senses, 3 (1978) 127-139.

[204] F. Nakayama, D. Bucks, Water quality in drip/trickle irrigation: a review, Irrigation science, 12 (1991) 187-192.

[205] Sadtler, The Infrared Spectra Atlas of Monomers and Polymers: Sadtler Research Laboratories, (1980).

[206] Y. Lanteri, A. Szymczyk, P. Fievet, Membrane Potential in Multi-Ionic Mixtures, The Journal of Physical Chemistry B, 113 (2009) 9197-9204.

[207] K. Asaka, Electrochemical properties of asymmetric cellulose acetate membranes, Journal of Membrane Science, 52 (1990) 57-76.